ABSTRACT

Title of Dissertation:	THE EFFECTS OF MECHANICAL CONFINEMENT ON CANCER CELL GROWTH AND MIGRATION MECHANISMS
	Rebecca A. Moriarty, Doctor of Philosophy, 2021
Dissertation directed by:	Associate Professor, Dr. Kimberly M. Stroka, Fischell Department of Bioengineering
	Stadtman Investigator, Dr. Stavroula Mili, National Cancer Institute

Cancer is a disease in which cell growth proceeds unchecked and cells accumulate mutations to adopt an invasive and migratory phenotype that promotes metastasis. Once a cancer becomes metastatic, survival rates plummet, and vast tumor heterogony and lesion formation leave current therapeutics and treatments unable to maintain pace. Therefore, there exists a clinical need to gain a more complex understanding of factors that promote and encourage metastasis. Cancer cells are subjected to mechanical forces *in vivo* that influence their behavior. Mechanical cues are transmitted through the cell from the membrane to the cytoskeleton, and ultimately to the nucleus where gene expression and subsequently protein output can be altered.

In this dissertation, we probed the effects of mechanical confinement, a restrictive force present at various stages during the metastatic cascade, on (1) cancer

cell growth and cell cycle progression, (2) global mRNA translational and its relationship to cell migration, and (3) mRNA localization mechanisms for use in confined cell migration. We modeled confinement *in vitro* through fabrication of microfluidic microchannel devices. We show here that mechanical confinement halts sarcoma cell cycle progression and division and leads to an increase in abnormal divisions. We explored the connection between mRNA translation and cell migration and found that global mRNA translation is spatially altered in confinement and that it is necessary for confined cell migration. We explored this idea further, investigating a subset of mRNAs that are known to influence cell migration in unconfined spaces and show that their regulation in confinement is cell type dependent, but that it primarily relies on cell mechanoactivity. Together, this work contributes a detailed understanding of key cell behaviors that are altered in confined environments and emphasizes the importance of studying mechanical cues that cells experience *in vivo*, in the context of understanding and treating cancer progression and metastasis.

THE EFFECTS OF MECHANICAL CONFINEMENT ON CANCER CELL GROWTH AND MIGRATION MECHANISMS

by

Rebecca A. Moriarty

Dissertation submitted to the Faculty of the Graduate School of the
University of Maryland, College Park, in partial fulfillment
of the requirements for the degree of
Doctor of Philosophy
2021

Advisory Committee:
Professor Kimberly Stroka, Chair
Dr. Stavroula Mili, Co-Chair
Dr. Steven Jay
Dr. Giuliano Scarcelli
Dr. Kan Cao

Personal Acknowledgements

It takes a village to finish a dissertation. Accordingly, I am forever grateful for the wise minds and shoulders that I leaned on to get to this point. I would first and foremost like to thank the woman that took a chance on a wide eyed and naïve student, Dr. Kim Stroka. Through her unyielding support, kind encouragement, and positive attitude on research, life, and everything in between I am so thankful to have learned from you.

To Dr. Voula Mili, thank you sharing your wealth of knowledge with me. Through your gracious mentorship over the last three years, I have grown as a scientist. You have taught me invaluable lessons on what the research world can offer, how to ask better research questions, and how to focus my often-jumbled efforts.

I could not have made it to this point without the support of my entire labmates, past and present. Those who created a warm environment in a perpetually cold cinderblock room, Dr. Kelsey Gray, Dr. Marina Pranda, and especially, Dr. Mary Doolin. Our times spent together in and out of lab have been some of my fondest memories of the last five years. To those who came after them, Ariana DeCastro, Dr. Li Yan, and Ian Smith, your positive personalities made the lab a welcoming place even though I was always moving in and out. At my second home, Dr. Tianhong Wang, Dr. Kostas Moissoglu, Dr. Alexander Gasparski, Dr. Devon Mason, and George Chrisafis, your endless supply of experimental knowledge and witty quips will always be a source of smiles. Also, thank you for giving me an outlet to test many a sweet treat.

I would like to thank the friends I found in the department, not limited to, but most notably, Dr. Joshua N. Webb, Dr. Anjana Jeyaram, and soon to be Drs. Eli Pottash and Barry Liang. Your supply of five years' worth of board games, podcast recommendations, and a friendly face accompanied by a pat on the back when an experiment didn't turn out as planned or most often, hoped, was most appreciated.

To my support system outside of the lab bench, I have to thank foremost, my incredible parents, Judy and Kevin. Thank you for providing us with a wide view of the world, especially the natural one, for us to go and forge our own paths. I am eternally grateful for your unyielding support of my wildest dreams. To my brother and sister, Daniel and Theresa, your work ethics and energy motivate me to be the best version of myself each and every day. And to *try* to stay one step ahead of you both. To Kim and Kelly, thank you for your unconditional love and for always accepting my calls when I need to vent or share my colorful mental musings. To my beautiful friends, Sukhi Gulati and Jeanne Dolan, your encouragement and reassurance from near and far has an effervescent light through it all.

Finally, I would like to thank the best roommate and my emergency contact over the last five years, Denise McPhilmy. Thank you for having my back through the tears, toils, and most importantly, triumphs that have come for us during this tenure together.

Scientific Acknowledgements

This body of work was achieved through the support of the following:

- Dr. Kim Stroka and Dr. Voula Mili for their mentorship, support in designing experiments, analyzing results, and manuscript and proposal writing and editing.
- My committee members Dr. Steven Jay, Dr. Giuiliano Scarcelli, and Dr. Kan Cao for their thoughtful feedback and support to make this document the best it can be.
- The Laboratory of Cellular and Molecular Biology at the National Cancer Institute, specifically Dr. Valarie Barr and Itoro Akpan, for their support in use of the confocal microscope. In addition, Dr. Larry Samelson, Elsy Hernandez, and Nancy Cruz for their leadership and administrative support.
- The Maryland NanoCenter Fabrication Laboratory for their assistance in providing and troubleshooting photolithography resources.

I would like to specifically acknowledge:

- Mary Doolin, for co-authoring sections in Chapter 2.
- Ian Smith, for his Auto-CAD renderings in Chapter 4.
- The University of Maryland Graduate School, for funding in the form of a Jacob K. Goldhaber Travel Award and a Summer Fellowship.
- The National Cancer Institute- University of Maryland Partnership for Integrative Cancer Research, for research funding.

Table of Contents

List of Figures

List of Abbreviations

EMT – epithelial-to-mesenchymal transition

YAP/TAZ – YES-associated protein 1/Tafazzin

ECM – extracellular matrix

LINC – linker of nucleoskeleton to cytoplasm

Arp2/3 – actin related protein 2/3

MMP – matrix metalloproteinase

ATP/ADP – adenosine triphosphate/adenosine diphosphate

pMLC – phosphorylated myosin light chain kinase

mRNA – messenger RNA

tRNA – transfer RNA

miRNA – micro-RNA

siRNA – small interfering RNA

UTR – untranslated region

μm – micron

M or k Pa – mega or kilo pascal

PDMS – polydimethylsiloxane

PEG – polyethylene glycol

qRT-PCR – quantitative reverse transcriptase polymerase chain reaction

FUCCI – fluorescent ubiquitination-based cell cycle indicator

ANOVA – analysis of variance

DMSO – dimethyl sulfoxide

PTL – Parthenolide

EtOH – Ethanol

CHX – Cycloheximide

APC – adenomatous polyposis coli

PDI – peripheral distribution index

FISH – fluorescent in situ hybridization

Chapter 1: Introduction

There are two major limitations when dealing with metastatic cancers; the first is that patients are often unresponsive to existing treatments, and secondly, once the cancer has begun to grow in a different organ, there is a vastly different microenvironment to treat and work with (*1*). Therefore, there is a current clinical need to develop new treatments aimed at both preventing and treating metastasis, but also to generate a broader understanding of how cells are encouraged to become metastatic through biophysical and biochemical cues that they experience during the metastatic cascade (*2*).

Cancer originates through mutations that deregulate cell growth and lead to a host of future mutations that can drive tumorigenesis and metastasis (*3*). A multitude of physical and chemical cues can influence cancer cell behaviors (*4*, *5*). First, an external stimulus is sensed by the membrane of the cell, either through mechanosensitive channels, focal adhesions, or cell surface receptors (*6*, *7*). This signal is then relayed into the cell where it can influence downstream signaling pathways or act upon cytoplasmic components, such as the cytoskeleton (*8*, *9*). Ultimately, these intracellular signals can translocate to the nucleus, either through openings in the nuclear envelope in response to mechanical tension placed on the LINC complex, or through active protein import, where they can affect gene expression that ultimately influences protein expression (*10–12*).

The majority of studies within the field of mechanobiology are focused on substrate stiffness, topography, matrix composition, and matrix rigidity. Here, we focus

on the physical cue of confinement. Cells experience confinement throughout the metastatic cascade, starting in the primary tumor, where they are exposed to high levels of solid stress (*13*, *14*). As they migrate out of the primary tumor through extracellular matrix with 1-30 μm diameter pores, or along thick, aligned collagen fibers they may also experience physically confining forces (*15*, *16*). Cells squeeze through the endothelium in gaps about 1-2 μm in diameter to enter the bloodstream, and within the bloodstream, cells move through capillaries as small as 3-4 μm in diameter (*17*, *18*). Cells extravasate through the endothelium, again through gaps between endothelial cells to a pre-metastatic niche site (*19*, *20*). While recent efforts have shown that confinement greatly impacts cell migration mechanisms, there is a still a gap in our understanding of how confinement affects other cellular behaviors.

The overall goal of this dissertation is to investigate the impact of mechanical confinement on metastatic cancer cell behaviors to improve our understanding to aid future development of therapies or treatments. We utilized microfluidic microchannel devices to model varying degrees of confinement, mimicking the microtracks that cancer cells are known to use as highways for invasion through the extracellular matrix in tissues. We utilized an engineered confining microenvironment to explore cancer cell growth and cell cycle progression, and cancer cell migration, specifically through modulation of global mRNA translation and local mRNA accumulations known to play a role in unconfined migration (Figure 1.1).

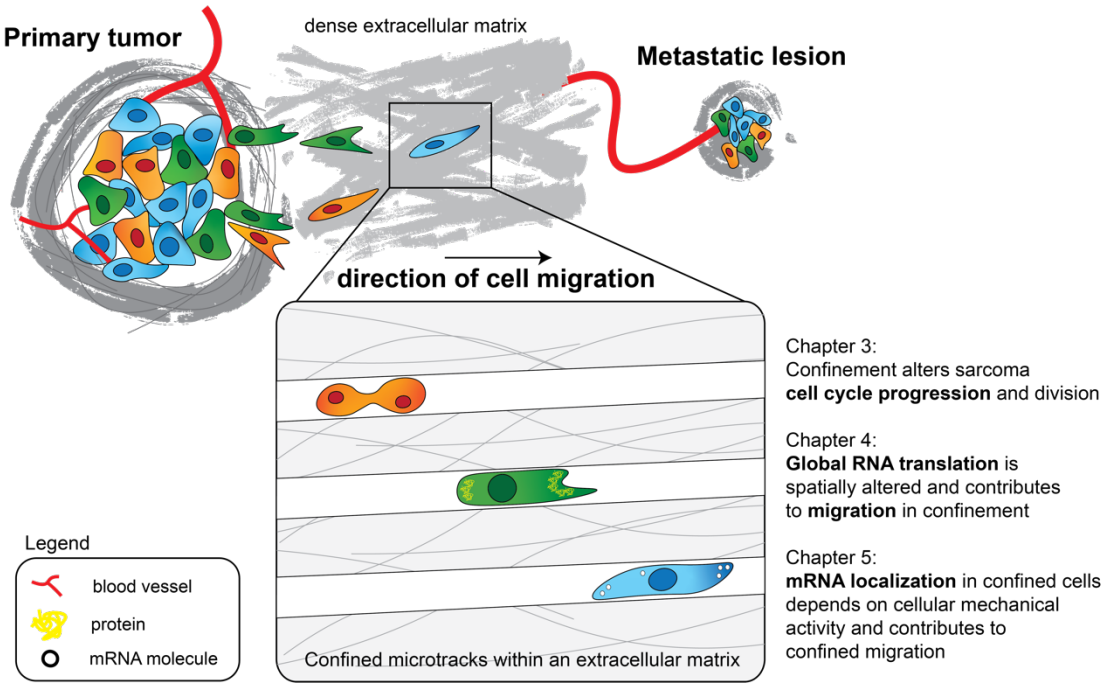

Figure 1.1: Dissertation overview and *in vivo* relevance.

In Chapter 3, we explored the effect of confinement on cancer cell division and progression through the cell cycle. We seeded mouse sarcoma cells stably expressing a fluorescent cell cycle indicator into microchannels of varying widths (50, 20, 10, 6, and 3 μm) to explore how the degree of confinement, in direct comparison to unconfined environments, affects tumor cell cycle progression. We found that cell divisions decrease as confinement increases. Interestingly, abnormal divisions increased as a function of increasing confinement, where cells in the 3 and 6 μm narrow, confined microchannels showed an increase in the number of cells that divided and then fused immediately afterwards, resulting in multinucleated cells. Our results here improve the understanding of the restrictive behavior of confinement on cell

growth but note that the unchecked regulatory pathways of cancer can mitigate this restriction and in turn adopt more invasive and metastatic characteristics.

We next explored the relationship between global mRNA translation and confined migration (Chapter 4). Here, we studied the spatial organization of newly synthesized protein in confined and unconfined environments and explored the role of mRNA translation in cell migration parameters, including cell directionality. Our results argue that there are two zones of protein accumulation in confinement, one at the leading edge of the cell, and one at the lagging edge. We showed that only a single zone of active translation is necessary to organize confined cell migration. We present a design for a novel 3-D printed transwell microchannel confining device to collect cell material for large scale RNA and proteome analysis to determine specific factors that may be involved in regulating confined migration. These results begin to explore the translational mechanisms in confinement which contribute to altered migratory behaviors.

We delved further into the mechanisms behind mRNA behaviors in the context of cell migration in Chapter 5. We explored mRNA localization at the peripheral regions of the cell and how its involvement in migration may or may not be altered in confined environments. In this chapter, through comparison of cells in confined or unconfined microchannels, we showed that mRNA localization at the periphery is cell type dependent in confinement. Specifically, peripheral mRNA localization occurs in a mechanically active cell type in confinement and is important for its ability to migrate through confinement. By contrast, a less mechanically active cell type does not localize the same set of RNAs at the periphery and does not rely on this mechanism for confined

migration. These results further expand upon the notion that cells are able to modulate their migratory behavior in confinement, with novel contributions to the fact that this can partially occur through directing subcellular RNA localizations.

Through an integrated biological, biophysical, and engineering approach, we provide evidence to advance the understanding of cancer cell behaviors. This work dually emphasizes the importance of both the study of the mechanical environment and the mechanoactivity of cells. We see this intersectionality as the future for targeted therapeutic developments.

Chapter 2: Background[1]

2.1: Cancer metastasis and the tumor microenvironment

2.1.1 Cancer progression and treatment

Cancer continues to be a leading cause of death worldwide, where in the United States alone, approximately 40% of the population will be diagnosed with cancer at some point during their lifetimes (*21*). While early diagnostic tests and improved therapeutics have led to an overall increase in survival rate, once the cancer becomes metastatic and begins to colonize secondary sites, the survival rate drops to anywhere between 5 to 30%, depending on the type of cancer, making it the primary cause of cancer related fatalities (*3*). Metastasis is characterized as the event in which cells leave the primary tumor and spread to other tissues within the body, through adoption of pro-invasive capabilities. Cells acquire these characteristics during the initial genetic modifications that are a hallmark of cancer. Metastasis is also the most difficult stage of cancer to treat as there can be inefficiencies in locating and treating the secondary tumors before they have become overgrown (*22*).

Current therapeutics to treat metastatic cancer include chemotherapy, immunotherapy, and/or targeted therapy. These therapies rely on small molecules or monoclonal antibodies to target the cancer cells' ability to divide or to mark them for recognition and degradation by the immune system, in addition to enhancing the overall

[1] Sections adapted from MT Doolin*, RA Moriarty*, and KM Stroka. "Mechanosensing of mechanical confinement by mesenchymal-like cells." *Frontiers in Physiology* (2020): 11, 365. * indicates equal contribution.

immune function. However, these treatments can lead to tumor cell resistance due to vast tumor heterogeneity and often have severe side effects, leading to the continuous need for novel therapeutic developments (*2*). Therefore, more targeted efforts can be focused on cancer cell growth and migration, to simultaneously prevent the spread of tumor cells while enabling easier removal of current tumors.

2.1.2 Tumor microenvironment

Genetic and epigenetic alterations have long been targeted as the primary regulators of cancer cell initiation and progression (*23*, *24*). Cancer initiation starts with a mutation in a driver gene within the cell. However, this single mutation alone is insufficient to result in tumor formation. Rather, this is the result of an accumulation of numerous mutations in additional driver genes (*25–27*). As the cell multiplies, it can acquire supplementary mutations, ultimately rendering the innate mutation repair mechanisms inadequate and the cell dysfunctional. There are ten common oncogenic signaling pathways that are altered in cancer: RTK/RAS, Nrf2, PI3K, TGF-β, Wnt, Myc, p53, Hippo, Notch, and the cell cycle (cyclins, CDKs) (*25*). These pathways modulate cell proliferation (RTK/RAS, PI3K, TGF-β, Wnt, Myc, Hippo), inflammation (Nrf2, Notch), and cell cycle checkpoints (p53, cyclins/CDKs).

At least one of these are mutated in 89% of cancers, from a sequencing study of more than 9,000 tumors (*25*). DNA sequencing technologies have ensured that the analysis of the genomic landscape can be relatively quick and cost-effective from a diagnostic viewpoint. Yet, there is a significant amount of variation within the cancer

genome and genes in these common pathways are not mutated at the same frequency, which can make diagnosis more complicated (*2*).

Once the cells have acquired an oncogenic mutation, they can create a pro-tumorigenic microenvironment to facilitate their growth and survival (*28*). The tumor microenvironment is a heterogenous environment comprised of both cancerous cells and the surrounding non-transformed cells, such as cancer associated fibroblasts, in addition to other immune cells (*29*). The interplay between the tumor and nontumorigenic cells, in the form of biochemical and biophysical cues, can influence cancer progression (*30*). From a biochemical standpoint, cancer cells can recruit and secrete various cytokines, extracellular vesicles, and inflammatory factors.

Tumor associated chemokines generate chemical gradients that can direct cell migration, immune cell recruitment, and blood vessel growth into the tumor (*31*). The hypoxic nature of the microenvironment, as well as proinflammatory cytokines (TGF-β, TNFα, IL6) and extracellular matrix components (collagen I, fibronectin, hyaluronan), can synergistically and individually promote epithelial-to-mesenchymal transition (EMT) (*32*). EMT occurs in epithelial cells, where numerous genetic changes primarily downregulate their cell-cell junction proteins and upregulate their invasive migratory behaviors, ultimately changing their cellular phenotype (*33*). Slightly counterintuitively, immune cells can be both anti-tumorigenic and pro-tumorigenic, the latter leading to enhanced cancer cell proliferation, which can facilitate the accumulation of genetic mutations in this feed forward cycle (*34*). Switches in the direction of pH gradients, where increases in ion channel expression alone in cancer cells can alter the cytoplasmic homeostasis, can drive switches in metabolic activity of

the cancer cells towards a glycolytic phenotype (*35*, *36*). The same can be said for the establishment of a hypoxic environment, where lack of O_2 diffusion into the center of the tumors can alter the metabolic gradients present within the tumor microenvironment (*31*).

Biophysical signals are also known regulators of cancer cell progression. Cells experience numerous mechanical cues within the tumor microenvironment, but also experience mechanical cues as they migrate out of the tumor environment, through surrounding extracellular matrix that is dense with collagen fibers. These matrix fibers can either be aligned to allow for cells to use them as "highways" or through intertwined fibers that need to be remodeled or degraded for cells to move through. Solid stress, substrate stiffness, tension, confinement, and matrix rigidity are just a few forces cells experience within this environment. Substrate stiffness and rigidity can dictate sites of secondary tumors and cancer cell growth (*37*, *38*), shear flow can encourage cancer cells to become more invasive (*39*), and interstitial pressure can drive cancer cell outgrowth into the surrounding matrix (*40*). Substrate stiffness, in particular, has been recently discussed (*41*) as a target for therapeutics and delivery approaches. **Meanwhile, this dissertation focuses on the mechanical cue of confinement, as it can affect cells at every stage of tumor formation, progression, and secondary tumor locations.**

2.1.3 Mechanical memory

Cancer cells can display symptoms of mechanical memory of their environment, in addition to changes in cell behavior at the time of force exposure. Specifically, there is a transcriptional memory phenomenon, after treatment with

certain drugs, bivalent histone modifications remain and spread to other loci, ultimately resulting in drug resistance by these genes (*42*). In depth analysis showed that these memory signals can be transmitted bioelectrically, via miRNA, or through the YAP/TAZ pathway, and can be traced to varying patterns of chromatin condensations (*43–46*).

More examples of this have begun to populate the literature. Mechanical conditioning of breast cancer cells on hydrogels of increased stiffness (8.0 kPa) for seven days before transfer to a soft (0.5 kPa) gel can lead to an increase of osteogenic markers via ERK mediated signaling and was strongly correlated with aggressive bone metastases (*47*). A new theoretical model predicts that the duration of substrate stiffness priming can direct extended protein production associated with cytoskeletal activation on stiff substrates through various epigenetic memory related factors (*48*). As a result, a more complete understanding of the effects of the physical microenvironment on cells may shed light on genetic alterations that can drive both cancer initiation and progression.

2.2 Clinical relevance of confinement

2.2.1 Confinement is a clinically relevant mechanical cue for cancer cells

Cancer is defined as an abnormal growth of cells, meaning that as cells continue to grow within the primary tumor, cells become confined due to the accumulation of solid stresses, derived from the compression of the surrounding ECM onto the overgrown cell mass (*13*, *49*). As the interstitial stress within the primary tumor

becomes overwhelming, cells are encouraged to move out of the tumor (*50*). Physical confinement has been shown to encourage cells to undergo EMT (*51*). Cells can migrate via collective invasion or single cell migration upon leaving the primary tumor; however, this mechanism depends on the degree of EMT (*17*, *18*). Recent work has also demonstrated that collective cell dynamics arise through cell-cell contacts facilitated by adherens junctions, but that the maintenance of this collective movement is modulated by polarized Rac1 activation in single cells which establishes a directional polarity and this leads to coordinated lamellipodial migration (*52*).

Cells are exposed to confining forces at numerous locations during the metastatic cascade (Figure 2.1). Some examples are noted here: as they migrate out of the primary tumor through ECM with 1-30 μm diameter sized pores, or along thick, aligned collagen fibers (*15*, *16*). Cells squeeze through 1-2 μm-sized gaps between endothelial cells to enter the bloodstream, and within the bloodstream, cells move through capillaries as small as 3-4 μm in diameter (*17*, *18*). Cells extravasate through the endothelium, and again through gaps between endothelial cells to a pre-metastatic niche site (*19*, *20*). It is important to note that only a very small population of cancer cells can survive to this point (*19*).

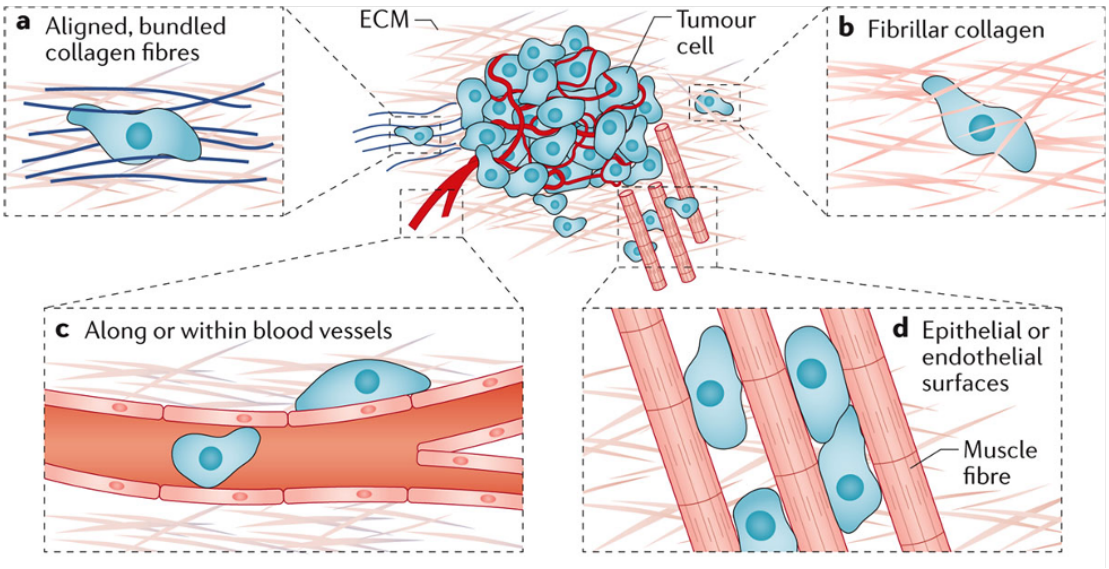

Figure 2.1: Cells experience confinement *in vivo* during tumor progression. Adapted from (*53*)**.**

2.2.2 A physical definition of confinement

There is a growing need to define confinement in quantitative physical terms due to the varying degrees of confining forces that cells can experience *in vivo* and within *in vitro* confinement assays. Here, we focus on cell confinement within microchannels as this is the basis for this work. We suggest it is the result of three main forces (*54*). First, the external force applied to the cell is hydrostatic pressure against the cell at any membrane area exposed to fluid. Hydrostatic pressure is determined by the fluid density, the gravitational pull, and the height. The density, which is an intrinsic property of the fluid calculated by its mass and volume, is in this case, that of the culture medium. The height of the seeding channels determines the pressure at the seeding channel to microchannel interface. The second force is the frictional force exerted on the cell by the microchannel walls. The frictional force is determined by the coefficient

of friction and the force exerted by the cell on the microchannel wall. Friction increases as contact pressure with wall increases (*54*). The third force is the contact force (or pressure) that is exerted on the cell by the microchannel walls.

Currently, there are a few ways to measure these forces within confined microchannels. One method is microelectrode reading of intracellular pressure, which could be an inverse reflection of hydrostatic pressure placed on the cell (*55*). Hydrostatic pressure itself can be calculated by knowing the dimensions of the microchannels and the intrinsic properties of the fluid (or those can be measured in an unconfined, static environment). In addition, the frictional force of cells against polydimethylsiloxane (PDMS) microchannels functionalized with polyethylene glycol (PEG) can be calculated (*56*). Two notable studies have quantified the magnitude of forces exerted by cells within confinement. Upon investigation of cell traction forces within the microchannels, NIH-3T3 mouse fibroblasts and human osteosarcoma cells exert lower traction forces upon entry into 40 μm^2 microchannels compared to 200 μm^2 microchannels (*57*). A study of macrophages within 66 μm^2 microchannels showed that confinement does not affect the amplitude of cell forces, but rather the directionality of the force (*58*). Whereby upon entry into a more confined microchannel, cells redirect their forces outward against the walls of the microchannel. This contrasts with cells in wider channels, or more unconfined environments that direct the forces at the edges of the cell inwards.

To offer a generalized definition of confinement for the purposes of *in vitro* studies, we highlight previous work where the speed of migration and nuclear morphology classified the environment (*59*). Tumor cells in environments greater than

70 μm^2 were unrestrained in their migration and morphology. Tumor cells in environments ranging from 7 to 70 μm^2 were impeded in their migration and altered their nuclear morphology. Environments below 7 μm^2 arrested cell migration. We suggest therefore, that environments at or below 70 μm^2 can be considered 'confining' and environments above are unconfined. **Here, we analyze cells in microchannels that range from 500 μm^2 in cross sectional area, to 100 μm^2 channels, to channels that are 30 μm^2. This allows us to compare unconfined, an approximate transitional state, and confined environments, respectively.**

2.3 Mechanosensing in confinement

2.3.1 Proteins transmit forces across the cell membrane

In the past two decades, there have been significant strides in understanding how cells sense mechanical forces in 2D environments, and the field is now moving towards understanding mechanosensing mechanisms in 3D environments (Figure 2.2). To attach to a 2D substrate, cells form nascent adhesions which may mature to focal adhesions or disassemble (*60*). Traction forces are generated as cells adhere to a substrate and contract via actomyosin interactions, thereby moving the cell forward (*61*). Traction forces are highly dependent on, or inter-linked with, actin dynamics, cell morphology, and cell migratory state (*61*), all of which may be altered by confinement. For example, human osteosarcoma cells decrease their traction forces as confinement increases, but inhibition of myosin II does not reduce cell traction forces in confinement as it does in unconfined spaces (*57*). Within PEG hydrogels, fibroblasts interrogate the

3D matrix via strong inward traction forces near the ends of long, slim extensions (*62*). Additionally, fibroblast adhesions to 3D matrices are much more stable over time than adhesions to 2D matrices (*63*), and 3D adhesions can be distinct from 2D adhesions in phosphorylation of focal adhesion kinase (FAK) (*64*).

Cancer cells in confinement can have fewer and more diffuse focal adhesions. Vinculin, paxillin, talin, zyxin, VASP, FAK, p130Cas, and α-actinin appear diffuse in human fibrosarcoma cells within 3D gels (*65*), while pY-paxillin appears diffuse in MDA-MB-231 cells within confined microchannels (*66*). Despite their diffuse appearance, these focal adhesion proteins still play a role in protrusive and matrix deforming activity (*65*), and are found in regions of curvature or edges (*67*), for instance, as cells begin to enter confinement. During these protrusive events, α4β1 integrins can engage with paxillin to drive myosin II-mediated contractility (*68*). Increased membrane tension, as may be observed in confinement, compresses the lamellipodium and subsequently aligns focal adhesions in fibroblasts (*69*). Increased membrane tension also inhibits SCAR/WAVE complex recruitment and RAC activation, which inhibits protrusion and leading-edge signals in migrating neutrophils (*70*). Hence, although in some situations focal adhesions appear more diffuse and punctate in confinement, reportedly leading to lower cell traction forces, these protein complexes still seem to play an important role in cellular mechanosensing of the physical environment, albeit in a possibly different manner than the classical 2D model (*71*).

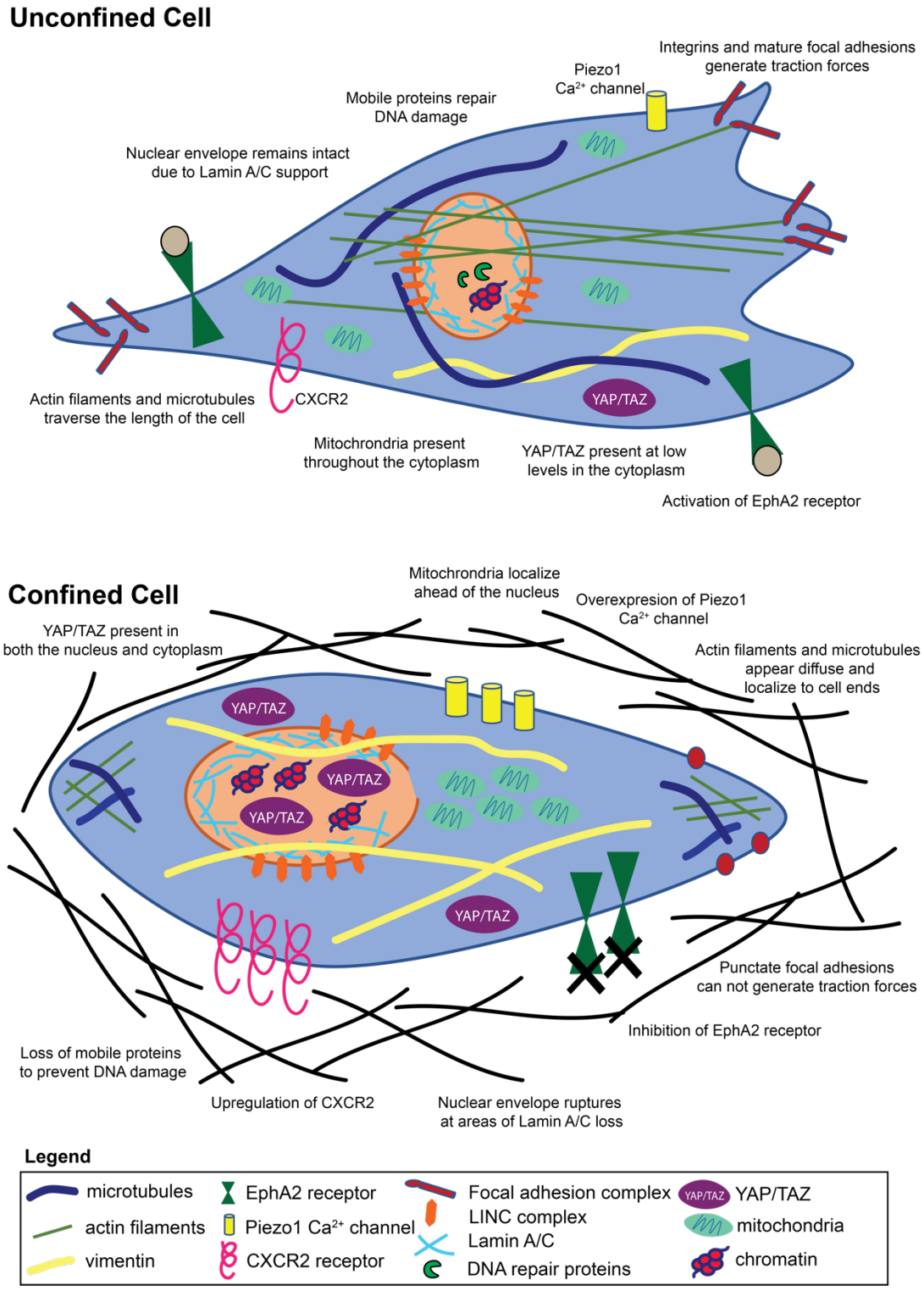

Figure 2.2: Cells within confinement undergo distinct structural changes yet contain many of the same mechanosensitive pathways as unconfined cells.

2.3.2 Confinement induces cytoskeletal reorganization

Typically, a force experienced by a cell at its membrane is transmitted to the cell's cytoskeleton. Physical alterations of boundaries around cells influence actin filaments, focal adhesions, and cell contractility (*67*). Carcinoma cells within microchannels show diffuse actin and microtubule structures that polarize to the leading and lagging edges of the cell (*66*). In confinement, cancer cells upregulate the CXCR2 chemokine receptor, which has been shown to control cytoskeletal remodeling and drive contractility (*72*). A well-known mechanosensitive ion channel is the Piezo1 Ca^{2+} gated ion channel, which can respond to both external and internal stimuli to alter Ca^{2+} levels in the cell. Mechanical stresses induced by confinement in Chinese hamster ovary (CHO) and A375 metastatic melanoma cells lead to increases in intracellular calcium levels via increased tension activation of the Piezo1 stretch-activated cation channel as measured by qRT-PCR, kick starting a feed-forward signaling loop to drive the PDE-1-dependent suppression of protein kinase A (*73*) and possibly enhancing myosin II activity. It is important to note here that Piezo1 expression varies across cancer cell types and stages, potentially leading to varying roles in terms of cell migration behaviors. In addition, there are several other membrane ion channels that are mechanosensitive and drive fluxes of ions across the membrane, such as sodium hydrogen exchangers (NHEs) and transient receptor potential channels (TRPs), which we discuss in further detail in the context of our work in Chapter 5.3.

Actin filaments work to provide the cell with a structural support system important in regulating cell shape, intracellular transport, and cell attachment and adhesion to the surrounding environment (*74*). The actin cytoskeleton reorganizes in

response to physical barriers, partially due to blocking of the membrane transport protein EphA2 (*75*), and in coordination with loss of linear, mature focal adhesions (*66*, *76*). Remodeling of the cytoskeleton also takes place during EMT, when cells adopt a more vimentin-based than keratin-based composition (*77*). Vimentin is critical for coupling to myosin to generate adhesion and traction forces (*78*), whereas keratin aids in cell-cell adhesions common in epithelial cells (*79*). Furthermore, accumulation of YAP/TAZ in the cytosol, as opposed to the nucleus, is seen in cells that have undergone actin remodeling during ciliogenesis (*80*), and in U2OS tumor cells in uni-axial confined microchannels (*81*). This sheds light on yet another possible mechanosensing mechanism for confined cells.

The cytoskeletal reorganization observed in confinement can also be driven by protein kinase C inhibition, which was shown to attenuate migration in conjunction with retinoic acid (*82*). Additionally, organelle positioning, which may vary in confinement, can regulate cell behaviors. For example, nuclear position can be a key factor in determining when a fibroblast undergoes fast or slow migration (*83*). Anterior localization of mitochondria in confined environments, via rhoGTPase-1 trafficking on microtubules, ahead of the nucleus in the direction of cell migration, increases cell velocities and directional persistence (*84*). **In this dissertation, we explore the role of the cytoskeleton in the subcellular localization of specific mRNAs in confined cells.**

2.3.3 Nuclear membrane proteins and chromatin reorganize in confinement

The nucleus is a dynamic organelle, with its volume changing in response to

altered extracellular environments (*85*). Nuclei from a variety of cell types have the capacity to deform in an anisotropic manner in response to applied force from an atomic force microscope tip (*86*), and this anisotropic behavior was confirmed for MDA-MB-231 cells within confining microchannels (*87*). Environmental radii of less than 7 μm seem to be the threshold for nucleus remodeling (*88*, *89*), though this value likely depends on unconfined nuclear size. It is likely that nuclear deformation is a critical pathway for cell mechanosensing of physical confinement (*12*, *90*).

Lamin A/C, a protein in the nuclear lamina that supports the nuclear envelope, has been shown to play a critical role in the successful migration of cells in confinement (*91*). Lamin A/C overexpression has been shown to increase the degree of anisotropic nuclear deformation in response to an applied force, underscoring its importance in nuclear mechanics and response to external forces (*86*). Cancer cells show reduced lamin A/C expression compared to healthy cells, which can facilitate nuclear deformations. Nuclear envelope rupture due to actin bundle accumulation at areas of low lamin A levels causes nuclear compression or stretching (*92*). This compression or stretch leads to herniation of chromatin or double stranded DNA breaks, but the nuclear envelope integrity is restored by ESCRTIII, a membrane remodeling protein, rapidly after cells clear confinement (*93*, *94*). This process has also been modeled extensively during transmigration studies (*95*). However, these DNA breaks can persist long after the cell has repaired the nuclear envelope.

Lamins and the cytoskeleton can transmit mechanical forces between each other via the linker of the nucleoskeleton and cytoskeleton (LINC) complex. The LINC complex consists of KASH-domain proteins, which reside in the outer nuclear

membrane, and SUN-domain proteins, which reside in the inner nuclear membrane (*11*). KASH-domain proteins include nesprin -1, -2, -3, and -4 which each contain binding sites for one or two cytoskeletal elements, and SUN-domain proteins include the commonly expressed Sun1 and Sun2, as well as the testis-specific Sun -3, -4, and -5. (*96*). Microtubules link to Dynein/Lis1, which connect to members of the LINC complex (nesprin to SUN to lamin A) to transmit forces across the nuclear membrane (*97*). In addition, nesprin-2 works synergistically with non-muscle myosin IIB to transmit forces to the nucleus (*98*, *99*).

Disruption of the LINC complex prohibits cells from responding to low magnitude vibrations, further indicating the LINC complex as a critical component of the cellular mechanosensing machinery (*100*). In line with this, transfer of strain from the cytoskeleton to the nucleus via the LINC complex has been shown to be essential for stretch-induced activation of the YAP/TAZ pathway (*101*). YAP/TAZ are consistently activated in human tumors, as they are key transcriptional regulators of cell proliferation and survival. Therefore, activated YAP/TAZ is associated with nuclear localization. Interestingly, evidence has noted that in confinement, tumor cells are unable to translocate YAP to the nucleus, due to cell softening (*81*).

The nuclear lamina interacts with the genome via lamin associated domains, controlling the location and accessibility of the genome (*102*). In fact, lamin A/C deficient cells have defective gene transcription regulated by NF-κB in response to mechanical strain (*103*). In addition to lamin A/C, confinement has been shown to alter dynamics of chromatin associated proteins. When confined to 2 μm pores, cancer cells squeeze mobile proteins involved in DNA repair or nucleases out of the nucleus to

allow chromatin to occupy the full volume of the nucleus. Yet, mobile proteins remain in the nucleus when cells encounter 8 μm pores (*104*). Both the cytoskeleton and nucleoskeleton have been shown to control chromatin dynamics within the nucleus. In one study, confined, isotropic cells contained lower lamin A/C levels and more dynamic heterochromatin foci (*105*). Conversely, polarized, elongated cells generated higher stress on the nucleus, had higher lamin A/C levels, and had less dynamic heterochromatin foci (*105*). These results have been confirmed by others who have shown that loss of lamin A/C leads to increased chromatin dynamics (*106*).

Histone acetylation patterns may also be affected by confinement. Nuclear levels of histone deacetylase 3 (HDAC3) were lower in cells with intermediate volume (3600-4800 μm^3), and higher when actomyosin contractility was inhibited with blebbistatin (*67*). This higher level of nuclear HDAC3 was also shown upon application of a compressive force to fibroblast cells to remove acetylation marks on histone tails to increase the level of heterochromatin. This subjects the cell to a less transcriptionally active state, but one that can be reversed upon removal of a compressive force (*107*). Nuclear confinement leads to alteration of around 180 genes, including increased expression of histones 4 and 3 (*108*). In addition, lateral confinement of MCF7 cells can facilitate their adoption of cancer stem cell likeness, likely through the modifications on histone H3 (*109*). Disruption of chromatin structure via chromatin decondensation can decrease fibroblast mechanosensitivity and dampen the anisotropic deformation of nuclei in response to an applied force (*86*). The structure and composition of the LINC complex, nuclear lamina, and nuclear contents can be altered by mechanical confinement, and may subsequently alter gene expression. **In this**

dissertation, we explore the relationship between altered nuclear morphologies and cell cycle progression and division of cells in confined environments, as the nucleus is the master regulator of the cell cycle.

2.4 Cellular confinement assays

Cells experience confinement in many different environments, whether in the context of *in vitro* or *in vivo* assays, and to many different degrees. As a result, published literature varies greatly when discussing confinement, and many labs have distinct strategies and devices to study cell behavior in confinement. The various models of confined cell migration have been reviewed extensively (*110*, *111*), but we focus on those of most relevance here. Hydrogels, PDMS, silicon, PEG, glass, and collagen are examples of the many materials applied in various confining devices (*111*). Cells can be "confined" on a 2D surface through chemical modifications of the growth surface or with plasma lithography (*112*, *113*). For example, micropatterned lines of adhesive protein can create a 1D track upon which cells can migrate (*114*, *115*). This 1D system can be easily fabricated and imaged, and it is a useful technique for single cell studies. Additionally, fibroblast migration on 1D lines has some similarities to its migration in 3D substrates (*114*). 1D patterning techniques are most similar to the migration of cells along extracellular matrix protein "tracks" *in vivo* (*116*). Similarly, grooved substrates have been harnessed to confine cell migration through a phenomenon known as contact guidance (*117–119*). Contact guidance aligns cytoskeletal features parallel to the grooves in a substrate, directing cell migration along the grooved axis (*120*).

Many groups study confinement using microfabricated devices, including uni-axial “sandwich” confinement (*121*, *122*) and bi-axial confinement which is the focus of this work (Figure 2.3, (*123–125*)). One such method encourages cell migration through confining microchannels or nanotubes of various widths (*66*, *126–129*). Useful to the study of cell mechanotransduction, these channels may be modified to measure forces exerted by cells or to exert forces on cells (*57*, *58*, *130*). Beyond microfluidic devices, confining cells within micropillar arrays can be an effective method to systematically control degree of confinement while simultaneously assessing cell behavior (*131–134*). Furthermore, microtracks can be created in softer materials, by patterning microchannels in polyacrylamide gels (*135*), or by fabricating collagen microtracks via micromolding (*136*) or two-photon laser microsurgery (*137*).

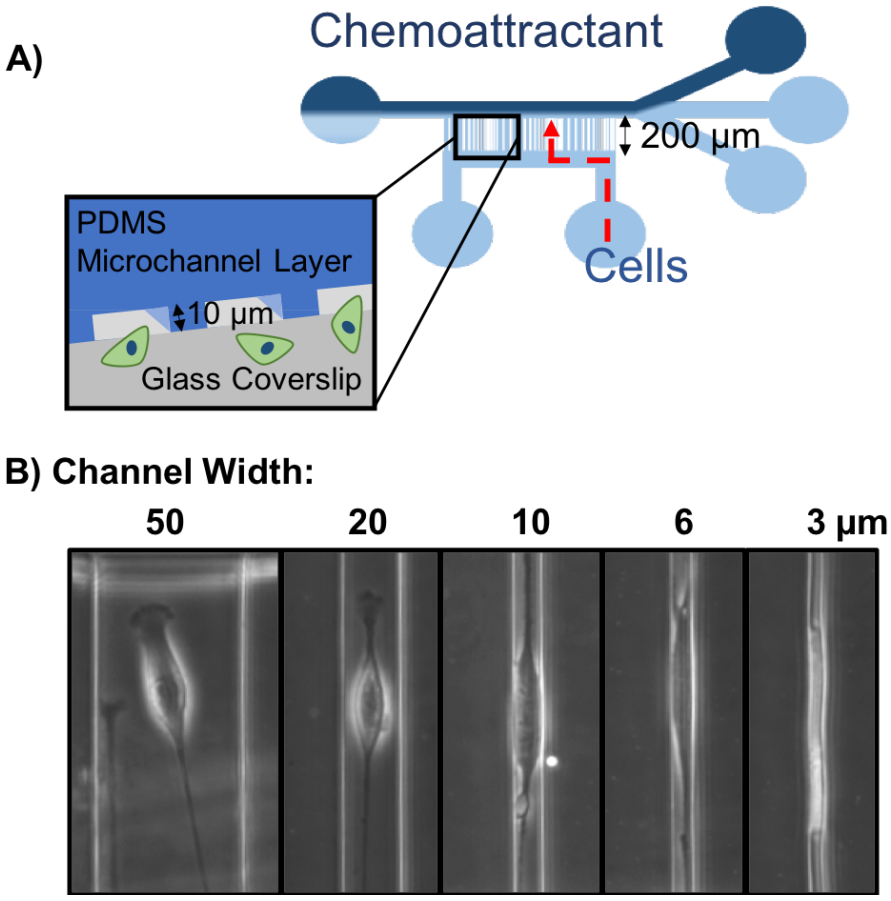

Figure 2.3: Microfluidic microchannels can bi-axially confine cells.

(A) Schematic depicting design of microfluidic channels. Cells are seeded at the bottom inlet and encouraged to migrate through the microchannels of varying widths and fixed height and length (10 µm and 200 µm, respectively) by the addition of a chemoattractant at the topmost inlet (dark blue coloring).

(B) Phase-contrast images of cells in microchannels of 50, 20, 10, 6, 3 µm in width.

Complete 3D confinement can be achieved by encapsulating cells in 3D hydrogels or scaffolds, though the degree of confinement may be difficult to systematically control in these assays (*59*, *138–140*). Within hydrogels, cell seeding

may be manipulated by external forces (*141*, *142*) or confinement may be dynamically controlled, for example by light-triggered expansion of gelatin hydrogel microstructures (*143*). Cells may also be confined within spheroids, where they experience increased cell-cell interactions and confinement due to greater intercellular pressures (*144*). Lastly, cells are confined as they intravasate and extravasate into or out of the vasculature, and numerous groups have modeled transmigration in this facet, usually either through Boyden chambers or cell monolayers (*145–148*). While these assays do not fully confine the entire cell at once, they do present *in vivo*-like constrictive environments through which the cell body, and its nucleus, must squeeze. Regardless of the confining mechanism used, mechanical confinement has the potential to drastically alter cell behavior when compared to traditional 2D culture. **Indeed, in this dissertation, we find that mechanical confinement alters tumor cell cycle progression, global mRNA translation, and subcellular mRNA localization in cells.**

2.5 Effect of confinement on cell behaviors

2.5.1 Migration

The classical model of haptokinetic cell migration occurs in three steps: extension of the leading edge lamellipodium, attachment to the surface, and contraction of the rear (*149*). Small GTPases are critical in the first two steps, where Rac1 encourages actin branching via recruitment of Arp2/3 at the leading edge, then RhoA facilitates integrin driven nascent adhesion association with the actomyosin

cytoskeleton in step two (*150*). Myosin II mediated contractility drives the retraction of the rear. We note that numerous cell types can utilize varying migratory mechanisms (e.g. macrophages, which can also utilize an ameboid blebbing mechanism), and this classical model presented above aligns mainly with mesenchymal cells, with a particular focus and relevance to cancer cells that have undergone EMT and adopted an invasive phenotype.

Of note, nuclear passage into a pore is widely regarded as the rate limiting step in migration through confinement, likely because the nucleus is significantly stiffer than the surrounding cytoplasm and other organelles (*151*). Lamin A/C is critical for successful confined migration, and the expression level of lamin A/C can influence the migration rate of cells through small pores. For example, overexpression or knockout of lamin A/C reduces cell migration rate, but a moderate knockdown of lamin A/C expression increases the migration rate of fibroblasts and tumor cells (*88*, *91*, *152*). Furthermore, migration is arrested in tumor cells, T cells, and neutrophils during migration through pores that are less than 10% of the size of their nuclear cross-section (*59*). Hence, nuclear deformability, nuclear morphology, and lamin A/C expression are all critical components in determining cell migration response in confined environments.

Cells are able to use a variety of mechanisms to move in confinement, including actomyosin contractility (*53*, *59*, *68*, *135*, *153*), water permeation through aquaporins (*154*) or asymmetric hydraulic pressure gradients (*155*), a nuclear piston-based mechanism (*156*), and nuclear rupture to promote squeezing through confined spaces (*93*). Meanwhile, recent reports have revealed new mechanistic insights. Breast

carcinoma cells use contact guidance via myosin IIA and B within microchannels (*120*) or in 3D aligned collagen matrices, which induce lamellipodia along with focal adhesions, to grow parallel to the direction of fiber alignment (*116*, *157*). Smaller, less elongated, and constrained focal adhesions correlate to non-aligned actin fibers, leading to frequent retraction of protrusions and decreased cell polarization (*116*). Interestingly, myosin IIA shRNA treatment has only a modest effect on the time required for MDA-MB-231 cells to squeeze their nuclei through 5 μm pores in a 3D invasion device (*98*). In contrast, myosin IIB shRNA treatment dramatically increases nuclear transit time through these pores. Hence, MDA-MB-231 cells use non-muscle myosin IIA as the primary force generation during active protrusion at the periphery, but use non-muscle myosin IIB as the primary force generator to move the nucleus through small pores through its perinuclear localization (*98*). Specifically, non-muscle myosin IIB links to nesprin-2 which traverses the nuclear membrane, then binding to Sun-1/2 in the inner nuclear membrane. This stimulates nuclear deformation, in a mechanism unique to mesenchymal-type migration (*98*).

Actin can be a key player in confined cancer cell migration. For example, carcinosarcoma cells use actin cortex flow to expand their ECM and use frictional force to migrate in confinement (*158*). Cells can mobilize Girdin, a prometastatic actin binding protein also involved in cell polarity, to aid in persistent directional cell migration in 3D confined collagen matrices with microtracks (*159*). More results have demonstrated a direct link between nesprin-2 and actin via fascin to aid in nuclear deformation as cells enter confined microenvironments (*160*). Fascin is important in regulating F-actin bundling, stability, or localization. Meanwhile, several types of

tumor cells can migrate in confined PDMS-based microchannels even when actin polymerization or myosin II is pharmacologically inhibited (*66*, *154*), and this result can be explained by an "osmotic engine" model of cell migration (*154*). Interestingly, though, cancer cells still require actin polymerization to migrate through collagen microtracks (*161*), which are porous and orders of magnitude more compliant than PDMS, and therefore may not be sufficient to induce osmotic pressures in the cell. Hence, cell migration experiments must be carefully interpreted and considered within the context of the cell models and specific microenvironment.

In addition to cytoskeletal elements, the nucleus can be an important contributor to efficient confined cancer cell migration. Fibroblasts can migrate in confinement via the use of a nuclear piston mechanism to generate varying pressure gradients (*156*), which can activate mechanosensitive ion channels to facilitate extension and propulsion (*162*). A follow-up study showed that, in fibrosarcoma cells, this migration mechanism is initiated by inhibition of MMP, potentially suggesting that the cell uses a single migration mechanism at a time (*163*). The higher pressure at the leading edge of the cell is derived from actomyosin contractility mechanisms, in which nesprin-3 (a LINC complex protein) exerts force on the nucleus to pull it forward (*163*).

While the reports above have noticed that cancer cells can migrate through confinement independent of MMPs, a new mechanism of cancer cell migration in confinement shows that confinement can trigger membrane type 1-MMP (MT1-MMP) endosomes to traffic along microtubules to the anterior of the nucleus, thereby enabling the cell to move forward. Dyenin-Lis1 in the LINC complex directly couple to the microtubule centrosome complex to direct MT1-MMP endosomes towards the leading

edge of the cell (*97*). As more research is published showing new mechanisms for cell migration in confinement, it seems that cells have a range of mechanisms at their disposal (Figure 2.4). Moving forward, it will be critical to identify specifically what aspects of the microenvironment push cells towards a specific migration mechanism, the degree to which cells can switch back and forth between these mechanisms, and why the mechanisms are cell-type dependent. **This dissertation provides evidence that the mechanical activity of the cells directs the migratory mechanism that cells utilize in confined environments.**

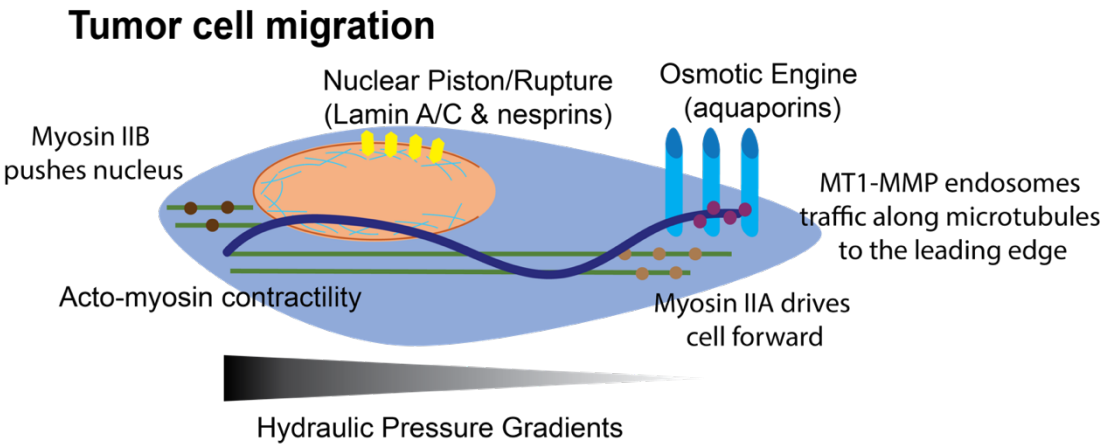

Figure 2.4: Tumor cells in confinement can employ a variety of mechanisms to migrate.

2.5.2 Metastatic potential and invasiveness

Invasiveness, or the ability to permeate confined spaces, is another critical property of both cancer and stem cells. We chose not to describe phenotypic changes in cells transmigrating through an endothelium, but rather we describe the effects of

longer, sustained confining forces. Confinement alone can encourage cells to undergo EMT. Pre-EMT MCF10A cells in narrow channels display a rise in EMT markers when compared to wide channels. These EMT markers include a loss of E-cadherin membrane localization, an increase in vimentin expression, and cytoplasmic localization of β-catenin (*51*). In addition, cells in narrow channels undergoing collective cell migration lose their cell-cell junctions, which is speculated to be a result of the stronger cell-ECM adhesions at the channel wall, leaving the cell-cell junctions susceptible to degradation (*164*). This response is controlled via cell polarization through microtubules. When microtubules are inhibited, epithelial cells lose their sensitivity to confinement and do not undergo EMT (*51*).

Cancer cells are able to negate contact-inhibition and migrate around other cells on narrow micropatterned fibrillar structures, where they would normally retract from cell-cell contact. This increase in migratory behavior is driven by an overexpression of metastatic genes, namely TGF-β and ErbB2, and a reduction in E-cadherin and PARD3 expression (*165*). Confinement can be more important than stiffness in determining how cells invade into surrounding 3D collagen matrices (*166*) and which migration mechanism they use (*167*). As mentioned above, metastatic outgrowth through cell invasion can occur through collective invasion or single cell invasion. Metastatic breast cancer cells can be encouraged to become leader cells through mechanical compression, resulting in changes to the cytoskeletal structure and an increase in focal adhesions (*168*). Similarly, non-muscle myosin (NMM) -IIA and –IIB have been shown to play differential roles in cancer cell invasion, with NMMIIA facilitating cell protrusion and NMMIIB facilitating nuclear translocation through small pores (*98*).

Confinement within the ECM can inhibit the number of cancer stem cells (CSCs) and their scattering from a cancer cell mass (*169*). However, this inhibition may be overcome by increased CSC motility or increased proteolysis (*169*). Meanwhile, intravital imaging is revealing that tumor cell metastasis likely involves invasion plasticity between collective groups of cells and single cell release (*170*).

2.5.3 Cell cycle, division, and proliferation

Circulating tumor cells become mitotic during late stage aggressive cancers, which correlates to poor patient prognosis (*171*). In addition, arrested metastatic tumor cells in the bloodstream can proliferate within the vasculature and form secondary tumors (*172*). However, *in vitro* analysis has shown that confinement has profound effects on cell cycle progression and proliferation specifically by delaying mitosis in healthy and cancer cells (*129*), and reduces proliferation of hematopoietic stem and progenitor cells (*173*). The nucleus is the master regulator of cell division, and nuclear shape and organization are critical regulators of cell division. Reportedly, 8 μm in diameter is the critical threshold for nuclear remodeling to occur in confinement (though this likely depends on cell type and nuclear size), and in glass tubes of 8 μm diameter, division and proliferation of osteosarcoma cells is inhibited (*174*). Confinement within a 3D spheroid forces nuclear elongation and as a result, delays cell division (*175*).

In Chapter 3, we show that sarcoma cells are halted in the S/G2/M stage of the cell cycle while in bi-axial confinement, reducing the number of cell divisions (*176*), and this has been supported by numerous reports from other labs (*177–179*). In single dimension confinement, HeLa cells specifically arrest in the M stage due to the inability

to correctly position the mitotic spindle during mitosis (*179*). In Chapter 3, we show that once cells exit confinement, they are able to improve division frequency, but not to the point where they recover frequency of division on 2D substrates where they were never confined (*176*). It is important to note that confinement reduces but does not eliminate cell divisions, and reports from others, as well as our work in Chapter 3, show that division in confinement results in an increase in abnormal daughter cell geometries, including multinucleated tumor cells and division into more than two daughter cells (*176*, *179*, *180*). These behaviors are relevant because single multinucleated sarcoma cells can form solid tumors significantly more often than mononucleated cells most likely through their enhanced clonogenic and asymmetric division capabilities. In addition, they are also more resistant to the chemotherapeutic agent, doxorubicin (*181*).

During mitosis, cells "round up" by increasing their surface area to volume ratio, through the formation of a cytokinetic actin ring. This mediates proper spindle assembly and positioning, which has been shown to positively influence correct daughter cell formation during mitosis (*182–184*). Disruption of actin can cause arrest in every cell cycle stage. Actin is involved in cyclin regulation and control which is critical in cell cycle progression (*185*). During mitosis, actin binding proteins link the centrosome to F-actin monomers to direct centrosome separation. In fact, treatment with latrunculin, which blocks F-actin assembly, prevents centrosome separation, and as a result, the spindle cannot be assembled (*179*). It has been proposed that F-actin can regulate spindle lengthening and shortening, suggesting a synergistic energy of mitotic spindle assembly and regulation (*186*). However, previous reports that treated cells

with latrunculin saw major effects during cytokinesis, not during mitotic rounding, suggesting that actin is primarily needed for cytokinesis (*179*).

During cytokinesis, the actin contractile ring forms in the cleavage furrow and provides the force needed to separate the two daughter cells (*187*). The contractile ring forms in the specified location due to feedback signals from the separated spindles. The spindle poles transmit Rho-GTPase regulators to the cleavage furrow to activate Rho, leading to contractile ring formation (*188*). There are contrasting reports that the mitotic spindle poles both activate and silence relaxation at the cleavage furrow, stimulating contraction. Recruitment of myosin II to the cleavage furrow generates the necessary intracellular pressure, counteracting the force against the cell (*189*). While myosin II may be able to resist the force of confinement, cytokinetic actin rings in non-spherical mitotic cells, as seen in high degrees of confinement, may be unstable and tenaciously tethered to the mitotic spindle (*190*).

In mitosis, microtubules are responsible for attaching to the kinetochores of the chromosomes (*191*), aiding in initial spindle positioning and force generation to move the centrosomes apart, reaching to the cell cortex to promote rounding (*192*), and packing the space between the centrosomes and the chromosomes to provide the force needed to keep the chromosomes in alignment as the kinetochore microtubules retract to separate the chromosomes (*193*). It seems that microtubules are limited in their growth length, which is why rounding occurs, allowing microtubules to correctly reach the chromosomes. However, during cell flattening, the microtubules are unable to fully cover the length of the cell and therefore, incorrect chromosome capture occurs (*179*). During cytokinesis, microtubules specify the location for the cleavage furrow by

transporting signals and proteins. **Hence, through disruptions to the nucleus and the cytoskeleton, physical confinement can place significant restrictions on mechanisms regulating the cell cycle and cell division events, which we show here in Chapter 3.**

2.5.4 Metabolism

Recent studies have begun to investigate the role of cancer cell metabolism and energy requirements in confined environments, as metabolic reprogramming is a key change observed in cancer cells. MDA-MB-231 cells in unconfined environments use ATP for a wide variety of cellular functions, but primarily cell growth (*194*). While it is not known exactly what cellular behaviors are altered metabolically in confinement, cellular energy consumption patterns change. In dense collagen matrices, where cells must overcome physical barriers or even remodel to move, cells utilize more energy as compared to cells on aligned collagen matrices, while migrating slower (*195*). Advancing these studies, investigation of MDA-MB-231 collectively invading stands showed that leader cells utilize significant more energy than follower cells as they indent into and remodel the matrix (*196*). However, after sufficient energy depletion, the leader cells can be replaced by a follower cell with a higher energy level. This evidence of collective invasion as a dynamic process controlled by the energetic outputs of the leader and follower cells could support two novel ideas about cell behavior in confinement. First, cells may coordinate their energy outputs as a mechanism for migration in confined environments, and second, that cells may be able to modulate their energy requirements to focus on specific functions in different environments.

2.5.5 Gene and protein expression

Ultimately, the phenotypic changes in cell behavior can usually be traced back to changes in gene and protein expression. Although we touched on this in previous sections, we highlight some findings here. On 2D surfaces, cells are able to control gene expression via spatial control of regulatory proteins (*197*), and studies are investigating if the same effect could be occurring in confinement. Constricted migration increases DNA damage and repair, as shown by an increased amount of γ-H2AX foci and the presence of nuclear blebs (*198*). DNA damage can potentially lead to aberrations in gene expression. HeLa cells exhibit altered gene expression of histones H4 and H3 in response to vertical confinement (*108*). Meanwhile, cancer cells that display high amounts of heterochromatin have a more difficult time entering and migrating through confinement (*89*). In general, deformation of the nucleus can subsequently alter gene expression. For example, force on the nucleus can open nuclear pores to YAP/TAZ entry (*199*).

There are still several key areas that need to be explored in greater detail, in particular, those that link mechanosensing mechanisms and cell behaviors. For example, there are some studies on mechanosensing of confinement (*73*, *200*), and many others investigating the effect of confinement on a particular cell behavior. However, there is still a need to link these two areas in greater depth. Merely knowing the behavior without its mechanism or knowing the mechanism without its impact is typically not enough to significantly improve therapeutic outcomes. Due to the pervasive nature of mechanical confinement *in vivo,* it is critical to understand how and why confinement alters cell behaviors. **Here, we address this gap in knowledge by**

exploring the effects of physically confining forces on cancer cell growth and migration mechanisms in relation to the mechanical state of the cell.

Chapter 3: Physical confinement alters sarcoma cell cycle progression and division[2]

3.1 Introduction

Cell growth and behavior have been shown to be dictated not only by soluble and matrix-bound biochemical cues, but also by the physical microenvironment, which includes factors such as matrix rigidity, shear stress, topography, and confinement (*201*, *202*). Initial studies sought to understand primarily the first three cues, but technical advances in microfabrication techniques and biomaterial synthesis have enabled insights into the impact of physical confinement on cell behavior within the last decade. Tumor cells experience confinement within the primary tumor, due to cell crowding caused by increased growth rates of cancer cells, and during metastasis, as tumor cells circulate through the blood stream within capillaries as small as 5 μm in diameter, intravasate or extravasate into or out of blood vessels, and migrate along anatomic features such as muscle and nerve fibers (*53*, *203*). Intriguingly, molecular mechanisms driving cell behavior can be altered in response to physical confinement. For example, some cell types migrating through three-dimensional physical confinement primarily use mechanisms driven by actomyosin contractility (*59*, *68*, *204*, *205*), but other cell types can employ a migration mechanism based on water permeation through aquaporins (*154*), a nuclear piston-based mechanism for migration in a 3D matrix (*156*), a mechanism based on asymmetric hydraulic pressure where cells can "push"

[2] Adapted from Moriarty, RA and KM Stroka. "Physical confinement alters sarcoma cell cycle progression and division." *Cell Cycle* (2018), 17 (19-20): 2360-2373.

water during migration in microchannels (*206*), and a mechanism whereby the cell's nucleus ruptures to promote squeezing through confined spaces (*207*).

Within confinement, the nucleus has been demonstrated to be the rate limiting step for cell migration (*88*, *208*), where altered nuclear shape and structure might also cause altered nuclear function. Indeed, the nucleus is responsible for regulating cell growth, replication, and ultimately division through various signaling cascades (*209–215*). Nuclear shape throughout cell division is an important regulator of cell cycle progression. The cell and nucleus enlarge during G1 to provide adequate room for DNA synthesis to occur in the nucleus during S stage, and the nucleus prepares for mitosis during G2, where the nucleus controls chromatid formation and correct alignment for daughter cell formation (*216*). The main cytoskeletal elements involved in cell division are microtubules, which control mitotic spindle formation within the nucleus and pull respective chromatin into separate areas of the cell to create identical daughter cells, and cortical actin, which drives cell rounding. During cell division, cell rounding is an important step to allow for proper spindle assembly and positioning and subsequently, correct daughter cell formation (*182*, *184*, *216*).

Given the critical role of nuclear shape and mechanics in cell division, we hypothesized that physical confinement of the cell body, and also the cell's nucleus, would alter cell cycle progression. Indeed, recent reports have shown that confinement in a 3D spheroid alters nucleus geometry and delays cell division (*175*), and that imposing confining forces on cells in the vertical direction impairs mitotic spindle rounding, results in abnormal daughter geometries, and can promote division into more than two progeny (*179*, *180*). Meanwhile, the effects of bi-axial cell confinement

should also be investigated, since intravital microscopy recently revealed that metastatic tumor cells migrate through small (1-30 μm) spaces *in vivo*, including through preexisting longitudinal microtracks in tissues (*15*, *16*). Hence, in this Chapter, we sought to understand the effects of bi-axial physical confinement on cell cycle progression and ultimately, division, using microfabricated devices with microchannels of defined geometry and varying cross-sectional area. Using a sarcoma cell line stably transfected with the fluorescence ubiquitination cell cycle indictor (FUCCI), we could visually distinguish cells between G1 and S/G2/M stages of the cell cycle and found that in the most confining microchannels, progression through the S/G2/M stage (but not G1) was delayed or halted. Together, our results in this Chapter suggest that as tumor cells migrate through physically confining spaces, cell division may either (1) be halted until the cell enters a less restrictive space, or (2) proceed but result in more frequent instances of abnormal division events that could lead to secondary tumor formation.

3.2 Results

3.2.1 Physical confinement decreases sarcoma cell divisions and restricts cleavage furrow angle

Given the physiological role of physical confinement in multiple stages of tumor progression, we first evaluated the effects of bi-axial confinement on the fraction of sarcoma cells that divided over the course of 18 hours, which is significantly longer than the 13-hour cell cycle length of these cells. We used two assays: (1) cells seeded

on fibronectin-coated glass-bottom dishes, which served as a two-dimensional (2D) control (Figure 3.1A), and (2) cells seeded in a microfluidic device containing fibronectin-coated microchannels of 10 μm in height and varying width (3, 6, 10, 20, and 50 μm) (Figure 3.1B). We note that cells in 3 and 6 μm narrow microchannels are 'confined' while cells in 10, 20, and 50 μm wide microchannels are 'unconfined'. A chemotactic gradient was initially set up within the microfluidic device to promote cell migration into the microchannels. After 24 hours, the gradient was removed and replaced with media containing full serum (Figure 3.1B) to reduce cell migration persistence and increase cells' time spent in channels. Cells divided within the microchannels of all widths, as demonstrated by imaging via phase contrast microscopy, with the morphology of cells during division in the widest 50 μm channels resembling that on 2D surfaces (Figure 3.1C). However, the fraction of cells that divided within all microchannel widths was significantly reduced in comparison with the 2D substrates (Figure 3.1D and Appendix Table 1). In addition, the fraction of cells dividing in higher degrees of confinement (3 μm narrow channels) was significantly lower in comparison with wider 10, 20, 50 μm channels (Figure 3.1D and Appendix Table 1).

Taking into account the abnormal cell divisions previously reported in cells that were confined in the z-direction (*179*), we broke down the division events in confinement. Cells in the 3 and 6 μm narrow channels experienced more abnormal division events than cells in the 10, 20, and 50 μm wide, unconfined channels (Figure 3.1E). Cells in the 3 and 6 μm narrow channels showed evidence of a distinct cleavage furrow and two individual daughter cells, but in some cells, the two daughter cells fused

together to create one multi-nucleated cell in the G1 phase (Appendix Movies 1 and 2). Furthermore, both 3 and 6 μm narrow channels contained cells dividing with a distinct cleavage furrow but with two daughter cells that immediately died upon completion of cytokinesis in the channels. In addition, some cells in the 6 μm narrow channels divided into 3 individual daughter cells (Appendix Movie 3). These are all in comparison to cells in the 10, 20, and 50 μm wide, unconfined channels that displayed a majority of normal divisions (Appendix Movie 4) and very few abnormal divisions (Figure 3.1E). Increasing confinement also restricted the angle of division, where cells in 3 and 6 μm narrow, confined channels were forced to divide with a cleavage furrow angle at 90 degrees with respect to the length of the microchannel, while cells in wider channels were free to divide in any direction (Figure 3.1F). Indeed, quantification of these results showed a significantly larger spread of cleavage furrow angles on 2D substrates and in wider microchannels, while cleavage furrow angles in narrower channels were limited to around 90 degrees (Figure 3.1G). Histograms demonstrated a relatively even distribution of all cleavage furrow angles in cells dividing in 2D control experiments, and cleavage furrow angle distributions centered about 90 degrees for cells dividing in microchannels, with the distribution width decreasing with increasing confinement (Figure 3.1H).

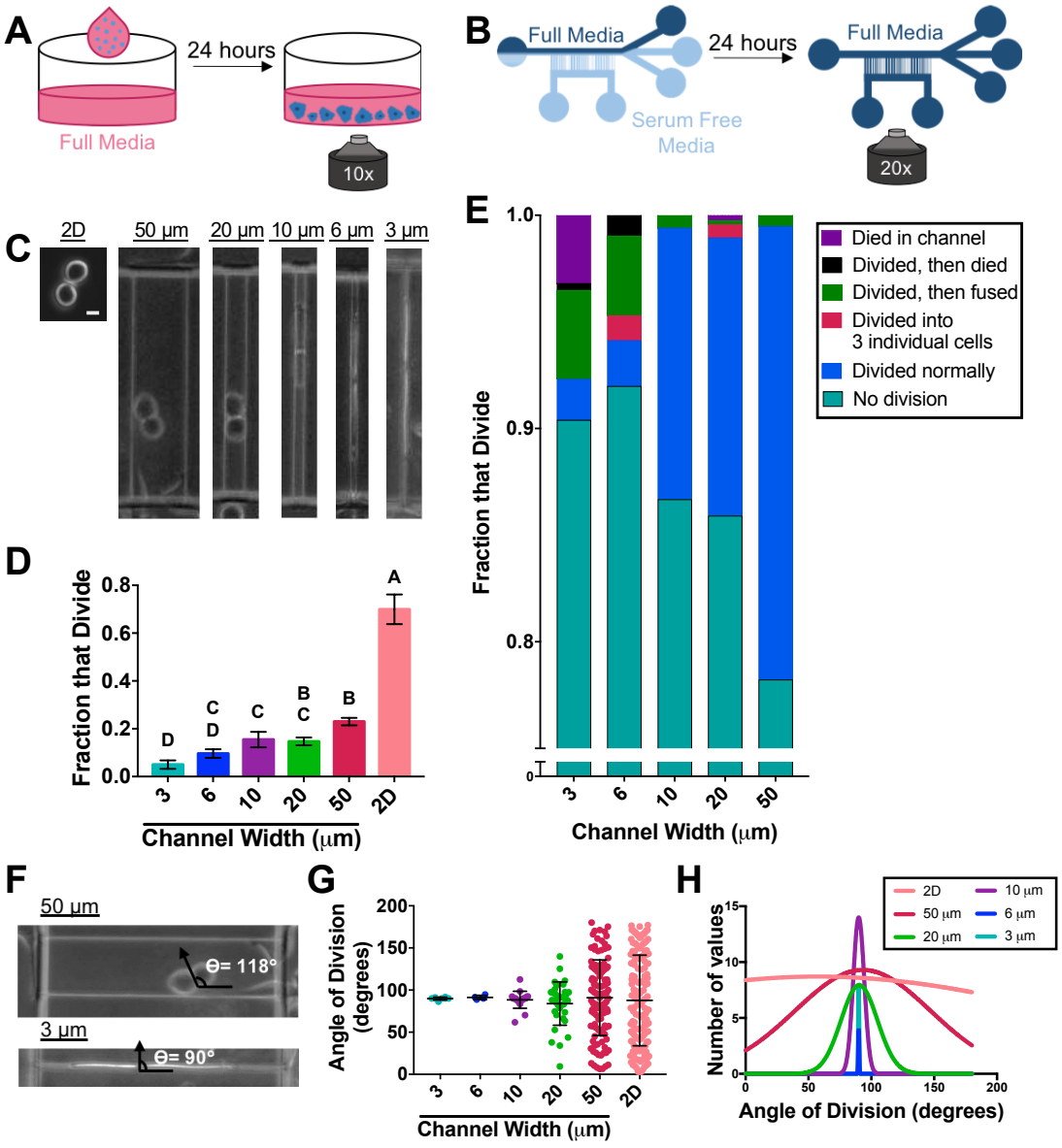

Figure 3.1: Cell divisions decrease in confinement.

Schematic of (A) 2D controls and (B) microchannel confinement devices. (C) Representative phase contrast images of cells dividing on 2D substrates, as well in 50, 20, 10, 6, and 3 µm wide microchannels. Scale bar for image showing 2D control represents 10 µm. (D) Effects of channel width on fraction of cells that divided, including normal and abnormal divisions. Bars that do not share a letter

are statistically different. (E) Breakdown of cell division events in all channel widths. (F) Representative image of quantification method for angle of cell division in 50 μm wide and 3 μm narrow devices, where *x*-axis is parallel to axis of channel. (G) Effect of channel width on angle of cell divisions. Each point represents one cell. (H) Gaussian curve fits to histograms of angle of division. Cell counts and full statistical comparisons for panel D are displayed in Appendix Table 1. Error bars represent standard error (D) and standard deviation (G).

3.2.2 Physical confinement alters cell and nuclear morphology during the cell cycle

We sought to determine why confinement reduced the fraction of sarcoma cells that divided, and we hypothesized that cell and/or nuclear morphology and deformation were playing a role. Taking advantage of the FUCCI system that allows for visual distinction of cells in the G1 versus S/G2/M stage (Figure 3.2A), we further evaluated the effects of confinement on sarcoma cell division. First, we confirmed that cells indeed expressed Cdt1-RFP during the G1 phase of the cell cycle, fluoresced yellow during transition from G1 to S/G2/M (co-expression of RFP and GFP), expressed geminin-GFP during the S/G2/M phase, and turned colorless while undergoing mitosis (Figure 3.2A). Using phase contrast images in conjunction with the FUCCI images, we outlined both the cells and their nuclei (Fig. 2B) and quantified morphology parameters of each, as described in the Materials and Methods section. Cell area (Figure 3.2C) decreased in all degrees of confinement as compared to cells in 2D unconfined controls

(Figure 3.2D and Appendix Table 2). The area of G1 stage cells was mostly similar across channel widths, while the area of S/G2/M stage cells decreased with increasing confinement (Figure 3.2D and Appendix Table 2). Interestingly, cells in the G1 phase had smaller areas than those in the S/G2/M stage, except for the case of the 3 μm narrow channels, where the trend was opposite (Figure 3.2D and Appendix Table 2). We expected cells in the S/G2/M stage to have replicated their DNA content and also enlarged to prepare for mitosis, which is consistent with our results in channels ≥6 μm in width, but the data also suggested that the highest degrees of bi-axial confinement (i.e., 3 μm narrow channels) could have a growth limiting effect on cells preparing for division. Nuclear area (red fluorescence in Figure 3.2C) in the G1 stage was not significantly different across the range of channel widths (Figure 3.2E and Appendix Table 2). Meanwhile, nuclear area in the S/G2/M stage displayed a biphasic trend across channel widths (Figure 3.2E and Appendix Table 2). Similar to cell area, cells in the G1 phase had smaller nuclear areas than those in the S/G2/M stage, except for the case of the 3 μm narrow channels, where the trend was opposite (Figure 3.2E and Appendix Table 2).

We also quantified the cellular aspect ratio (Figure 3.2F), where an aspect ratio of 1 correlated with a highly circular cell, and aspect ratios >1 tended towards more elongated cells. Most notably, the aspect ratio of cells in both G1 and S/G2/M increased as channel width decreased (Figure 3.2G and Appendix Table 2). Nuclear aspect ratio trends also matched those of the cells themselves, where nuclear aspect ratio increased with decreasing channel width (Figure 3.2H and Appendix Table 2). Breaking down nuclear morphology further, we compared the major and minor axis lengths of the

nucleus fit to an ellipse (Figure 3.2I). In both the G1 and S/G2/M stages, the major axis of the nuclear ellipse decreased as channel width increased, while the minor axis increased as channel width increased (Figure 3.2J,K and Appendix Table 3). It seems that once the nucleus becomes confined (3 and 6 μm narrow, confining channels; Figure 3.2B) the cell experiences a growth constraining force that impacts the S/G2/M stage.

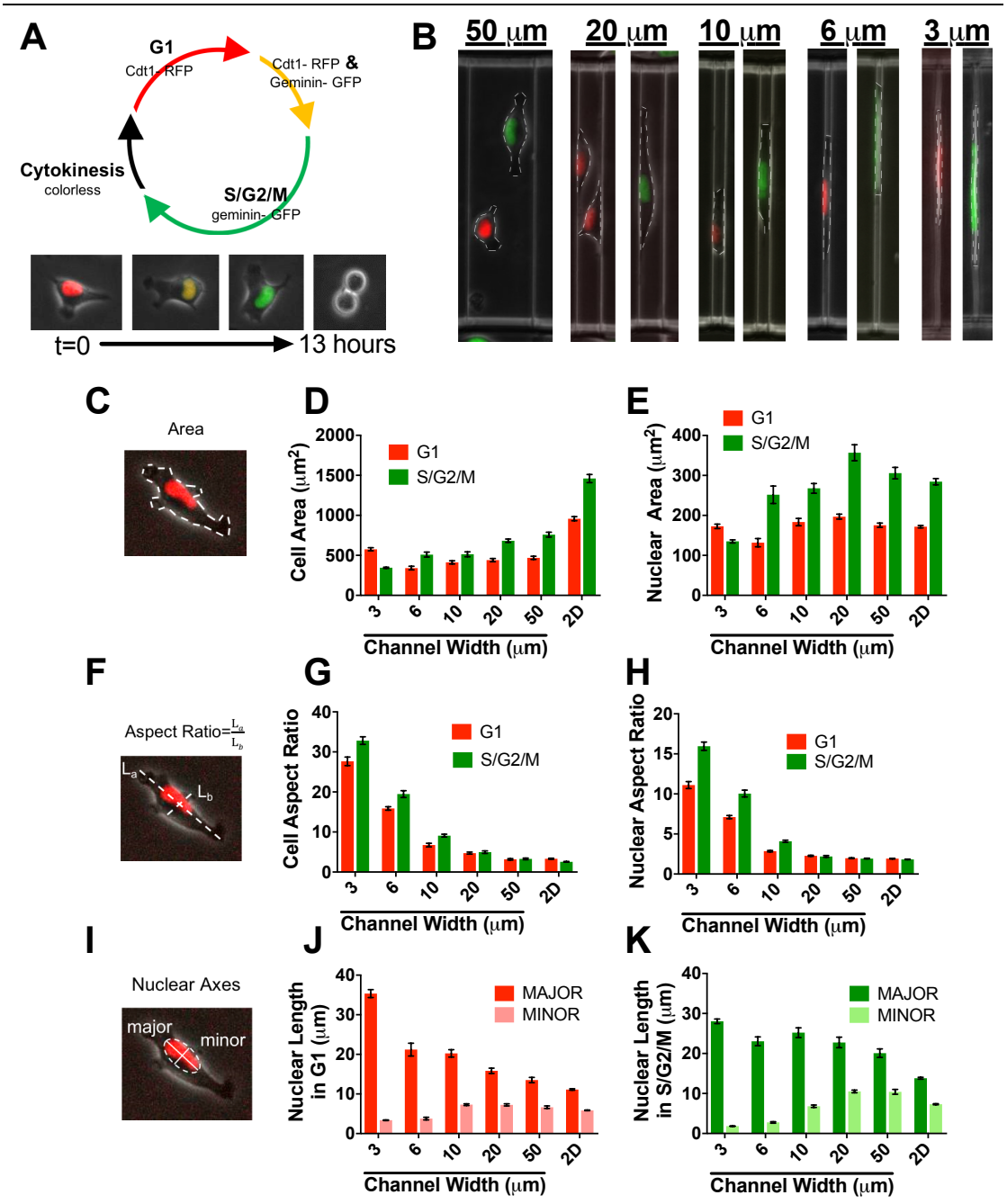

Figure 3.2: Cell and nuclear morphologies are altered in confinement.

(A) Schematic depicting FUCCI reporter construct design and corresponding fluorescent expressions to cell cycle stages. Scale bar for images showing FUCCI progression represents 10 μm. (B) Representative images of cell morphology in various channel widths. Fluorescent images showing FUCCI expression were overlaid on the phase contrast images, and white dotted lines were added to improve visualization of cell outlines. (C) Image demonstrating area calculation. White dotted outline represents manual tracing of cell border, while red fluorescence from FUCCI expression was used to calculate nuclear area. (D) Cell area and (E) nuclear area as a function of channel width. (F) Image demonstrating aspect ratio calculation. (G) Cell aspect ratio and (H) nuclear aspect ratio as function of channel width. (I) Image demonstrating determination of nuclear major and minor length. (J) Major and minor axes of nuclei in G1 stage and (K) S/G2/M stage as a function of channel width. Cell counts and full statistical comparisons are displayed in Appendix Table 2 (for panels D, E, G, and H) and Appendix Table 3 (for panels J and K). Error bars represent standard error.

3.2.3 Physical confinement alters sarcoma cell migration during the cell cycle

Next, we aimed to understand if migration through confinement could be playing a role in the reduced division frequency in confinement, possibly through alteration of time spent in the channels. Previous studies by us and others have shown

that tumor cells display novel mechanisms of migration through confined spaces (*59*, *68*, *154*, *156*, *204–207*), and that there are cell cycle stage dependent differences along 3D collagen fibers (*217*). Using a combination of phase contrast and fluorescence timelapse imaging, we tracked cells migrating through the microchannels in our fabricated devices (Figure 3.3A), and then quantified cell speed (Figure 3.3B) and persistence (Figure 3.3C). For cells in the G1 phase, cell speed in all microchannel widths was significantly greater than cell speed in 2D controls (Figure 3.3B and Appendix Table 4). For cells in the S/G2/M phase, cell speed in wider, unconfined channels (10, 20, 50 μm) was significantly larger than cell speed in 2D controls, while cell speed in narrow channels (3, 6 μm) was not significantly different from 2D controls (Figure 3.3B and Appendix Table 4). Cell speed in G1 and S/G2/M phases generally decreased with increasing confinement, though there was a slight statistically significant biphasic behavior in the G1 phase across channel widths (Figure 3.3B and Appendix Table 4). Interestingly, cells in 2D controls had similar speeds in G1 and S/G2/M phases, while all cells in all microchannel widths were significantly faster in the G1 phase in comparison with the S/G2/M phase (Figure 3.3B and Appendix Table 4). In both G1 and S/G2/M phases, the persistence of migrating cells increased with confinement from 2D controls to 10 μm wide microchannels and then remained the same between 10, 6, and 3 μm narrow, confined channels (Figure 3.3C and Appendix Table 4). Hence, while migration speed was dependent on microchannel width, reduced cell division in narrower channels cannot be attributed to the cells spending less time in the channels, since the cells did not migrate faster in these channels.

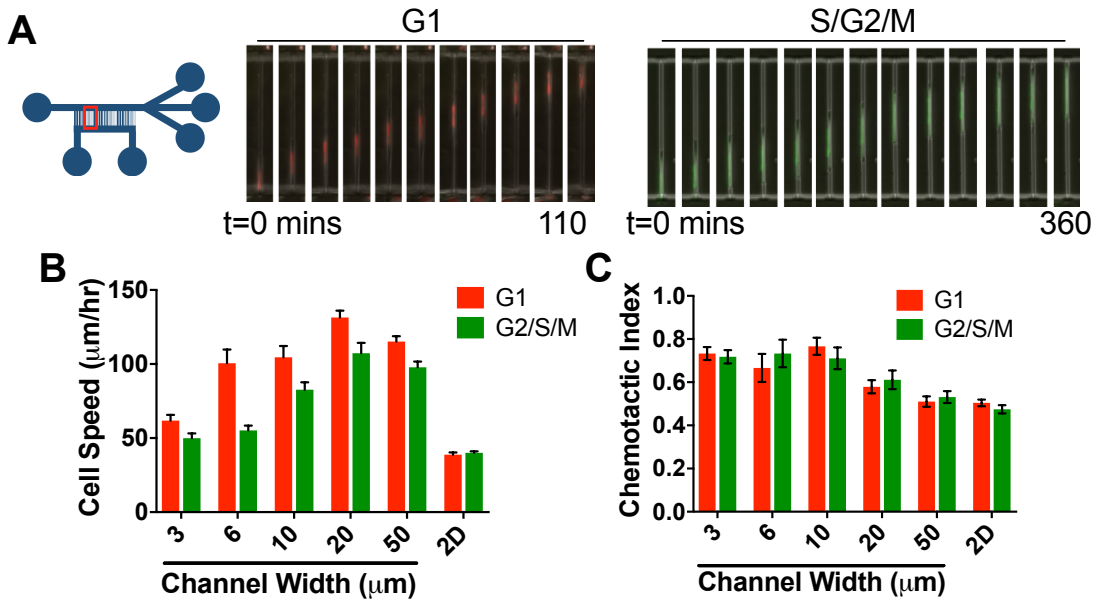

Figure 3.3: Cell migration is altered in confinement.

(A) Representative images of cells in G1 and S/G2/M stages migrating through 6 μm wide channels. (B) Cell speed and (C) persistence as a function of channel width. Cell counts and full statistical comparisons for panels B and C are displayed in Appendix Table 4. Error bars represent standard error.

3.2.4 Confinement increases time spent in the S/G2/M phase of the cell cycle

Considering the results from the morphological and migration analysis, we hypothesized that physical confinement (i.e., 3 and 6 μm narrow channels) impacts the S/G2/M stage of the cell cycle, possibly by preventing cell division or lengthening time spent in S/G2/M. To probe this idea further, we compared the time that cells spent in G1 versus S/G2/M stages of the cell cycle in the varying channel widths. In line with

our hypothesis, the time that cells spent in the G1 stage of the cell cycle was independent of degree of confinement (Figure 3.4A and Appendix Table 5). However, the time that cells spent in the S/G2/M stage drastically increased as channel width decreased (Figure 3.4A and Appendix Table 5). Cells in the 3 and 6 μm narrow channels spent more than double the time in the S/G2/M stage than cells in 10, 20, 50 μm wide channels and cells in 2D controls, with most cells still in the S/G2/M phase by the end of the timelapse experiment. Indeed, within the microchannels, fraction of cell division (from Figure 3.1D) seemed to correlate with the average time cells spent in channels (Fig. 4B). In line with this, the cumulative fraction of cells that successfully transitioned from the G1 to S/G2/M phase was similar across channel widths (Figure 3.4C), while the cumulative fraction of cells that divided decreased with decreasing channel width (Figure 3.4D). Hence, time spent in the G1 phase remained unaffected by confinement, while the S/G2/M stage was primarily affected, thus supporting our hypothesis that confinement decreases the fraction of cells that divide by altering the S/G2/M stage of the cell cycle.

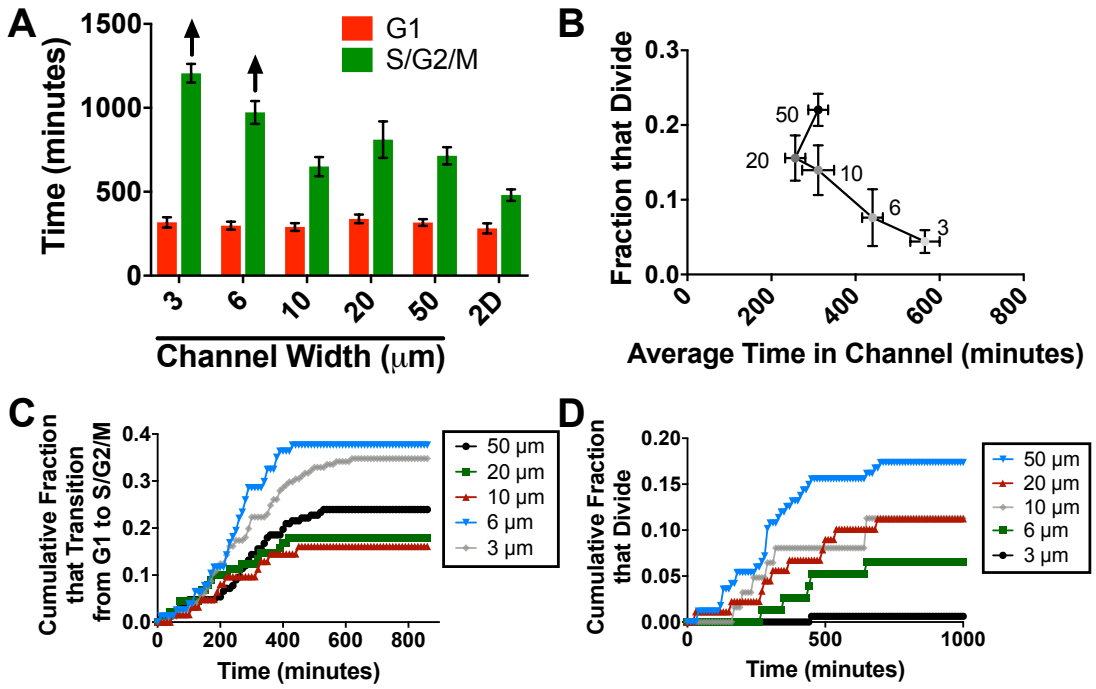

Figure 3.4: Confinement lengthens time spent in S/G2/M, but not G1, stage of cell cycle.

(A) The amount of time that cells spend in G1 stage in confinement as a function of channel width. Upward pointing arrows above bars for 3 and 6 μm narrow channels for S/G2/M stage indicate that the actual values extend longer than the length of the timelapse. The values for the bars shown were calculated using the last frame of the time lapse as the end of the S/G2/M phase and therefore underestimate the actual length of the S/G2/M phase. (B) The fraction of cells that divide (also shown in Fig. 1D) versus the average amount of time that cells spent in various channel widths. Data point labels indicate microchannel width. (C) Cumulative fraction of cells that progress from G1 stage to S/G2/M stage over time for varying channel widths. Only cells that transitioned from G1 to S/G2/M

over the course of the timelapse were counted in the fraction denominator. (D) Cumulative fraction of cells that divide over time for varying channel widths. Only cells that entered the channel over the course of the timelapse were counted in the fraction denominator. Cell counts and full statistical comparisons for panel A are displayed in Appendix Table 5. Error bars represent standard error.

3.2.5 Some effects of confinement disappear upon cell exit from confinement

We sought to understand the degree to which confinement affected cells after they had migrated through the microchannels and returned to an unconfined environment. Therefore, we tracked and analyzed cells in the upper region of the device and compared them to cells in the microchannels (Figure 3.5A). We found that cells post-confinement divided less frequently than cells in 2D unconfined controls, but more frequently than cells in confinement (Figure 3.5B and Appendix Table 6). Cells post-confinement spent similar amounts of time in each stage of the cell cycle as compared to cells in 2D controls (Figure 3.5C and Appendix Table 7), suggesting that the effects of high degrees of confinement in lengthening the S/G2/M phase of the cell cycle were reversed upon exit from confinement. Cells post-confinement were larger than cells in confinement for all microchannel widths and for both stages of the cell cycle but were still smaller on average than cells in the 2D controls for the corresponding cell cycle stage, which could contribute to the reduced divisions post-confinement (Figure 3.5D and Appendix Table 8). Interestingly, nuclear area of cells post-confinement was smaller than that of cells in confinement, and also significantly

smaller than 2D controls for the S/G2/M stage cells (Figure 3.5E and Appendix Table 8). Finally, the cell (Figure 3.5F) and nuclear (Figure 3.5G) aspect ratios, and the cell speed (Figure 3.5H) and persistence (Figure 3.5I) mostly were similar to 2D unconfined control values when the cells were post-confinement (Appendix Tables 8 and 9). Based on these results, it seems that confinement has a transient effect on cell migration and the time regulation of the cell cycle stages. However, traveling through confinement may have a lasting effect on cellular ability to divide and morphological area, at least over a 16-hour time window.

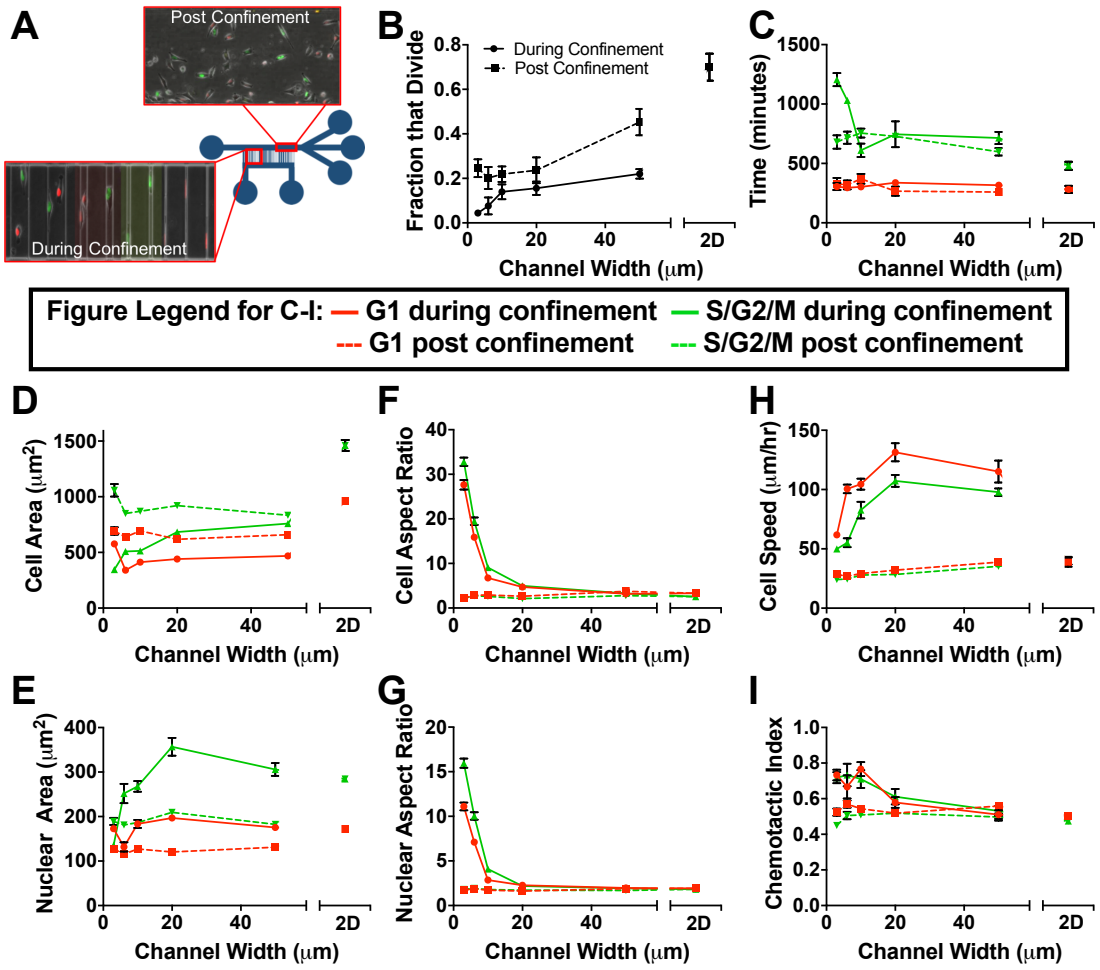

Figure 3.5: Some effects of confinement disappear upon cell exit from confinement.

(A) Representative schematic of cells in confinement versus cells post-confinement. Cells were observed post-confinement for up to 16 hours. Scale bar on post-confinement image represents 20 μm. (B) Comparison of fraction of cells dividing as a function of channel width during and post-confinement. (C) Time spent in G1 and S/G2/M stages of the cell cycle as a function of channel width, during and post-confinement. (D) Cell area and (E) nuclear area as a function of channel width during and post-confinement. (F) Cell aspect ratio and (G) nuclear aspect ratio as a function of channel width during and post-confinement. (H) Cell speed and (I) cell persistence as a function of channel width during and post-confinement. Cell counts and full statistical comparisons are displayed in Appendix Tables 6 (for panel B), Appendix Table 7 (for panel C), Appendix Table 8 (for panels D-G), and Appendix Table 9 (for panels H-I). Error bars represent standard error.

3.3 Discussion

There has been a growing appreciation in the field of cancer metastasis and cell mechanobiology for the role of physical confinement in many aspects of tumor cell behavior, including cell division. Furthermore, it is becoming evident that tumor cells must navigate heterogenous microenvironments during metastasis, including

microchannels that impose bi-axial physical confinement on the cell body and nucleus (*15*, *16*). Hence, in this work, we sought to understand how systematic control of bi-axial confinement in a microchannel device impacts cancer cell cycle progression. Our work, using cells derived from mouse sarcoma tissue in combination with the FUCCI reporter system, indicates that bi-axial physical confinement: (1) reduces frequency of cell division; (2) increases frequency of abnormal division events; (3) constricts the cleavage furrow angle; (4) alters cell and nuclear morphology, with the most confining channels preventing cells from increasing in size in the x-y plane from G1 to S/G2/M during cell cycle progression; (5) alters cell migration speed and persistence; (6) increases time spent in the S/G2/M phase of the cell cycle and/or halts progression through mitosis, and (7) has some lasting effects on cell division and morphology, even after cells have exited confinement.

It has been established for several decades that cancer cell growth occurs mainly on the peripheral outer layers of the tumor (*218*). Circulating tumor cells have the ability to become mitotic during late stage aggressive cancers (*219*), and metastatic tumor cells in the blood stream have been shown to attach to the endothelium and proliferate within the vasculature (*220*). Following extravasation, cancer cells attach to the extravascular side of vessels, flattening themselves out and enlarging, then dividing rapidly (*20*). This literature is in line with our results that less confined cells (outer layers of the tumor) experience more cell division events than those in the interior (higher degrees of confinement). Furthermore, the increased abnormal division events occurring in confinement may be associated with chromosomal abnormalities that are

a hallmark of cancer. It is also worthwhile to note that single multinucleated sarcoma cells have been previously shown to form solid tumors (*181*).

Recent reports have shown that cells undergoing mitosis in 3D collagen matrices maintain a highly elongated shape, and this behavior can be recapitulated in collagen-coated microchannels independent of β1 integrin (*221*, *222*). However, these studies have been limited in their inability to distinguish other stages of the cell cycle or assess beyond the cleavage furrow. Our work supplements these findings, as our primary focus was not M stage but rather the cell cycle as a whole, by demonstrating that confinement imposes morphological and migratory abnormalities at potentially earlier stages than just mitosis. It has also been shown that external forces and uni-axial confinement prevent actin cortex-driven cell rounding, which can lead to incorrect spindle assembly, pole splitting, and delays in mitotic progression (*179*). Furthermore, in some tumor cells, microtubule inhibition results in drastic migratory changes in cells in 3D physically confining microenvironments, as compared to perturbations of integrins, actomyosin, or the Rho/ROCK pathway (*66*, *179*, *223*). Indeed, our previous work has demonstrated that bi-axial confinement promotes a more diffuse actin and microtubule network in cells (*66*, *154*, *224*), and therefore it is possible that these altered cytoskeletal arrangements may improperly position the mitotic spindle, thus preventing division. Along with this, uni-axial confinement has been reported to increase the number of abnormal division events and delay mitotic progression caused by the incorrect spindle machinery assembly. Our work supports the appearance of these abnormal division events in bi-axial confinement as well.

We also found it interesting that the highest degrees of physical confinement resulted in deformation of the nucleus (i.e., in 3 and 6 μm narrow, confined channels), as well as a lack of cell area increase from G1 to S/G2/M (i.e., in 3 μm narrow channels), as compared to wider channels. Nuclear deformation due to mechanical forces can lead to numerous alterations in cells, including restructuring of the lamin A/C network, increased mobility of chromatin, redistribution of biophysical stresses within the cell, as well as time-dependent transcriptional silencing or activation (reviewed in (*225*)). These changes reflect a possible mechanism by which confinement lengthens the later stages of the cell cycle and promotes abnormal division events. It is also possible that there exist cell cycle checkpoints that are tension dependent. Furthermore, the unexpected decrease in x-y projected cell area from G1 to S/G2/M in 3 μm narrow channels lead us to hypothesize that confinement promotes cell volume dysregulation, thus preventing cells from undergoing the normal mitosis-associated increase in cell volume while cell material is replicating.

We have previously shown through experimental and theoretical analysis that tumor cells can utilize aquaporin water channels for migratory mechanisms in confinement (*154*). Similarly, recent theoretical work has shown that active pumping of water and ions at the cell poles can explain cell shape changes during cytokinesis, and that this process can be actomyosin-independent, assuming that the intercellular fluid flow is above a threshold magnitude (*226*). However, they also suggest it is likely that water flux works together with the actomyosin cortex ring and actin cortex to regulate cell shape during division (*226*). We are currently working to understand the effects of aquaporin distribution and water flux on tumor cell cycle progression and

division in confinement, given the striking connection between cell shape, migration, and confinement.

The tumor microenvironment is not spatially or temporally homogeneous, as cells are constantly exposed to varying environments as they move and proliferate. Interestingly, non-neural cells (especially stem cells) display mechanical memory of their exposure to stiffness or fluid flow, and these memory signals can be transmitted bioelectrically, through miRNA, or mechanically through the YAP/TAZ pathway (*43–45*). There can also be epigenetic regulation of bivalent chromatin domains on cancer cells in response to drug re-expression (*42*). In this regard, our results suggest that cells may retain a mechanical memory of physical confinement, thus affecting cell size and ability to divide even after cells leave confinement. Future work could elucidate if this is truly mechanical memory and how, whether epigenetically, or genetically, this memory is imposed, and whether it is temporal or permanent.

Our combination of FUCCI-transfected sarcoma cells and microchannel devices presents several advantages over other *in vitro* systems used to study cell division. First, the device design and fabrication procedure allow us to impose systematic control of bi-axial confinement on cells. Second, the device provides excellent imaging capabilities, both in phase contrast and fluorescence microscopy, given that the bottom surface is a glass coverslip. Hence, we could quantitatively analyze and compare multiple parameters of cell division, cell cycle progression, cell morphology, and cell migration in varying degrees of physical confinement. Third, using a cell line stably transfected with the FUCCI vector allowed us to circumnavigate other hurdles associated with transient transfection, such as loss of FUCCI expression

over the course of the experiments, low transfection efficiency, and possibility for cells to be expressing Cdt1-RFP but not geminin-GFP, or vice versa. We encountered these issues when attempting to create new cell lines with Fisher Scientific's Premo FUCCI Cell Cycle Sensor and BacMam 2.0 delivery system.

We also acknowledge several limitations of our work. First, the microchannel devices were composed of PDMS, which has a stiffness in the MPa range, larger than most physiological tissues which are in the kPa range. However, we note that our goal in this study was to explore the effects of bi-axial confinement, not stiffness, on cell cycle progression. Other labs have recently developed other systems, such as polyacrylamide-based devices, to alter microenvironment stiffness (*204*), and hence future work could explore the interplay between confinement and stiffness on cell cycle progression. Second, this work was carried out on only one cell line that was stably transfected with FUCCI, but ideally, we would have used multiple cell lines to determine whether our results are cell line-dependent or general phenomena. As mentioned above, we attempted to transfect several other cell lines, including MDA-MB-231 and human bone marrow-derived mesenchymal stem cells, with Fisher Scientific's Premo FUCCI Cell Cycle Sensor using the BacMam 2.0 delivery system. However, we experienced extremely low transfection rates of both Cdt1-RFP and geminin-GFP, which would have prevented us from gathering sufficient numbers of cells in the microchannel devices to form meaningful conclusions on those cell lines. Hence, our future work will be aimed at using other FUCCI vectors and delivery systems to create new stable cell lines expressing FUCCI.

Other future work should focus on exploring whether there are specific molecular signaling pathways or processes that prolong the S/G2/M phase in confinement, and whether cell cycle checkpoints are affected, perhaps in a tension-dependent way. We note that we did perform some experiments in which cells were treated with indisulam and RO-3306 (data not shown), previously shown to induce cell cycle arrest in G1 and G2, respectively. On 2D fibronectin coated plates, we observed a near complete cell cycle arrest in the corresponding cell cycle stage. Cells treated with indisulam were morphologically identical to untreated cells in the G1 stage; meanwhile, cells treated with RO-3306 were noticeably larger and more circular than untreated cells in the S/G2/M stage. However, we experienced difficulties seeding the cells into our PDMS microfluidic devices and retaining cell cycle inhibition, which may be due to the absorption of the drug by the surrounding PDMS (*227*).

In summary, we have integrated mouse sarcoma cells stably expressed FUCCI into microfluidic devices that impose bi-axial physical confinement during cell migration in microchannels and shown that confinement reduces frequency of cell division while increasing frequency of abnormal division events, which in other work has been shown to lead to solid tumor formation. Confinement also alters cell and nuclear morphology, with the most confining channels preventing cells from increasing in size from G1 to S/G2/M during cell cycle progression, and with lasting effects even after exit from confinement. Finally, confinement does not seem to affect the G1 phase of the cell cycle, but increases time spent in the S/G2/M phase of the cell cycle and/or halts progression through mitosis. Together, our results suggest that as tumor cells migrate through physically confining spaces, cell division may either (1) be halted until

the cell enters a less restrictive space, or (2) proceed but result in more frequent instances of abnormal division events that could lead to secondary tumor formation. Finally, our results provide new insights into the possible impact of mechanical forces on primary and secondary tumor formation and growth.

3.4 Materials and Methods

3.4.1 Cell culture

S180 mouse sarcoma cells stably transfected with a fluorescent ubiquitin cell cycle indicator (FUCCI) were gifted from Jean Paul Thiery, who is currently at the Cancer Science Institute of Singapore. Cells expressed Cdt1-RFP during the G1 phase of the cell cycle and geminin-GFP during the S/G2/M phase of the cell cycle (Fig. 2A). Cells were grown in medium comprised of Dulbecco's modified Eagle's medium with high glucose (ThermoFisher Scientific) supplemented with 10% heat inactivated fetal bovine serum (ThermoFisher Scientific), and 1% penicillin/streptomycin 1000 U/mL (P/S; ThermoFisher Scientific). Cells were passaged when they reached approximately 90% confluency and passages up to 30 were used in experiments. Cells were washed with phosphate buffered saline (PBS; VWR) and lifted using 0.25% Trypsin-EDTA (ThermoFisher Scientific). All cells were cultured at 37C, 50% humidity, and 5% CO2: 95% air.

3.4.2 Microfluidic device fabrication

Microfluidic devices were fabricated as previously described (*66*, *128*). All fabrication was carried out in the University of Maryland Nanocenter Fabrication Lab. To summarize, two masks were designed in AutoCad (AutoDesk), one with the microchannels, the other with the larger feed lines. A layer of SU-8 3010 negative photoresist (MicroChem) was spincoated onto a silicon wafer (University Wafer). An EVG620 Mask Aligner (EV Group) was used to UV crosslink the SU-8 through the mask containing the microchannel design. The uncrosslinked photoresist was washed away using the SU-8 developer (MicroChem). A second layer of SU-8 3025 negative photoresist was spincoated on the wafer, and the mask containing the feed lines was aligned and the photoresist was UV crosslinked again. Excess SU-8 3025 was dissolved and washed away. Wafers were then silanized using tridecafluoro-1,1,2,2,tetrahydrooctyl-1-trichlorosilane (97%; Pfaltz & Bauer) overnight in a vacuum desiccator. The completed silicon wafer contained microfluidic devices with microchannels of 3, 6, 10, 20, 50 μm in width; all channels were 200 μm in length and 10 μm in height, and the feed lines were 50 μm in height. Polydimethylsiloxane (PDMS, Robert McKeown Company) was mixed at a 10:1 base-to-crosslinker ratio, poured over the silicon wafer, vacuum desiccated for 1 hour, and baked at 85°C for 3 hours. The PDMS was removed from the wafer, cleaned with ethanol and water, dried at 85°C for 5 minutes and then plasma treated for 2.5 minutes. The PDMS devices were then bonded to glass coverslips (which were also cleaned and plasma treated simultaneously with the PDMS) for 5 minutes and the PDMS device-coverslip unit was UV sterilized for 10 minutes. 20 μg/mL fibronectin (ThermoFisher Scientific) was

added to all wells of the device and allowed to adsorb for one hour. The device was then washed with PBS 3 times for 5 minutes each to remove excess protein. Cells were added according to the description in the section below.

3.4.3 Microscopy time lapse experiments

Cells were washed with PBS and then lifted using 0.25% trypsin-EDTA as previously mentioned. Cells were counted using a hemocytometer and resuspended in DMEM containing 1% P/S to give a final concentration of $4x10^5$ cells/mL. Twenty-five μL of the final cell suspension was added to the inlet of the lower feed line and allowed to incubate in the device for 5 minutes. Excess media was removed from the lower feed line inlet and outlet lines and DMEM containing 1% penicillin/streptomycin 1000 U/mL was added to all wells, except for the topmost upper feed line well, which received DMEM containing 1% P/S and 10% FBS to serve as the chemoattractant to encourage cells to migrate through the microchannels. The device was then cultured for 24 hours and then all media was replaced with DMEM containing 1% P/S and 10% FBS in all wells. The device was then imaged on an Olympus IX83 microscope (Olympus) using a 20x objective. For 2D control experiments, we used 24 well glass bottom dishes (Mattek) that were coated with 20 μg/mL fibronectin which was allowed to adsorb for 1 hour, and subsequently they were washed 3 times with PBS for 5 minutes each. Cells were plated on the glass at a concentration of $2x10^5$ cells/mL and allowed to attach and grow for 24 hours before they were imaged on the Olympus IX83 microscope. A chamber adjusted to 37°C, 50% humidity, and 5% CO_2:95% air was used on the microscope stage to sustain cell viability. Images were taken at 10 min

intervals for durations longer than 18 hours. Following overnight timelapse, cells plated on 24 well glass bottom plates were imaged using a 20x objective for morphological analysis.

3.4.4 Data & statistical analysis

All cell and nuclear morphological parameters were manually traced and quantified using ImageJ. Cell and nuclear perimeters were traced to quantify area and aspect ratio (ratio of the width to the length). The outline of the nucleus was fit to an ellipse and the major and minor axes were calculated. Cells were tracked using the Manual Tracking ImageJ plug in and then speed and persistence values were calculated using a custom written Matlab code by KMS. We calculated persistence as the end-to-end distance the cell traveled divided by the total distance. Data for cells was pooled from at least 3 biologically independent trials, comprised of a similar number of cells, and was assumed to be normally distributed. An ANOVA with post-hoc Tukey test was conducted to evaluate significance across all samples, as presented in the Supplementary Tables S1-S9. An individual cell within a single microchannel was noted as N=1. First, this allowed for the heterogeneity within a single cell line population to be factored into the analysis. Second, as each microchannel could have slight differences in shape, introduced during fabrication, or exposure to nutrients due to its position within the device, each cell within was in a unique experimental environment and could be counted as an individual entity. A significance level of 0.05 was used, and error bars represent SEM unless otherwise noted in the figure caption.

3.5 Conclusion

Here, we explored the effects of bi-axial confinement on cell cycle progression given the critical role of nuclear shape and mechanics in cell division and cell cycle progression. Our results demonstrate that bi-axial physical confinement reduces the frequency of cell division, which we found to be attributed to an arrest in the S/G2/M phase of the cell cycle and increases the frequency of abnormal division events. Cell and nuclear morphology were both altered in confinement, with the most confining channels preventing cells from undergoing the normal increase in size from G1 to S/G2/M during cell cycle progression. Finally, our results suggest that confinement induces a mechanical memory to the cells, given our observation of lasting effects on cell division and morphology, even after cells exited confinement. Together, our results provide new insights into the possible impact of mechanical forces on primary and secondary tumor formation and growth.

Chapter 4: Global mRNA translation is spatially altered in confinement and contributes to confined migration

4.1 Introduction

Single cell migration is a hallmark of cancer cells that have undergone EMT and adopted an invasive phenotype (*3*, *228*). This can be partially explained through an induction of actin polymerization, vimentin, and MMP related genes and proteins. In the surrounding tumor stroma, cells encounter an obstacle course of dense ECM and mechanical forces, including, but not limited to, interstitial pressure, confined forces, and fluid shear (*229*, *230*). As cells invade into the stroma, they can remodel their environment through MMP-assisted degradation when they are unable to pass through small pores, or they can migrate using MMP-independent mechanisms, likely through pre-existing microtracks or larger gaps in the matrix (*59*). Cells can rupture their nuclear envelope to fit into small spaces within the ECM, which results in double stranded DNA breaks that persist even after nuclear envelope integrity has been restored (*207*, *231*).

Movement of cells through confined microtracks (1-30 μm in diameter) has been extensively studied (*17*). Cells in confinement can modulate their migration mechanisms, transitioning to an ameboid-based myosin II contractility method or employing a nuclear-piston propeller method that generates pressure gradients through use of the vimentin cytoskeleton (*68*, *156*, *162*, *163*, *232*). Specifically, MDA-MB-231 cells, a triple negative breast cancer line, can migrate in the absence of actomyosin contractility, instead utilizing methods of microtubule-based migration, or can employ

an osmotic engine model, which drives migration through aquaporin mediated water fluxes in and out of the cell (*66*, *154*). As such, cells have a variety of migratory mechanisms to choose from. These above-mentioned studies have shown that while cell migration can be altered due to inhibition of actomyosin contractility, microtubules, or knockdown of aquaporins, results do not show a complete inhibition of migration in confinement. Individual cells are able to employ multiple modes of migration in a single environment (*233*), but currently it is unclear if they utilize these in combination or separately until one is inhibited or no longer favorable.

In traditional 2D migration, extension at the forward edge of the cell is mediated through new actin monomer addition to the growing end of the filament (*234*, *235*). Notably, β-actin mRNA as well as the actin polymerization factor, Arp2/3, localize at the protrusive regions of cells, and technologies to image sites of translation show β-actin translation at these peripheral sites (*236–238*). Integrin binding to the ECM can induce the movement of ribosomes and mRNA sequences to the site of attachment, potentially driving localized translation (*239*). Evidence also shows that *RAB13* mRNA, which encodes a Rab GTPase known to be involved in intracellular transport and actin reorganization, is localized to the protrusive regions of cells and that its active translation is seen at the leading edge (*240*, *241*). Interestingly, the peripheral translation of *RAB13* correlates with different protein associators than *RAB13* that is translated perinuclearly, motivating a functional significance for localized translation (*242*). Inhibiting translation at the protrusions of cells renders the protrusion unstable, and affects forward migration (*243*). This suggests a link between the state of active translation and the ability of the cell to migrate.

Here, we sought to understand the role of global mRNA translation in confined cell migration, specifically in MDA-MB-231 cells that can alter their migration mechanisms within confined environments. Similar to Chapter 3, here we utilized microfluidic microchannels to contrast confined and unconfined environments. We first explored the spatial distribution of newly synthesized proteins in both environments. We showed that newly synthesized proteins become significantly peripherally enriched in confinement. We briefly explored the diffusion limitations of confined microchannels to ensure that these results were not due to experimental constraints. We then probed the relationship between peripheral zones of newly synthesized protein and showed that just a single functional zone of translation is sufficient to facilitate confined migration. This work highlights the role of dynamic, active translation for confined cell migration, and emphasizes the plasticity of cells to adapt their functional mechanisms for diverse environments.

4.2 Results

4.2.1 Newly synthesized proteins accumulate at the extreme peripheral edges of cells in confinement

To explore the spatial orientation of newly synthesized protein accumulation of cells in confinement, we utilized a previous protocol (*244*) aimed to freeze the translating ribosomes and fluorescently tag their localization in the cell. We first treated the cells with cycloheximide to halt translation at the E site within the ribosome

complex and prevent the tRNA from moving along the mRNA sequence, and then followed with puromycin, which attaches to the C-terminal end of the nascent protein (Figure 4.1A). We then probed for the location of puromycin within cells in the microchannels. The cells in the 50 μm wide microchannels displayed a relatively uniform distribution within the cell, with a slightly elevated perinuclear distribution (Figure 4.1B). In contrast, the cells in the 3 μm narrow, confined microchannels display a significant enrichment of puromycin signal at the peripheral edges of the cells (Figure 4.1B). We quantified the intensity of the signal as a function of the horizontal distance along the cell and showed that the cells in the 3 μm narrow microchannels display a significant increase in puromycin signal compared to the 50 μm wide microchannels at the peripheral regions of the cell (Figure 4.1C&D). This is notably similar to the pattern we present later in Figure 5.1, where the accumulation of ribosomal subunit protein RNAs is also significantly enriched at the peripheral edges of the cells in the 3 μm narrow microchannels in comparison to the cells in the 50 μm wide microchannels.

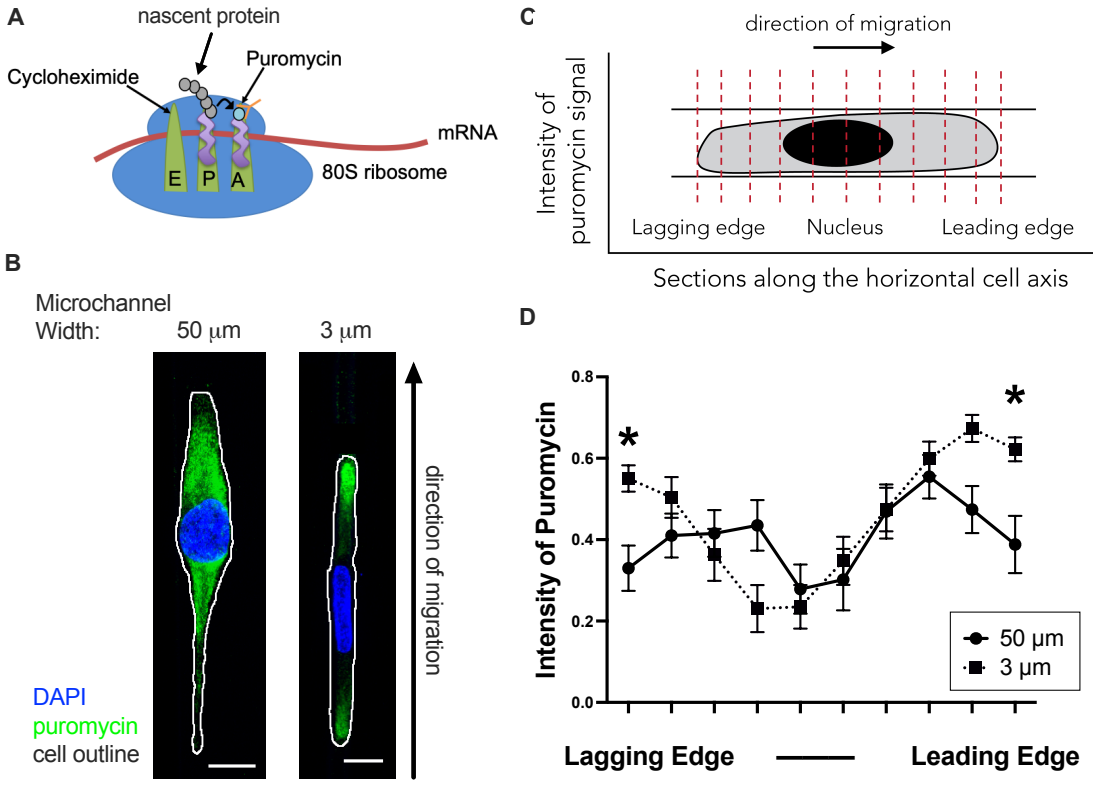

Figure 4.1: Newly synthesized proteins are spatially altered in confinement.

(A) Schematic depicting workflow for imaging translating ribosomes within the cell. (B) Representative immunofluorescent images of puromycin staining in cells in 50 μm wide or 3 μm narrow microchannels. Scale bars: 10 μm.

(C) Schematic showing fractionation of the cell in the direction of migration, from the lagging edge through the nucleus, to the leading edge. The intensity of the puromycin signal was calculated within ten evenly spaced horizontal sections starting and ending at the cell boundaries. (D) Quantification of the intensity of puromycin staining across the horizontal axis of the cells in 50 μm wide and 3 μm narrow microchannels. Data points represent the mean of 22 cells pooled from

two individual experiments. Error bars represent standard error. P value; *<0.05, a two-way ANOVA with Šídák's test was used.

We acknowledge that the cells in the 3 μm narrow microchannels may pose a unique barrier for adequate diffusion of reagents through the cytoplasmic regions. Cells within the 3 μm narrow microchannels occlude the entire volume of the channel (*68*, *128*, *154*). As a result, we explored the relative diffusion limits for antibodies within the 3 μm narrow, confined microchannels. We allowed cells to migrate into the microchannels and then added FITC-dextran (155 kDa) to the microfluidic device inlets and allowed it to diffuse through the channels and into the cells (Figure 4.2A). We chose this molecular weight as it is similar to the size of an IgG primary and secondary antibody. We note that within seconds after addition of FITC-dextran the reagent is at the cell boundary, and also within the cell cytoplasm itself. One hour after addition of FITC-dextran (which mimics the time we treat with a secondary antibody for immunostaining), we see that the overall intensity of the FITC-dextran signal within the cell has increased, but that the relative slope of the intensity signal has not significantly increased (Figure 4.2B). We note that there is a positive slope from the linear regression line in both time points, but there is not a significant difference in points across the trend line. Therefore, we believe the variations in diffusion do not correlate to the striking increase in signal in the newly synthesized protein accumulations seen at the peripheral edges of the cells in the 3 μm narrow microchannels (Figure 4.1B&D). Moving forward, we worked to investigate the functional significance of these peripherally enriched areas of newly synthesized

protein in confinement. As the microchannel devices are uniquely equipped to analyze cell migration, we probed for a link between translation and cell migration in confinement.

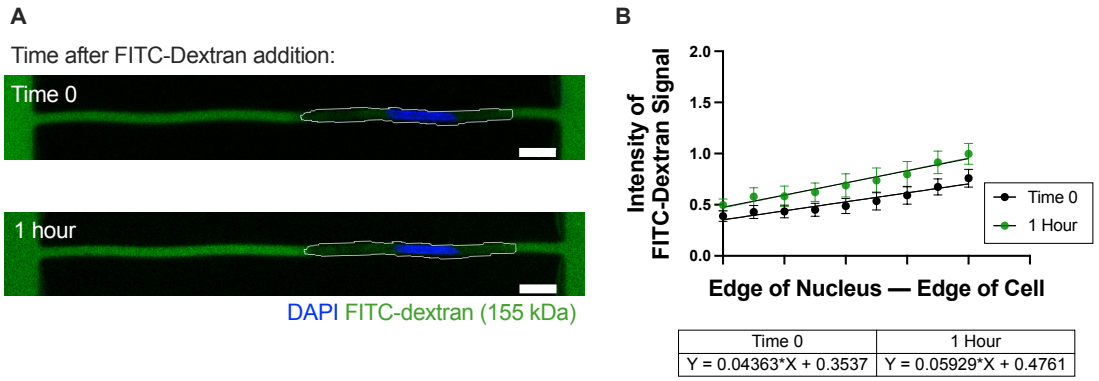

Figure 4.2: Diffusion within the cytosol of cells in microchannels is not significantly limited. (A) Images of cells in 3 μm narrow, confining microchannels after FITC-dextran addition. White line marks the cell outline. Scale bar: 10 μm. (B) Quantification of the intensity of FITC-dextran signal across the cytoplasmic regions of cells in 3 μm narrow, confining microchannels. The front and back regions of the cytoplasm were pooled together from 8 cells over two independent experiments. Error bars represent standard error, and a linear regression model was fit to the data, the equations of the lines are stated below the graph.

4.2.2 Inhibition of translation impacts cell migration in confinement

Previous studies have suggested that there is a preferential accumulation of mitochondria and plus-ends of microtubules to the leading edge of cells in confinement (*66*, *84*). We speculated whether there was a preferential translation of factors in cells

in confinement that accumulated at either edge of the cell. We demonstrated that the nucleus is a large diffusion barrier, where FITC-dextran signal both immediately upon addition and after 1 hour was not able to accumulate within the nuclear region (Figure 4.2A). We investigated how large of a diffusion barrier this presented. As the cells in the 3 μm narrow microchannels occlude the entire volume of the channel, we hypothesized that we could isolate the leading and lagging cytoplasmic regions of the cell if the nucleus truly acts as a restrictive barrier to reagent diffusion. As a result, we treated the cells with two different fluorescent ATTO probes, which tagged the polyA tail of mRNA within the cell, adding one at the leading-edge side, and the other at the lagging edge side (Figure 4.3A). We observed that the cells in the 50 μm wide microchannels, which do not occupy the entire height or width of the channel, did not accumulate either the leading or lagging probe at either side, they were both evenly distributed throughout the cytoplasm of the cell (Figure 4.3B). In contrast, the cells in the 3 μm narrow microchannels displayed a side specific staining and the nucleus acts as barrier to diffusion across the entirety of the cell (Figure 4.3B, (*154*)). This allowed us to test the relationship between translation in confinement and cell migration in a side dependent manner.

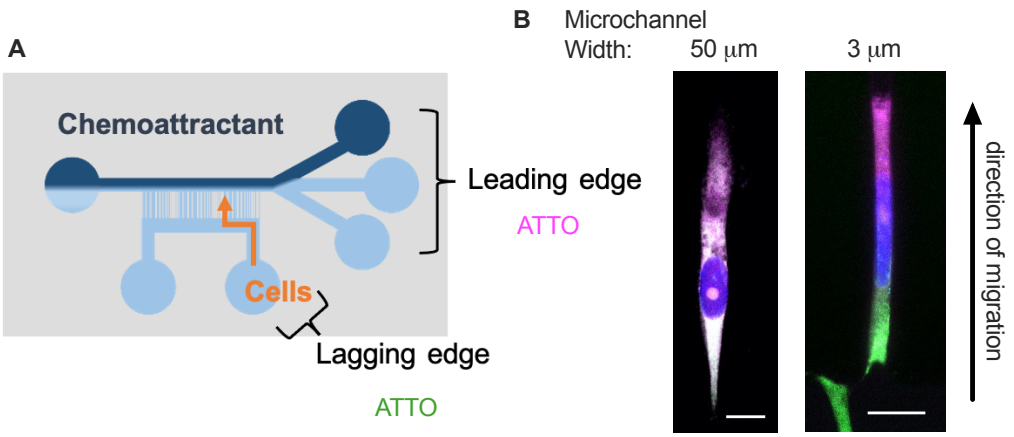

Figure 4.3: The nucleus acts as a diffusion barrier in confinement. (A) Schematic detailing the experimental setup to test the ability of the nucleus to act as a diffusion barrier in confinement. (B) Representative images of cells in 50 μm wide and 3 μm narrow, confining microchannels where magenta ATTO signal was placed at the top of the cell and green ATTO signal was added to the wells at the bottom. Scale bar: 10 μm.

We treated cells in both the 50 μm wide and 3 μm narrow microchannels with cycloheximide, a translation inhibitor (Figure 4.4A), and quantified the migratory capability of the cells. We treated cells on both sides, or only on the leading side or the lagging side, which were determined by the location of chemoattractant (Figure 4.4A). Upon treatment on both the leading and lagging sides with cycloheximide, we observed a significant decrease in speed of cells in both the 50 μm wide and the 3 μm narrow microchannels (Figure 4.4B, C). When we treated cells on the leading edge alone with cycloheximide, there was no effect on cell migration in either the 50 μm wide or the 3 μm narrow microchannels (Figure 4.4D, E). Similarly, when we treated the lagging edge of the cells alone, there was no effect on cell speed (Figure 4.4F, G) in either channel. These results suggest that translation on a single side is sufficient for cell migration in confinement, but that global translation does indeed contribute to confined migration.

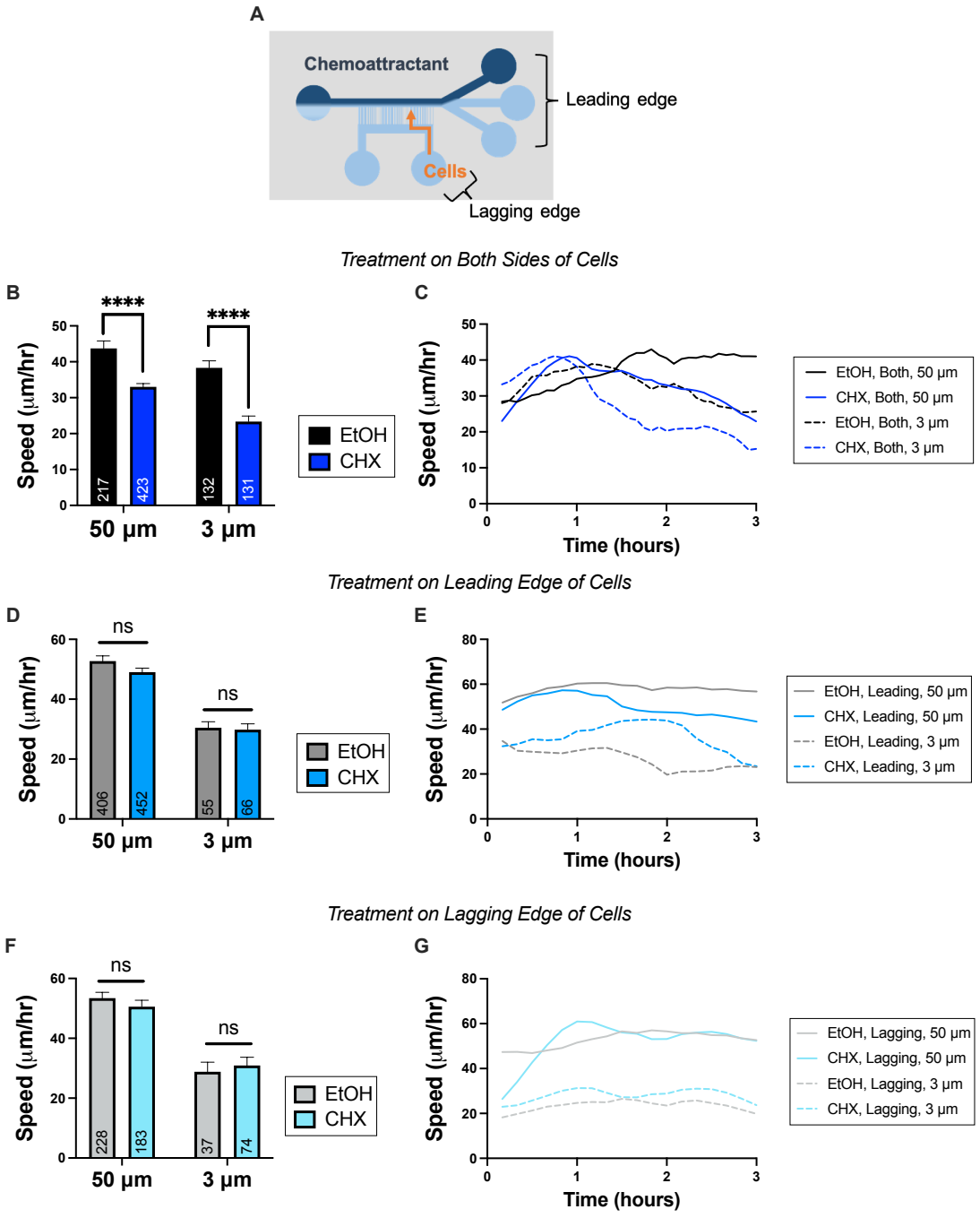

Figure 4.4: Cell migration in confinement is dependent on mRNA translation. (A) Schematic detailing sites of leading or lagging edge location for inhibitor addition. (B and C) Overall speed (B) and average speed over time (C) of cells treated on both the leading and lagging edges with ethanol (vehicle control) or cycloheximide.

(D and E) Overall speed (C) and average speed over time (D) of cells treated with ethanol or cycloheximide at the leading edge only. (F and G) Overall speed (F) and average speed over time (G) of cells treated with ethanol or cycloheximide at the lagging edge only. Numbers in bars (B, D, F) represent individual cells, pooled from three independent experiments. P values **<0.0001, a two-way ANOVA with Šídák's test was used.**

4.2.3 Global inhibition of translation does not affect the directional polarization of the cell

Previous work has identified that MDA-MB-231 are able to migrate in confinement using an osmotic engine model, whereby aquaporin channels are able to directionally pump water into and out of the cell to impart a motion (*154*). In addition, MDA-MB-231 cells are unable to migrate in confinement upon treatment with nocodazole, a microtubule destabilizing agent, and the growing tips of microtubules are primarily localized towards the leading edge of the cell (*66*, *154*). We speculated whether translation is needed in order to assist in establishing a directional polarization in confined cell migration. To test this, we seeded cells into the microchannels and allowed them to infiltrate completely. We then treated the cells either with ethanol as a vehicle control, or with cycloheximide to inhibit translation, and then switched the location of the chemoattractant in order to repolarize the cells to migrate in the opposite direction (*154*). We then quantified the ability of the cells to repolarize and migrate (Figure 4.5A).

Initially, cells migrated with a positive speed and velocity in both the 50 μm wide and 3 μm narrow microchannels (Figure 4.5B, C, black bars). Cells in the 3 μm narrow microchannels migrated with a greater persistence than the cells in the 50 μm wide microchannels, likely due to contact guidance (Figure 4.5D, black bars). After addition of the translation inhibitor and the switch of the chemotactic gradient, the control cells in both the 50 μm wide and 3 μm narrow channels displayed a slower speed, a negative velocity, and a decrease in persistence (Figure 4.5B, C, D, gray bars). In short, a fraction of cells was able to switch direction, but some were also able to continue to migrate on their established path. In comparison, the cycloheximide-treated cells reduced their cell speed further in both the 50 μm wide and the 3 μm narrow microchannels. This is supported by the results above, where broad treatment across both sides of the cell with the translation inhibitor significantly reduced cell speed (Figure 4.4B). However, the cells did not significantly alter their velocity after treatment with cycloheximide compared to the control; in both the wide and the narrow channels, the cells were able to repolarize and migrate in the opposite direction after the chemotactic gradient direction was switched. It is important to note that in the 3 μm narrow microchannels, the cells did move slower and had a less negative velocity compared to the control, but it was not significant in either case. After treatment with cycloheximide and chemotactic gradient switch, cells displayed a further decrease in cell persistence compared to the ethanol treated controls, but only in the 3 μm narrow microchannels (Figure 4.5D, blue bars). Taken together, these results suggest that in confinement, translation functionally contributes to aid in cell migration direction and motion.

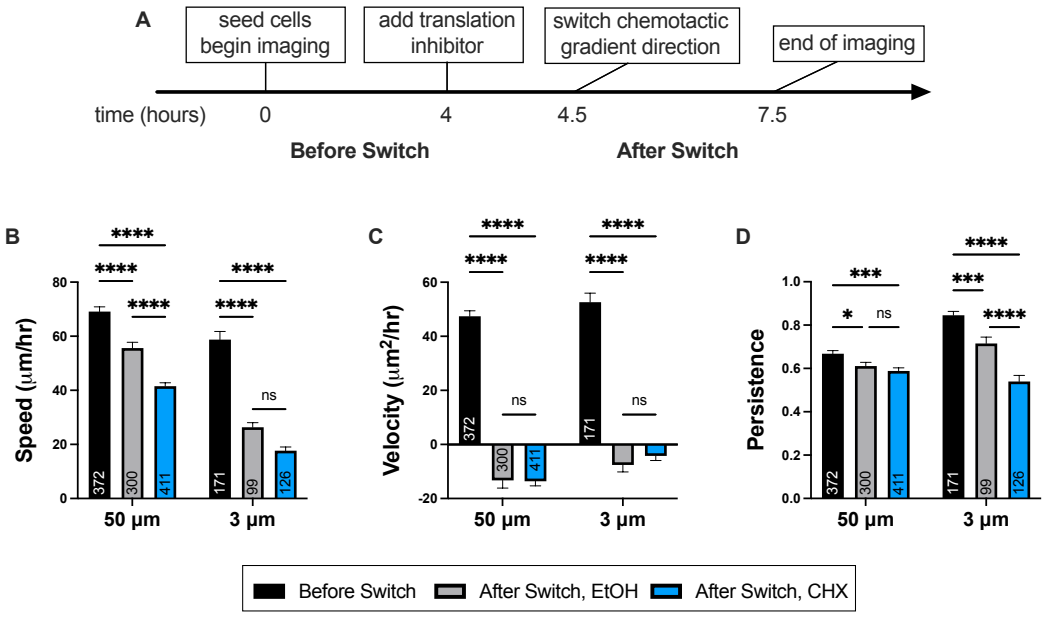

Figure 4.5: Inhibition of translation impacts the direction and persistence of cells migrating in confinement. (A) Schematic showing the workflow of the chemotactic gradient switching experiment. (B, C, and D) Speed (B) and velocity (C) and persistence (D) of cells seeded with chemotactic gradient in the positive direction (blacks bars), which was then subsequently reversed to the negative direction and cells were treated with ethanol (vehicle control, gray bars) or cycloheximide (blue bars). Numbers on bars indicate number of cells for each condition, pooled from three individual experiments. P values, *<0.05, *<0.001, ****<0.0001, a two-way ANOVA with Šídák's test was used.**

4.2.4 A novel confining device to collect RNA and protein from cells in confinement

At this point, we wanted to collect cells in confined microchannels for analysis of the translatome and proteome to explore what mRNA sequences could be

contributing to confined cell migration. However, the microfluidic microchannel device that we have used to this point presented several constraints. First, there were cells present in the seeding regions that are unconfined, therefore adding lysis buffer to the device would inherently mix the unconfined and confined cell populations. To work around this, we could remove the cells by trypsinization. However, to ensure that all cells were out of the seeding regions, we would likely need to incubate for a sustained period where the enzyme would also be able to diffuse or flow into the microchannels, potentially altering any membrane proteins or the entirety of the cells themselves. Second, we are only able to confine ~100 cells in each microchannel device, which is not on the order of a cell lysis concentration for sensitive analyses. As a result, we redesigned our microchannel device to isolate confined cell acquisition and generate a high cell yield.

We took advantage of the well-established and characterized transwell culture system that introduces an insert onto a cell culture plate well (Figure 4.6A). This insert acts a barrier between the fluid and cells in the upper unit, and the fluid and cells in the lower unit. The barrier, or filter, of the transwell can then be modified to allow for cells or fluid to migrate or flow in between the compartments based on the size of the pores. Commercially available membranes range in pore size from 0.4 μm to 8 μm, however, they are only 10 μm tall, therefore, they would not be sufficient for whole cell confinement. As a result, we opted to design a novel 3-D printed confinement device that would modify the transwell membrane to be 100-200 μm tall and contain the rectangular dimensions of our microchannels (30 μm^2 or 500 μm^2 in cross-sectional area) (Figure 4.5A). We could then seed cells into the top of the insert and encourage

them to move through the unconfined or confined pores by the addition of a chemoattractant to the lower compartment. As the cells would be completely confined within the microchannel pores, we could scrape the remaining unconfined cells off the top or bottom of the membrane and then isolate the cells within the pores for RNA and protein analysis.

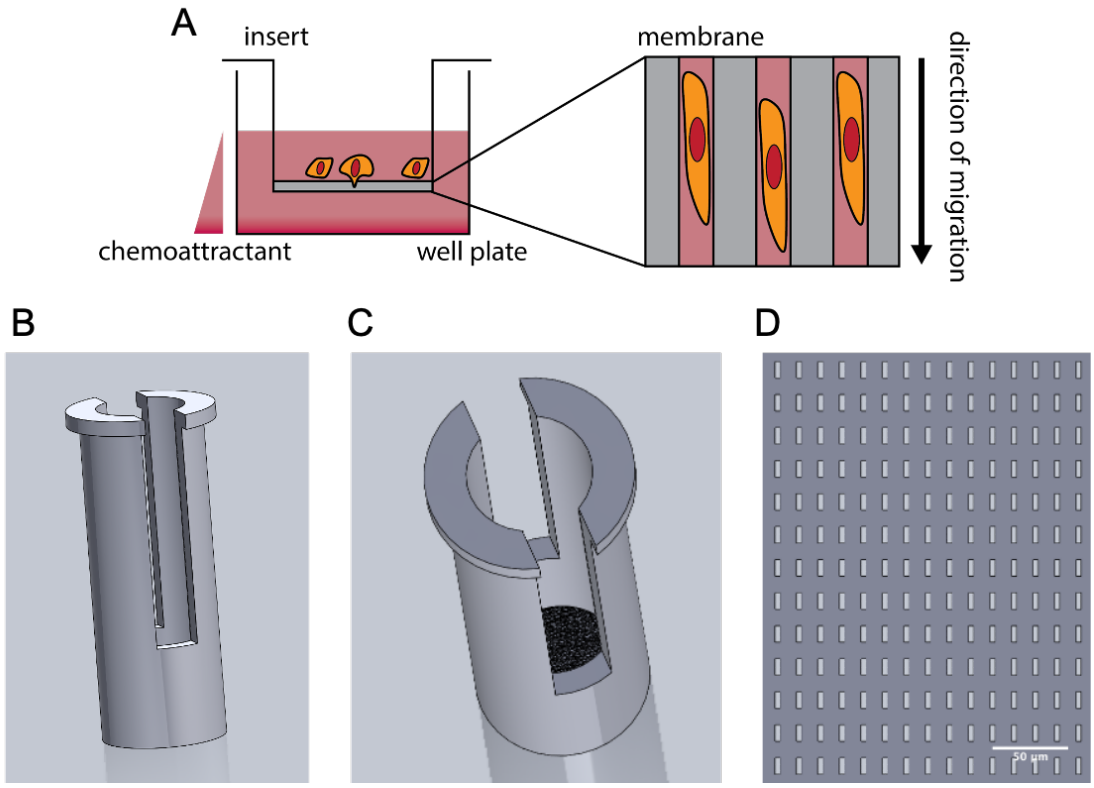

Figure 4.6: A novel 3-D printed microchannel transwell device to increase cell yield and isolate confined cells.

(A) Schematic depicting application of transwell filter, showing location of cell seeding in upper insert compartment and cells encouraged to invade into the membrane through the addition of a chemoattractant in the bottom well. Cells will subsequently become confined within the membrane.

(B, C) Auto-CAD renderings of transwell insert design. Height and width of device will depend on well-plate size but will be identical to commercial sizes. (D) A 100-200 μm thick membrane will be printed on to the bottom of the insert containing pores of 30 μm^2 or 500 μm^2 to mimic microfluidic microchannel devices. Scale bar: 50 μm.

The advantages to using this system are that it is customizable, the size of the membrane diameter (and accordingly, cell seeding number) can be easily modified, and the cells within the confined microchannel pores can be isolated without mixing with the unconfined cells. The only constraint is the volume capability of the 3-D printer, but it is larger than our calculations for a 6-well plate transwell insert. At this point, we are in touch with the Nanoscribe printing personnel through TerrapinWorks to print our device renderings (Figure 4.6B-D). Upon successful completion of the print, we would need to confirm that cells are able to infiltrate into the device, to which we will stain for cell membrane and the nucleus and image in z-slices from the bottom to the top of the device. We will also need to confirm that the removal of the cells from the top and bottom of the microchannel pore membrane is sufficient. Following successful validation of our novel 3-D printed microchannel transwell device, we will collect RNA and protein from the MDA-MB-231 cells in confined and unconfined microchannel pores to study the differences between the two. This global analysis of the translatome and proteome of cells in confinement will provide information on how cells in confinement are able to modulate their migratory mechanisms through upregulation or suppression of mRNA transcripts and proteins involved in various pathways.

4.3 Discussion

An active field of research is aimed at developing new 'migrastatics' or drugs that target cancer cell migration and invasion as this metastatic process is the primary cause of cancer related deaths (*245*). There are several candidates that target the contractility pathway, including actin destabilizers, myosin inhibitors, or kinase inhibitors. However, as cells in confinement can employ contractility-independent modes of migration, there exists a gap in targeted compounds or therapies. Here, we sought to understand the role of global mRNA translation in confined cell migration, specifically in cells that do not utilize contractility mechanisms to migrate. We show that there is a striking accumulation of newly synthesized protein accumulation at the peripheral edges of cells in confinement. We further demonstrate that these zones of active translation are critical in unconfined and confined migration.

In general, cancer cells alter their translatome as a result of the genetic changes that occur. Cancer cells exist in a state of hyperactive translation, and have altered their energy processes to meet the energy requirements (*246*). It is well established that protein synthesis is one of the main energy consumers of the cell, using approximately 30% of the total energy created (*247*). In line with this result, recent studies have shown that cells alter their metabolic consumption when moving through collagen matrices of varying orientations and densities; cells in denser matrices used more energy to promote migration which was slower than cells in aligned matrices that used less energy to move faster (*195*). In addition, during collective invasion, leader and follower cells dynamically rearrange once the leader cells' ATP/ADP ratio falls below a critical

threshold (*196*). Therefore, cells in a restrictive, confined environment may utilize more energy for the purposes of migration and prioritize protein synthesis of key migratory proteins.

Ribosomes translate RNAs to become proteins. They are traditionally assembled in the nucleolus, which is the site of ribosomal RNA synthesis. Interestingly, the nucleolus can have very dramatic responses to stress. Stresses such as ultraviolet light, hypoxia, heat shock, chemotherapeutic agents, and starvation can lead to morphological changes in the nucleolus, shuttling a number of its components out into the nucleus (*248*). As confinement imposes stress on the cell, there may be effects on the nucleolus that impact ribosome biogenesis and their subsequent function. The location of ribosomes can also vary within the cell, where ribosomal subunits are found in the protrusive regions of many cell types ((*240*, *243*, *249*), Figure 5.1). Interestingly, various ribosomal subunit protein RNAs can be transported to protrusions in MDA-MB-231 cells specifically via LARP6, an actin binding protein that is upregulated after EMT (*250*). This could suggest that a potential effect of tumorigenesis may be the sustained or increased localization of ribosomal subunit proteins to peripheral regions of cells and begs the question of what the function of peripheral ribosomal subunits is.

Mechanical forces can impact gene transcription and mRNA translation, affecting protein expression. In cancer cells, hypoxia can alter gene transcription through numerous factors, including the hypoxia inducing factor (HIF) itself (*251*), or through various splicing mechanisms. Mechanical forces are directly involved in protein synthesis, especially in protein folding (*252*). Ribosomes utilize mechanical forces to initiate translation, to unwind secondary structures in the mRNA sequences,

and during co-translational folding of the nascent polypeptide chain. Eukaryotic translation elongation factors 1A and 5A can associate with the actin cytoskeleton and have been known to associated with the β-actin mRNA at sites of integrin attachment. Actin depolymerization can lead to a decrease in protein translation, through inhibition of eukaryotic initiation factor. As mechanical forces can impact the cytoskeleton in confinement, it seems likely that translation may be altered as well.

Numerous studies have analyzed the proteome of cells migrating in 2D substrates, or even in 3D matrices. However, within 3D matrices there are numerous mechanical factors at play, so isolating the effect of singular forces on the proteome changes remains a challenge. Recently published data introduces the first attempt to quantify protein expression in confined microchannels, and suggests that confined migration can induce chemotherapeutic resistance due to increased protein expression of drug-efflux transporters such as ABCG2, MDR1, and nucleoporin-62 (NUP62) (*253*). In addition, cells in confinement also upregulate cancer stem cell-like properties such as CD133, aldehyde dehydrogenase (ALDH). Interestingly, these proposed alterations in a confined cell proteome, specifically ABCG2, ALDH, and CD133 were elevated in MDA-MB-231 cells post-confinement for four days. To drive increased transporter expression, there should likely be increased *ABCG2, ALDH* mRNA sequences within confinement. This suggests that the translatome in confinement is altered in accordance with signaling changes. In addition, vimentin expression increases in confinement and can be utilized in the nuclear-piston method to pull the nucleus. In contrast, other reports demonstrate that vimentin hinders migration in small spaces, emphasizing the need to untangle these effects (*254*).

In summary, our work demonstrates that cells in confinement peripherally enrich zones of translation with functional roles in cell migration, where one active zone is sufficient to direct confined cell migration. Future research direction could be focused on understanding what specific mRNA sequences are translated in confinement and how they contribute to migration. Future work should also target adding to the growing literature detailing altered proteomes and translatomes in mechanically active environments.

4.4 Materials and Methods

4.4.1 Cell culture

MDA-MB-231 cells (ATCC) were cultured in Leibovitz's L-15 medium (ThermoFisher Scientific) supplemented with 10% fetal bovine serum (ThermoFisher Scientific) and 1% Penicillin/Streptomycin (1000 U/mL; ThermoFisher Scientific) in a 37°C incubator with 50% humidity and 0% CO_2.

4.4.2 Microfluidic device fabrication

Microfluidic devices were fabricated as previously described and summarized here in Chapter 3.4.2. Twenty μg/mL collagen type I (Sigma) was added to all wells of the microfluidic device and allowed to adsorb for 1 hour at 37°C or overnight at 4°C. All wells were washed 3 times with PBS for 5 minutes each. Cells were trypsinized for 5 minutes and centrifuged. $2x10^4$ cells were resuspended in 25 μL of serum free media (basal media supplemented with 1% Pen/Step), added to the bottom inlet, and allowed

to incubate for 5 minutes at 37°C. Any remaining cell media was removed, and serum-free media was added to the bottom three inlets, while FBS-containing media was added to the top inlet to act as the chemoattractant.

4.1.3 Immunofluorescent staining of newly synthesized protein

Cells were allowed to enter the channels for at least 3 hours. Media was replaced with serum free or serum containing media supplemented with 100 μg/mL cycloheximide or 9.4 μM anisomycin. Devices were then incubated at 37°C for 15 minutes. Media was then replaced with serum free or serum containing media supplemented with 100 μg/mL puromyocin. Devices were then incubated for 7 minutes at 37°C. Cells were then permeabilized on ice for 2 minutes with a solution containing 50 mM Tris-Cl pH 7.5, 5 mM $MgCl_2$, 25 mM KCl, 100 μg/mL cycloheximide, 0.15 mg/mL digitonin, 1X EDTA-free protease inhibitors, and 0.5 U/μL RNAse inhibitor. Cells were rinsed with permeabilization buffer twice more and then fixed in 4% paraformaldehyde for 20 minutes and stored in PBS overnight at 4°C. Cells were then blocked for 30 minutes with a blocking buffer solution consisting of 0.05% saponin, 10 mM glycine, and 5% goat serum in PBS. Puromycin primary antibody (Kerafast) was diluted to 1:500 final concentration in blocking buffer and allowed to incubate on the cells overnight at 4°C. Devices were then washed three times in PBS for 5 minutes each and then incubated with secondary antibody (1:500, ThermoFisher Scientific). Cells were stained with DAPI and then imaged.

4.4.4 Diffusion experiments

Cells were seeded into the channels and allowed to migrate for 3 hours. Cells were then fixed and permeabilized with 0.3% Triton X (Sigma) for 5 minutes. The device was then placed on a Leica SP8 confocal microscope (with a HC PL APO 63X oil CS2 objective) and imaged for a pre-stained background value. FITC-dextran (0.6 μg/mL) was then added into the device and images were taken one hour after addition of the molecule.

4.4.5 Inhibitor treatment and timelapse imaging

Cells were seeded into the device and then media was replaced with serum-free or serum-containing media with cycloheximide or DMSO. For treatment on both sides of the cell, all inlet wells received media with 100 μg/mL cycloheximide. For treatment on the leading edge only, cells in the top three inlet wells were treated with serum-free or serum-containing media supplemented with 133 μg/mL cycloheximide. For treatment on the lagging edge only, only the bottom inlet well received serum-free media containing 400 μg/mL cycloheximide. This ensured that all cells received 20 μg of cycloheximide in total. Devices were then placed onto an Olympus IX83 inverted light microscope (LUCPlan FLN 20X phase objective) with an environmental chamber to maintain appropriate culture conditions. Images were taken every 5 minutes for 3 hours.

4.4.7 Quantification and statistical analysis

Immunofluorescence images of newly synthesized protein and FITC-dextran intensities were quantified using ImageJ. Cells for migration analysis were tracked using the Manual Tracking ImageJ plugin. Speed, velocity, and persistence values were calculated using a custom MATLAB code by K.M.S. We measure persistence as the stepwise distance divided by the total distance the cell travelled, such that a persistence of 1 reflects a cell that moved in a straight line. All values are represented as mean ± standard error (SEM) and data represents individual cells pooled from similarly sized, biologically independent trials. An individual cell within a single microchannel was noted as N=1. First, this allowed for the heterogeneity within a single cell line population to be factored into the analysis. Second, as each microchannel could have slight differences in shape, introduced during fabrication, or exposure to nutrients due to its position within the device, each cell within was in a unique experimental environment and could be counted as an individual entity. Prism 9 (GraphPad) was used for all statistical analysis; the significance level was set at 0.05. For multiple comparisons, a two-way ANOVA with Šídák's test was performed.

4.5 Conclusion

In summary, we found that MDA-MB-231 cells display a different spatial pattern of newly synthesized proteins in confinement, enriching these tagged sequences at the peripheral edges of the cell in comparison to unconfined cells, where the spatial distribution preferentially accumulates around the nucleus. We ruled out diffusion constraints within the microchannels to explain this peripheral accumulation. We

sought to understand the role of global mRNA translation in confined cell migration and found that active translation is required to specify the direction of migration and the magnitude of movement. We designed a novel 3-D printed transwell device to collect confined cell lysate to study RNA and protein alterations within this environment. Together, this work emphasizes that confined migration is the result of continuous protein synthesis and motivates exploration of the proteome in cells in confinement.

Chapter 5: RNA localization in confined cells depends on cellular mechanical activity and contributes to confined migration[3]

5.1 Introduction

Cell behavior can be influenced by biochemical as well as mechanical cues (*4*, *5*). Among the latter, cancer cells experience mechanical confinement *in vivo* in a multitude of environments during metastasis. For example, as cancer cells migrate out from the primary tumor, they are confined by the surrounding extracellular matrix, comprised of collagen fibers where pore spacing can range from 1-30 μm in diameter (*15*, *16*). Generally, pores below 15 μm in diameter are considered confining because they often require nuclear deformation for cells to fit into and impede MMP-independent cell migration (*59*). Additionally, tumor cells experience confinement as they intravasate, circulate through, and extravasate from the bloodstream, where they can travel through narrow capillaries as small as 3 to 4 μm in diameter (*17*, *18*). Mounting evidence over the past decade has revealed that confinement impacts cell migration mechanisms and phenotypes (*53*, *111*). For example, while traditional haptokinetic actomyosin contractility is often utilized by migrating cells on unconfined 2D substrates, in confinement cells can employ ameboid-based methods relying on myosin II-mediated contractility (*68*, *232*). Other migratory mechanisms in confinement have included (but are certainly not limited to) a nuclear-piston propeller

[3] Adapted from RA Moriarty, S Mili, KM Stroka. "RNA localization in confined cells depends on cellular mechanical activity and contributes to confined migration." Submitted to *iScience* (2021).

method (*156*, *163*), an osmotic engine mode, involving aquaporin mediated water flux (*154*), or a dependence on microtubule dynamics (*66*).

Many RNAs are enriched in protrusive regions of migrating cells (*255*). This spatial accumulation can be controlled through targeting sequences found within the mRNA transcripts (*256*, *257*). These localization elements are thought to direct association with molecular motors such as kinesins or myosins, usually through recognition by specific RNA binding proteins, in order to direct movement along cytoskeletal elements within the cell (*257–259*). RNAs can be targeted to protrusions in different ways. In one pathway, RNAs are directed to peripheral protrusions in association with the kinesin motor KIF1C (*260*). This pathway transports RNAs such as *RAB13* and the *KIF1C* RNA itself. Peripheral localization of these RNAs additionally requires the tumor suppressor protein adenomatous polyposis coli (APC) and stable detyrosinated microtubules (*240*, *249*, *261*). A different pathway, that relies on the RNA-binding protein LARP6, directs RNAs encoding ribosomal proteins to protrusions (*250*). Finally, transport of the β-actin mRNA to protrusions relies on ZBP1 and involves both microtubules and actin filaments as well as different myosins and kinesins, depending on the cell type (*262–264*).

Protrusion localized RNAs are functionally important for cell migration. Indeed, inhibiting translation at protrusions leads to protrusion destabilization (*243*). Furthermore, preventing protrusion localization of specific RNAs impedes the efficiency of cell migration in various 2D *in vitro* models (*242*, *249*, *265*). Localized RNAs of the APC-dependent group are additionally important for collective 3D

invasion of multicellular cancer spheroids, as well as for directing blood vessel morphogenesis *in vivo* (*266*, *267*).

RNA localization at protrusions can be affected by the mechanical properties of the extracellular matrix (ECM) and actomyosin contractility. Mechanical tension at sites of integrin attachment promotes localization of polyadenylated RNAs (*239*). Accumulation of APC-dependent RNAs at the front of collectively invading cell strands requires integrin-mediated contact with the ECM and coincides with areas of high laminin concentration (*266*). Furthermore, stiff substrates promote peripheral localization of APC-dependent RNAs (*249*). Stiff surfaces promote actomyosin contractility, formation of fibrillar actin and focal adhesions (*7*, *268–270*). Actomyosin contractility promotes the formation of detyrosinated microtubules, and consequently APC-dependent RNA localization. The underlying signaling pathway involves the GTPase RhoA and the formin mDia1, factors central in organizing actin and microtubule outgrowth at cell protrusions (*249*, *271–273*). Contractility-dependent localization does not likely apply to all protrusion localized RNAs. Indeed, ribosomal protein mRNAs become preferentially enriched in protrusions that are apparently less contractile, characterized by low levels of active myosin (*249*).

In this study, we sought to understand how RNA localization is controlled by the mechanical cue of confinement. We employed microfluidic microchannel devices to model unconfined and confined environments. We imaged RNAs in two cells lines: (1) the MDA-MB-231 metastatic breast cancer cell line, which can use microtubule-based methods (*66*) and/or an osmotic engine model (*154*) to migrate in confined spaces; and (2) the A375 metastatic melanoma line, which utilizes ameboid-based

myosin II contractility in confinement (*68*). We show that RNA localization patterns change in confinement in a cell type dependent manner. We focused on the APC-dependent *RAB13* RNA, which remains peripherally localized only in confined A375 cells. We show that *RAB13* RNA localization depends on detyrosinated microtubules and the mechanical state of cells. Specifically, the Piezo1 mechanosensitive ion channel and myosin II activity act redundantly to upregulate the detyrosinated tubulin network in confinement, leading to peripheral *RAB13* RNA localization. This mechanism functionally contributes to confined migration of A375 cells. By contrast, confined MDA-MB-231 cells do not exhibit peripheral *RAB13* RNA and do not rely on it for migration in narrow spaces. This work highlights the contribution of peripherally localized RNAs during confined migration. It indicates that different migration modes adopted by cancer cells to navigate through confined spaces variably depend on specific localized mRNAs.

5.2 Results

5.2.1 RNA localization patterns are altered in cells in confined microchannels

To examine the effect of confinement on mRNA localization, we seeded cells into microchannels of two distinct widths, either 50 μm in width by 10 μm in height to represent a relatively wide, unconfined environment, or 3 μm in width by 10 μm in height to represent a narrow, confined environment. The latter requires cells to remodel their nucleus to enter, as the cross-sectional area of this environment is below the 'nuclear limit' (*59*, *207*). We chose to compare two cell lines, MDA-MB-231 and

A375, as they seem to use two separate mechanisms to migrate in confined microchannels (*66*, *68*, *154*). We used fluorescence in situ hybridization to assess the distribution of four different mRNAs, *RAB13* and *KIF1C* (APC-dependent) and *RPL27α* and *RPS20* (APC-independent) in both cell lines (Figure 5.1A&B). To quantify RNA patterns, we measured a peripheral distribution index (PDI) which describes the normalized distance of an RNA population from the centroid of the nucleus (Figure 5.1C; (*274*)). The MDA-MB-231 cells displayed a peripheral RNA enrichment of the two APC-dependent mRNAs in the 50 μm wide microchannels (Figure 5.1D), consistent with previously published data on 2D surfaces (*242*, *243*). Interestingly, for cells in the 3 μm narrow microchannels, the APC-dependent mRNAs had a more perinuclear distribution, resulting in a significantly lower PDI. In contrast to the APC-dependent mRNAs, the APC-independent mRNAs (*RPL27α* and *RPS20*) were less peripheral in unconfined environments (Figure 5.1A&D; (*249*)). However, for cells in the 3 μm narrow microchannels, the APC-independent RNAs were significantly more peripherally enriched. Therefore, distinct mRNA species undergo opposing changes in their distributions as MDA-MB-231 cells enter confinement.

The A375 cells also displayed a peripheral APC-dependent RNA enrichment in the 50 μm wide microchannels (Figure 5.1E), consistent with the broadly observed localization of these RNAs in various cell types (*240–243*, *249*). Interestingly, in contrast to what we observed in MDA-MB-231 cells, A375 cells maintained the same degree of peripheral APC-dependent RNA enrichment in confinement. The APC-independent RNAs exhibited a similar behavior in both cell types with a significantly increased peripheral distribution in the 3 μm narrow microchannels. We believe that

this increased peripheral distribution is the result of specific RNA targeting and cannot be accounted for by non-specific, overall redistribution of the cytoplasmic volume, which we assessed through detection of total polyadenylated (*polyA*) RNA in the same cells (Figure 5.1A-E). Overall, r-protein mRNAs (APC-independent) consistently became more peripheral in confinement, while localization of APC-dependent mRNAs is maintained or not in confinement depending on the cell type.

To assess whether the observed peripheral RNA localization is uniform around the cell or whether it exhibits polarity, we measured an RNA polarization index for each cell, which is defined as the normalized distance between the centroid of the overall RNA signal and the centroid of the cell body (*274*, *275*). In MDA-MB-231 cells, APC-dependent RNAs (*RAB13* and *KIF1C*) exhibited a similar polarization index between 50 μm wide and 3 μm narrow microchannels, while, in contrast, the polarization of these RNAs was significantly increased in confined A375 cells. The APC-independent r-protein mRNAs exhibited an increased polarization upon confinement in both cell types (Figure 5.2A,B). Nevertheless, this type of polarization metric does not allow us to distinguish the particular site of RNA accumulation and its potential correlation with the direction of migration.

Cells in the 3 μm narrow microchannels are linearly confined and their direction of migration is specified by the site of chemoattractant addition (Figure 5.1A&B). Thus, we can segment the cells perpendicular to their direction of migration and measure RNA presence along the lagging to leading edge axis (Figure 5.1F). Interestingly, while r-protein mRNAs showed an increased polarization index in both cell types (Figure 5.2A&B) they did not exhibit a consistent preferential distribution

towards either the leading or lagging edges (Figure 5.2C&D). It therefore appears that r-protein mRNAs polarize either towards the front or the back of individual cells and when averaged across a population of cells the resulting overall distribution lacks a preference for either side. While the implications of this behavior, in the context of ribosome function or translation, might be interesting to explore, we think this observation indicates that peripheral localization of r-protein mRNAs is likely not directly linked to the directionality of cell movement in confined spaces.

On the other hand, the APC-dependent RNAs revealed an interesting directional behavior. In MDA-MB-231 cells, which did not maintain peripheral localization of *RAB13* or *KIF1C* RNAs in confinement (Figure 5.1D), these RNAs also did not preferentially polarize towards the leading or lagging edges (Figure 5.1G). In contrast, in A375 cells, where *RAB13* and *KIF1C* RNAs were peripheral in cells in confinement (Figure 5.1E), they also preferentially accumulated towards the leading edge (Figure 5.1H). Given that localization of APC-dependent RNAs is important in unconfined migration (*242*, *249*), we reasoned that this result might indicate that APC-dependent RNAs have a differential regulation and contribution in confined migration depending on the cell type. We thus focused on the *RAB13* mRNA and sought to understand the mechanism leading to its differential distribution in confined MDA-MB-231 or A375 cells, and to assess its functional role in confined migration of these cell types.

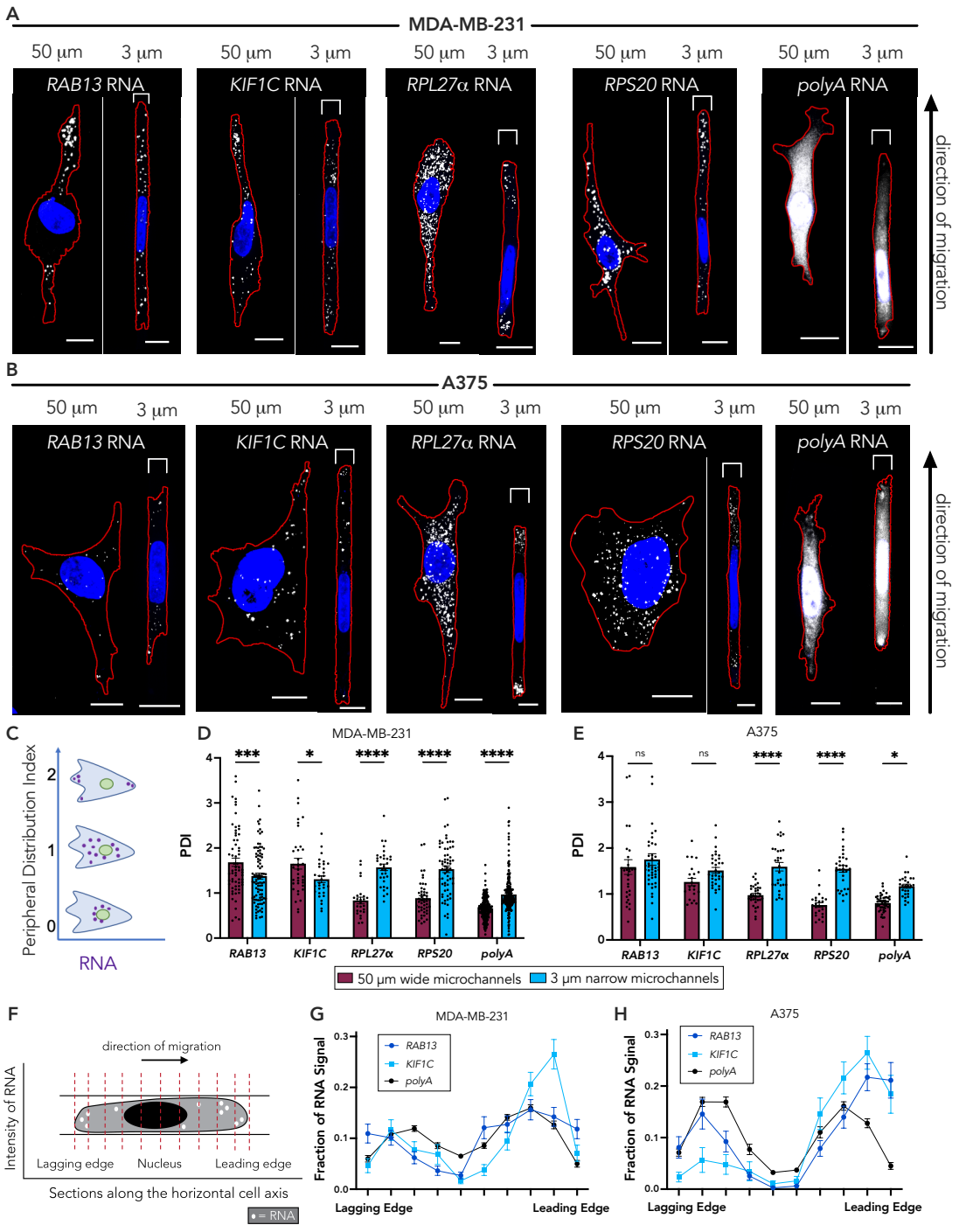

Figure 5.1: RNA localization patterns are altered in a cell type-dependent manner in confinement.

(A and B) Representative FISH images of *RAB13*, *KIF1C*, *RPL27α*, *RPS20*, and *polyA* RNAs in (A) MDA-MB-231 and (B) A375 cells in either 50 μm wide or 3 μm narrow microchannels. RNA signal is shown in white, nucleus in blue, and cell outline in red. Brackets above cells in 3 μm groups denote the microchannel width. The leading edge of the cells (determined by the side of chemoattractant addition) is towards the top of the page.

(C) Schematic showing PDI index values of the indicated hypothetical RNA distributions. A more peripherally enriched RNA exhibits a PDI>1, a diffuse RNA exhibits a PDI=1, and a perinuclear RNA a PDI<1.

(D and E) PDI calculations of *RAB13*, *KIF1C*, *RPL27α*, *RPS20*, and *polyA* RNAs for (D) MDA-MB-231 cells or (E) A375 cells. Dots on graphs in (D and E) represent individual cells pooled from at least three independent experiments. Note that the PDI of *polyA* RNA, which is used as a proxy for the cytosolic volume, is slightly higher in cells in the 3 μm narrow microchannels. This is likely because in confined cells the cytosolic volume is more equally distributed throughout the cell body, while in unconfined cells most of the cytosol is found perinuclearly, leading to higher and lower PDIs, respectively. This difference is not sufficient to account for the more substantial PDI increase observed for r-protein mRNAs in the 3 μm narrow microchannels.

(F) Schematic showing segmentation of the cell in the direction of migration, from the lagging edge through the nucleus, to the leading edge. The intensity of the RNA signal was measured within ten evenly spaced sections starting and ending at the cell boundaries.

(G and H) Quantification of the intensity of APC-dependent RNAs (*RAB13, KIF1C)* compared to *polyA* RNA in (G) MDA-MB-231 and (H) A375 cells along the length of cells in 3 µm narrow microchannels.

Error bars represent standard error. Scale bars: 10 µm. P values represent *<0.05, *<0.001, ****<0.000; two-way ANOVA with Šídák's test.**

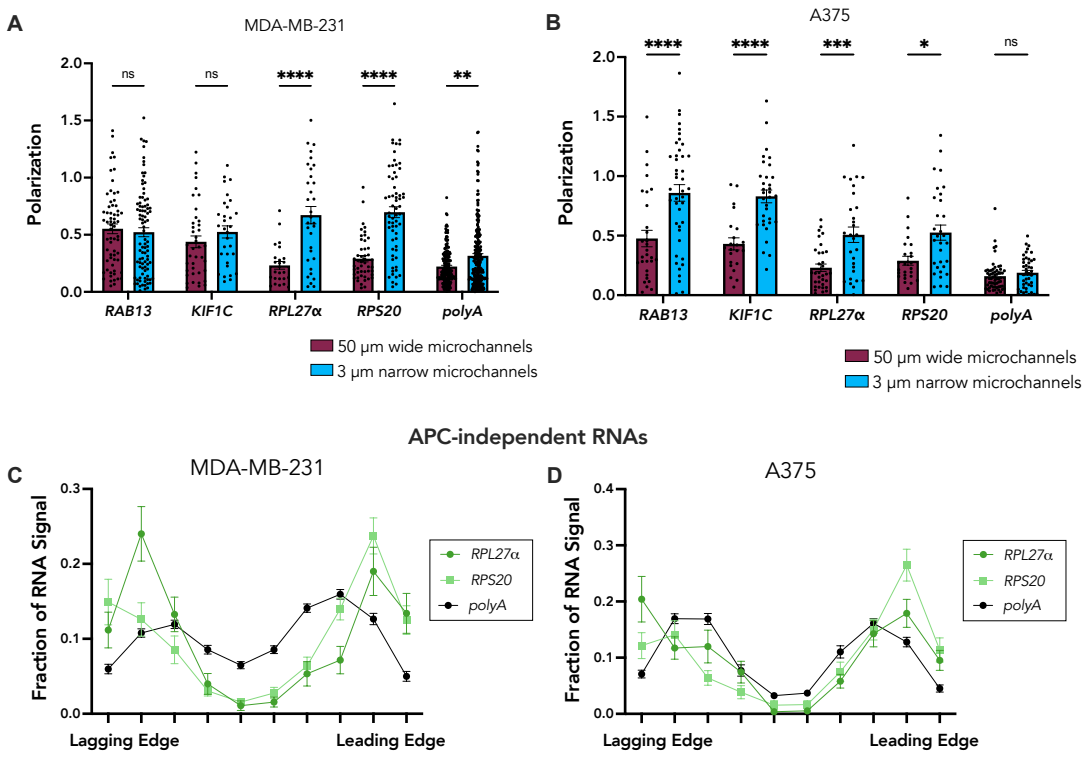

Figure 5.2: RNA polarization metrics are altered in confinement in a cell type dependent manner.

(A and B) Polarization index of *RAB13, KIF1C, RPL27α, RPS20,* and *polyA* RNAs in (A) MDA-MB-231 and (B) A375 cells in 50 µm wide and 3 µm narrow microchannels. Individual dots represent individual cells pooled from at least

three independent experiments. P values; *<0.05, **<0.01, *<0.001, ****<0.0001, a two-way ANOVA with Šídák's test was performed.**

(C and D) Quantification of the intensity of APC-independent RNAs (*RPL27α*, *RPS20)* compared to *polyA* RNA in (C) MDA-MB-231 and (D) A375 cells along the length of cells in 3 μm narrow microchannels. All error bars represent standard error.

5.2.2 Detyrosinated tubulin network drives APC-dependent RNA peripheral localization in confinement

Prior studies have shown that *RAB13* and other APC-dependent RNAs rely on detyrosinated (Glu)-microtubules for their peripheral localization (*240*, *249*, *261*). Detyrosinated (Glu)-microtubules are a subset of stable microtubules that arise upon removal of the C-terminal tyrosine from the tail of the α-tubulin subunit (Figure 5.3A). We therefore hypothesized that differences in APC-dependent RNA distribution between confined MDA-MB-231 and A375 cells could be driven by differences in the Glu-tubulin network. In the 50 μm wide microchannels, there was a fibrillar detyrosinated tubulin and α-tubulin network in both the MDA-MB-231 and A375 cells (Figure 5.3B), consistent with the peripheral RNA localization in both cases. However, in the 3 μm narrow microchannels, the Glu-tubulin network was fragmented and diffuse in the MDA-MB-231 cells, in direct contrast to the A375 cells, which maintained an obvious fibrillar presentation of Glu-tubulin staining (Figure 5.3C). The total α-tubulin network in the 3 μm wide microchannels appeared similar in both cell

lines. Quantification of the detyrosinated tubulin signal indeed showed that MDA-MB-231 cells exhibit a lower Glu-tubulin signal than the A375 cells (Figure 5.3D).

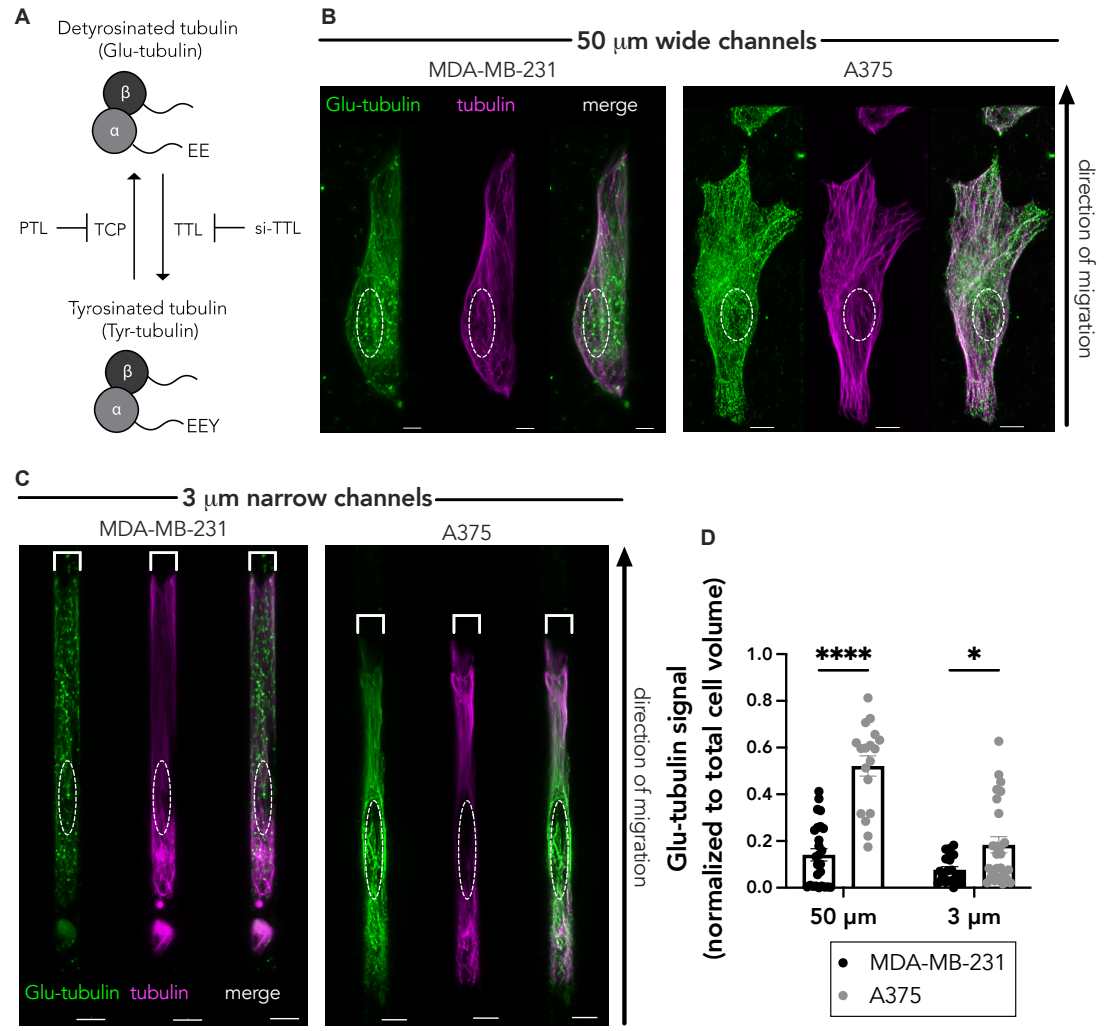

Figure 5.3: MDA-MB-231 cells have less detyrosinated (Glu) tubulin than A375 cells.

(A) Schematic representing the tubulin tyrosination and detyrosination cycle and the enzymes involved. The C-terminal tyrosine of a-tubulin can be removed by a tubulin carboxypeptidase (TCP), an enzyme that can be inhibited by parthenolide

(PTL). The tyrosine can be added back through the action of tubulin tyrosine ligase (TTL), whose expression can be knocked down through targeted siRNA (si-TTL).

(B and C) Representative immunofluorescence images of Glu-tubulin and tubulin in MDA-MB-231 or A375 cells in (B) 50 μm wide microchannels or (C) 3 μm narrow microchannels. White dashed lines indicate positions of nuclei. Scale bars: 5 μm.

(D) Quantification of Glu-tubulin signal volume (after diffuse background signal was thresholded out and normalized to total cell volume) in the indicated cells. Dots represent individual cells pooled from three independent experiments; error bars represent standard error. P values: *<0.05, **<0.000; two-way ANOVA with Šídák's test.**

To directly test whether Glu-tubulin is involved in peripheral RNA localization in cells in confinement, we took advantage of the fact that we can modulate the levels of Glu-tubulin by manipulating the enzymes involved in the α-tubulin tyrosination/detyrosination cycle (Figure 5.3A). Tubulin carbopeptidase (TCP), the enzyme that cleaves the tyrosine at the end of the α-tubulin monomer, can be pharmacologically inhibited with Parthenolide (PTL), leading to a reduction in detyrosinated tubulin (Figure 5.5A&B). Consistent with prior reports for cells on 2D substrates (*249*), in unconfined 50 μm wide microchannels, treatment with parthenolide reduced the peripheral localization of the *RAB13* RNA in both MDA-MB-231 and A375 cells (Figure 5.4A-D). Importantly, in 3 μm narrow microchannels parthenolide

reduced the peripheral *RAB13* localization in A375 cells but did not affect its distribution in MDA-MB-231 cells (Figure 5.4C&D). Therefore, the remaining fibrillar Glu-tubulin network in confined A375 cells is functionally important to support peripheral RNA localization, while the fragmented network seen in MDA-MB-231 cells does not have a determining impact on the already less localized *RAB13* RNA.

To test whether we could rescue Glu-tubulin formation and consequently RNA localization in confined MDA-MB-231 cells, we employed siRNA-mediated knockdown of the tubulin tyrosine ligase (TTL) protein (Fig 5.3A, Figure 5.5C). TTL restores the tyrosine at the end of the Glu-tubulin monomer; therefore, its knockdown can increase the levels of Glu-tubulin. Indeed, treatment of MDA-MB-231 cells with the TTL siRNA led to an increase in the visible fibrillar detyrosinated tubulin network in 3 μm narrow microchannels (Figure 5.5D&E). Importantly, this also led to a significant increase in the *RAB13* PDI in the confined MDA-MB-231 cells (Figure 5.4E&F). Together these data show that detyrosinated microtubules support the peripheral localization of the *RAB13* RNA in confined A375 cells, while the absence of detyrosinated microtubules underlies the reduced *RAB13* localization observed in confined MDA-MB-231 cells.

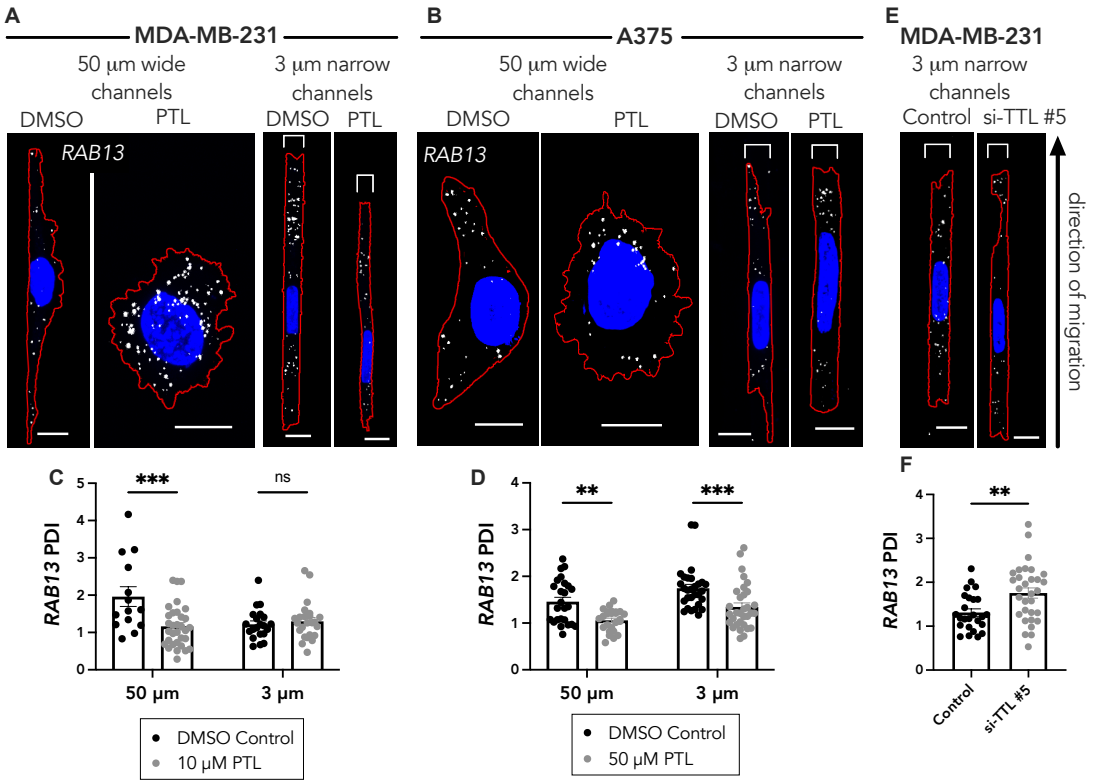

Figure 5.4: Glu-tubulin levels drive *RAB13* RNA localization in cells in confinement.

(A and B) Representative *RAB13* FISH images of (A) MDA-MB-231 cells and (B) A375 cells in 50 µm wide and 3 µm narrow microchannels after 3-hour treatment with DMSO (vehicle control) or Parthenolide (PTL; 10 µM in (A) and 50 µM in (B)). RNA signal is shown in white, nucleus in blue and cell outline in red. Brackets above cells in 3 µm groups denote the microchannel width.

(C and D) PDI calculations of *RAB13* RNA distribution of (C) MDA-MB-231 cells and (D) A375 cells.

(E) Representative *RAB13* FISH images of MDA-MB-231 cells treated with control siRNA or TTL siRNA. (F) PDI calculations of *RAB13* RNA distributions

of MDA-MB-231 cells treated with control or TTL siRNA. Individual dots on graphs in (C, D, and E) represent individual cells pooled from three independent experiments; error bars display standard error. P values, **<0.01, *<0.001 by two-way ANOVA with Šídák's test was performed (in C and D) or by unpaired t-test assuming equal standard deviations (F).**

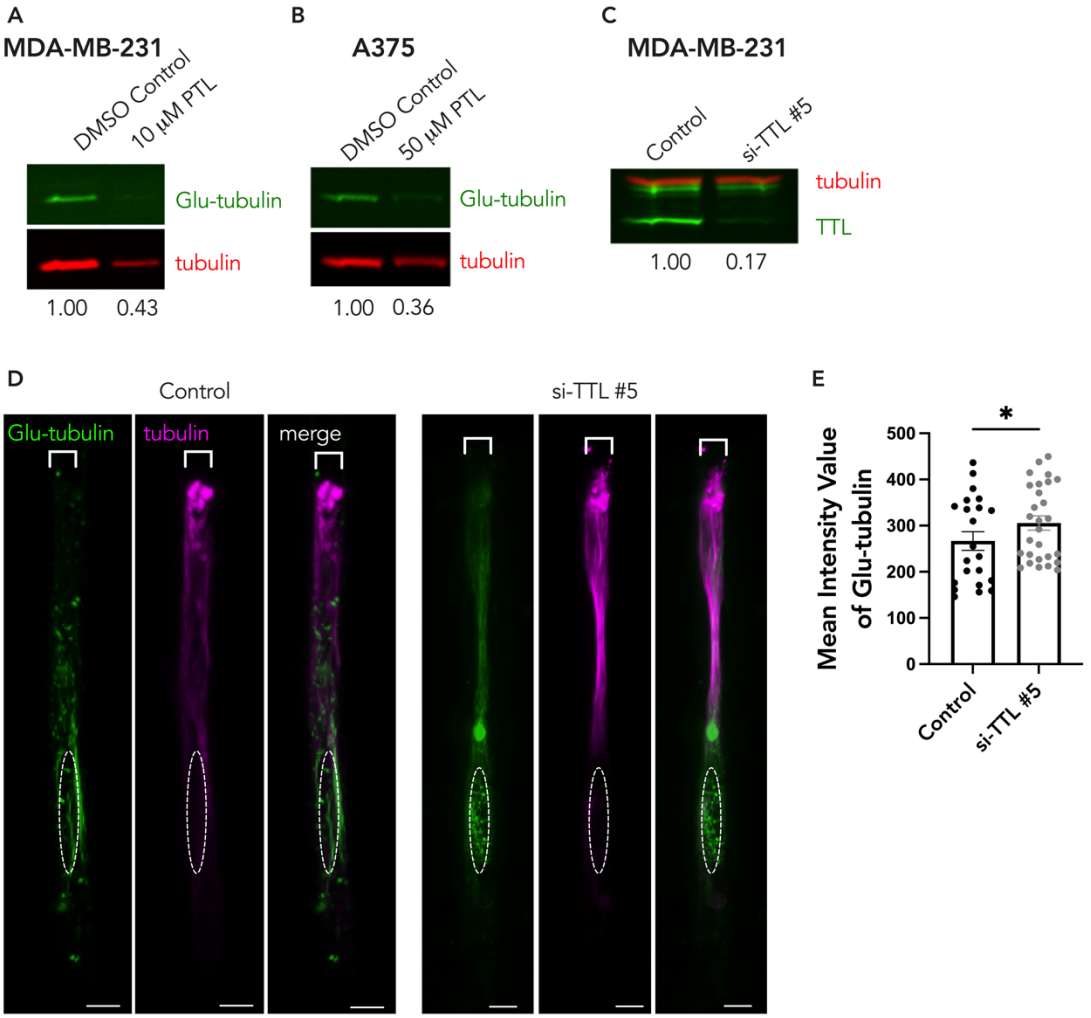

Figure 5.5: Modulation of Glu-tubulin levels.

(A and B) Western blots showing effect of DMSO (vehicle control) or Parthenolide (PTL) treatment on Glu-tubulin and tubulin protein levels for (A) MDA-MB-231

or (B) A375 cells. Numbers below tubulin bands represent quantification of Glu-tubulin to tubulin signal.

(C) Western blot showing the effect of Control or tubulin tyrosine ligase (TTL) siRNAs on tubulin and TTL protein levels. Numbers below tubulin bands represent quantification of TTL to tubulin signal.

(D) Representative immunofluorescence images of MDA-MB-231 cells in 3 μm narrow microchannels treated with either Control or TTL siRNAs. White dashed lines represent position of the nucleus. Scale bar: 5 μm.

(E) Quantification of mean intensity of Glu-tubulin signal of Control or TTL siRNA treated MDA-MB-231 cells. Individual dots represent individual cells pooled from two independent experiments. P value, *<0.05, an unpaired t-test assuming equal standard deviations was used. Error bars represent standard error.

5.2.3 Myosin II activity alone does not promote peripheral RNA localization in cells in confinement

Previous work from our lab showed that mechanical properties and actomyosin contractility can drive formation of the detyrosinated tubulin network, leading to peripheral RNA localization in cells (*249*). We speculated that differences in these parameters could account for the differences observed in Glu-tubulin levels and RNA localization between cell types. First, we investigated YAP distribution since higher nuclear YAP has been shown to correlate with a more mechanoresponsive cell (*81*,

199, *276*). In the 50 μm wide microchannels, there was a high degree of nuclear YAP in both cell lines (Figure 5.6A&B), such that the cytoplasm to nuclear signal ratio was close to 1. In the 3 μm narrow microchannels, the MDA-MB-231 cells excluded YAP from the nucleus, leading to a high cytoplasm to nuclear signal ratio. A375 cells in 3 μm narrow microchannels also had increased cytoplasmic YAP in comparison with cells in 50 μm wide microchannels, but they maintained a higher relative level of nuclear YAP in comparison with MDA-MB-231 cells. These results are consistent with the idea that A375 cells may maintain a higher degree of mechanoresponsiveness in confinement compared to MDA-MB-231 cells.

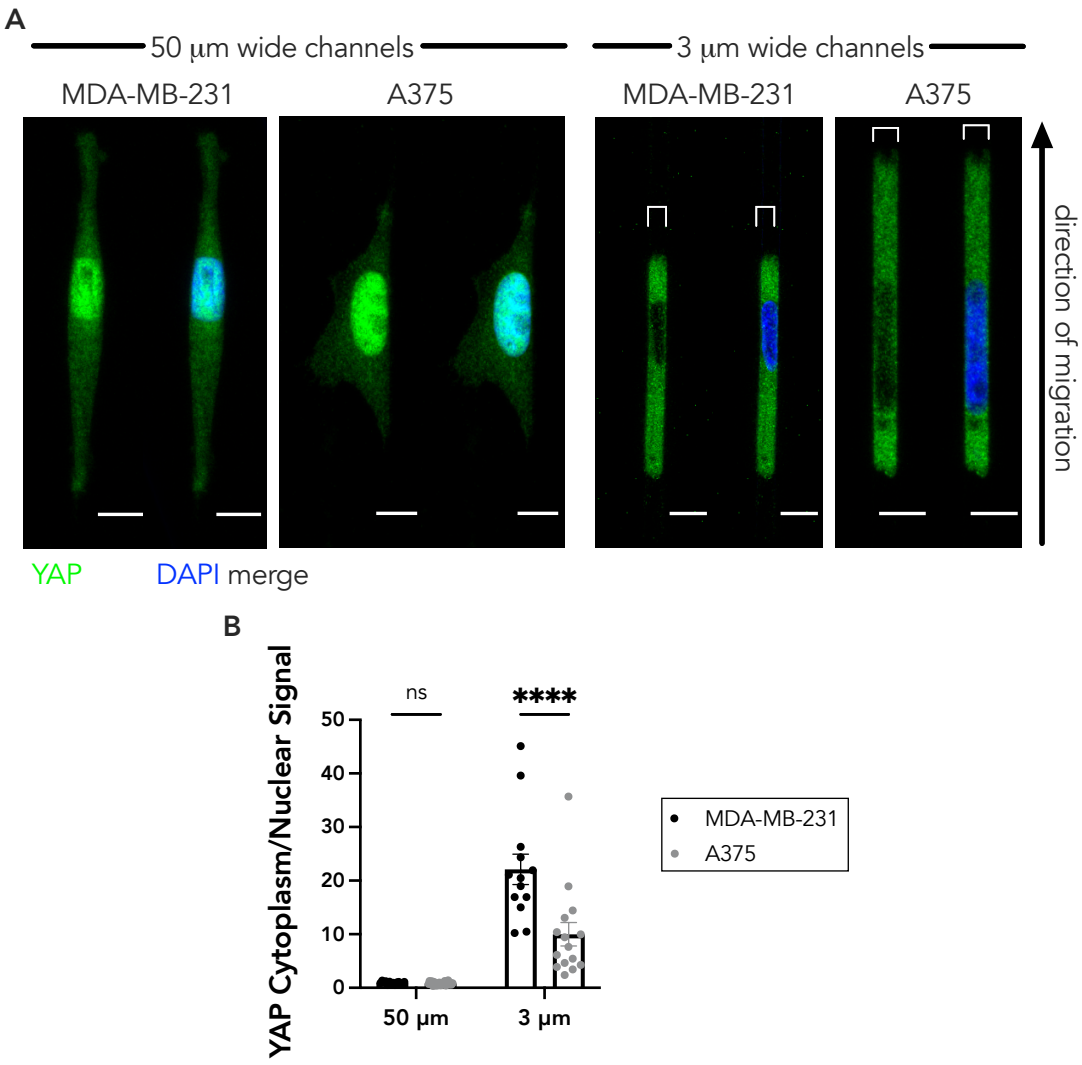

Figure 5.6: YAP localization is altered in cells in confinement.

(A) Representative immunofluorescence images of YAP staining in MDA-MB-231 and A375 cells in 50 μm wide and 3 μm narrow microchannels. Scale bar: 10 μm. Brackets above cells in 3 μm narrow microchannels show channel outline.

(B) Quantification of YAP cytoplasmic to nuclear signal ratio of MDA-MB-231 and A375 cells in 50 μm wide and 3 μm narrow microchannels. Individual dots

represent individual cells pooled from two independent experiments. P value, **<0.0001, a two-way ANOVA with Šídák's test was performed.**

To further test this, we explored the presentation of the actin and myosin networks within cells in confinement. We did not detect discernable differences in the actin network between either cell line in confinement (Figure 5.8A&B). In both cell lines in confinement, the actin network seemed to be largely cortical, which is a hallmark of ameboid migration that is dependent on myosin II contractility. Staining with an antibody against active phosphorylated myosin (Ser19) revealed that both unconfined MDA-MB-231 and A375 cells displayed a fibrillar active myosin network (Figure 5.7A). In the 3 μm narrow microchannels, the A375 cells maintained a fibrillar active myosin network. Meanwhile, the MDA-MB-231 cells did not show any fibrillar staining; rather, they accumulated active myosin at the extreme peripheral edges of the cells. Quantification of the fibrillar signal revealed significantly more fibrillar myosin in the A375 cells compared to the MDA-MB-231 cells in both the 50 μm and the 3 μm wide microchannels (Figure 5.7B). Interestingly, the levels of active myosin mirrored those of Glu-tubulin (compare Figure 5.7B and 5.3D), highlighting a potential connection between them.

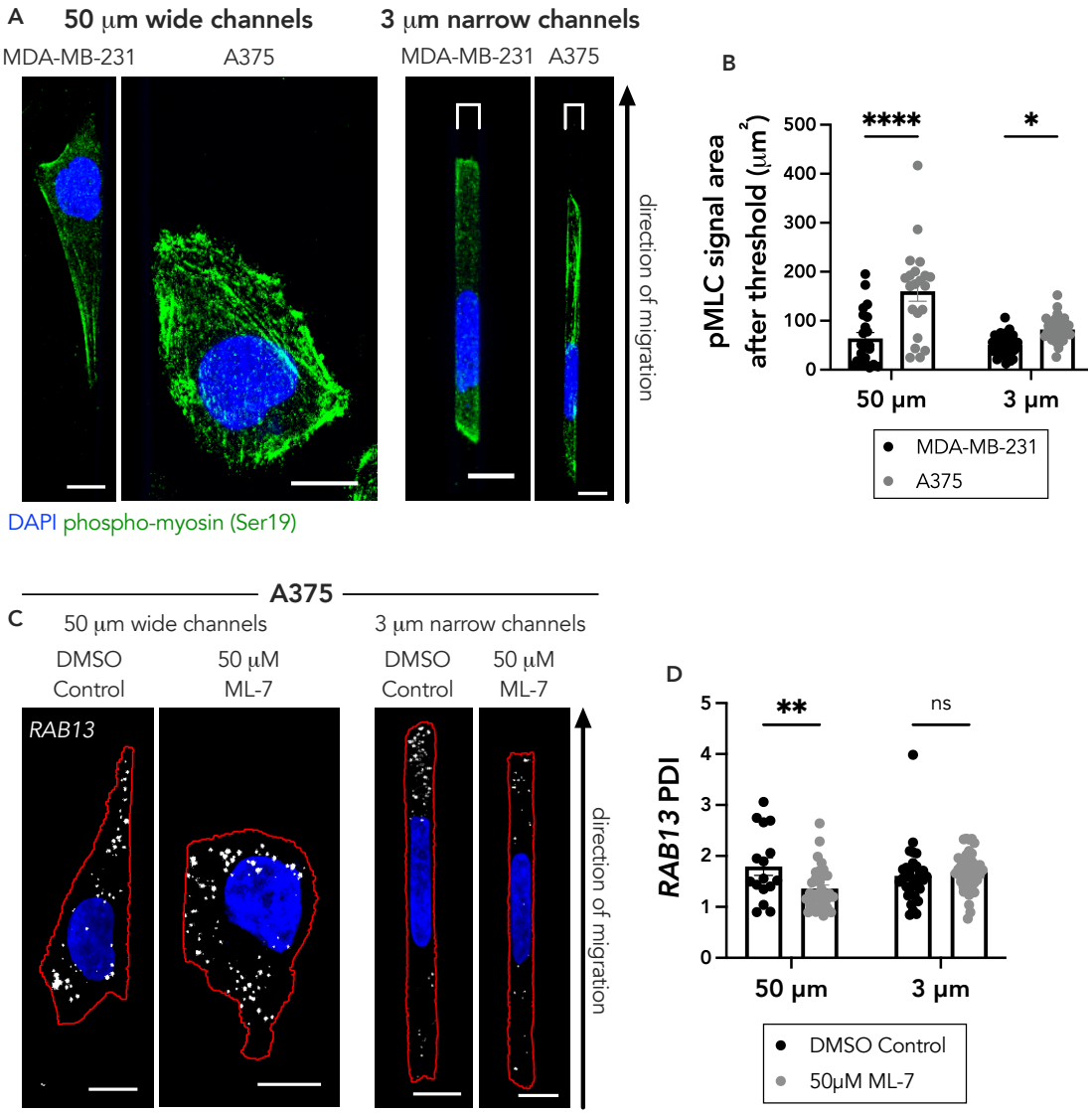

Figure 5.7: Loss of myosin activity is not sufficient to disrupt peripheral *RAB13* RNA localization in cells in confinement.

(A) Representative images of phospho-myosin light chain (er19) (pMLC) staining in MDA-MB-231 and A375 cells in 50 μm wide and 3 μm narrow microchannels. Brackets above cells in 3 μm groups denote the microchannel width.

(B) Quantification of pMLC signal (after thresholding out diffuse background signal) of MDA-MB-231 and A375 cells in 50 μm wide and 3 μm narrow microchannels.

(C) Representative *RAB13* FISH images of A375 cells treated with DMSO (vehicle control) or 50 μM ML-7 in 50 μm wide and 3 μm narrow microchannels. RNA signal is shown in white, nucleus in blue and cell outline in red.

(D) Quantification of *RAB13* PDI of DMSO control or 50 μM ML-7 treated cells. Individual dots on graphs represent individual cells pooled from three independent experiments; error bars display standard error. P values, *<0.05, **<0.01, *<0.001 by two-way ANOVA with Šídák's test. Scale bar: 10 μm.**

To explore this possibility, we sought to disrupt myosin activity through treatment with the myosin light chain kinase inhibitor, ML-7. We chose to use ML-7 in lieu of blebbistatin as it specifically targets myosin light chain kinase, which phosphorylates the myosin light chain residue that we imaged above. As expected, treatment with ML-7 led to a decrease in phosphorylated myosin signal (Figure 5.8C&D). Intriguingly, when we examined the *RAB13* RNA patterns in these cells, we saw that while myosin activity was required for *RAB13* RNA localization in unconfined microchannels, its loss was not sufficient to affect *RAB13* RNA localization in cells in confinement (Figure 5.7C). We conclude that in confined A375 cells a factor different than, or in addition to, myosin activity is required for peripheral RNA localization.

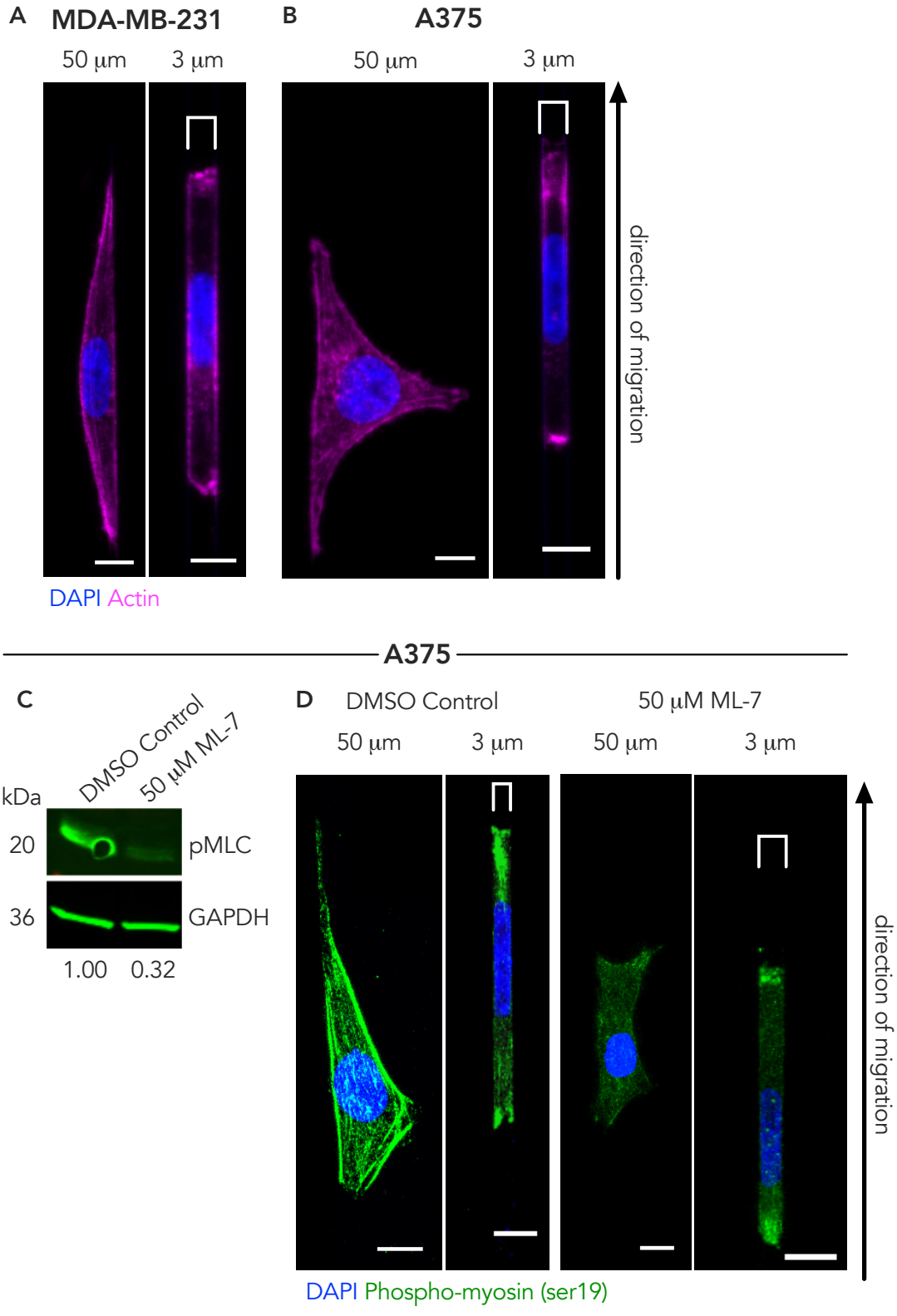
A
MDA-MB-231
50 μm
3 μm
B
A375
50 μm
3 μm
direction of migration
DAPI Actin
A375
C
DMSO Control
50 μM ML-7
kDa
20
pMLC
36
GAPDH
1.00
0.32
D
DMSO Control
50 μM ML-7
50 μm
3 μm
50 μm
3 μm
direction of migration
DAPI Phospho-myosin (ser19)

Figure 5.8: The actin network is largely cortical in cells in confinement and the myosin network can be modulated by an inhibitor of the myosin light chain kinase.

(A and B) Representative immunofluorescent images of phalloidin staining in (A) MDA-MB-231 and (B) A375 cells in 50 μm wide and 3 μm narrow microchannels. (C) Western blot of phosphorylated myosin light chain (pMLC) and GAPDH of A375 cells treated with DMSO (vehicle control) or 50 μM ML-7. Numbers below GAPDH band are quantification of pMLC/GAPDH signal.

(D) Representative immunofluorescent images of phospho-myosin light chain (Ser19) staining of A375 cells treated with DMSO (vehicle control) or 50 μM ML-7 in 50 μm wide or 3 μm narrow microchannels. Scale bar (A, B, and D): 10 μm.

5.2.4 The Piezo1 channel and myosin activity function redundantly to promote peripheral RNA localization in cells in confinement through the detyrosinated tubulin network

It has been suggested that in confinement, A375 cells maintain mechanoactivity through two independent factors, myosin II and the Piezo1 Ca^{2+} mechanosensitive ion channel, which initiates a downstream signaling cascade that controls myosin-mediated contractility (*73*). Intriguingly, only dual inhibition of these factors resulted in a change in cell stiffness on 1D micropatterned substrates (*73*). We speculated that the additional factor involved in peripheral RNA localization postulated above is the Piezo1 channel. Hence, we investigated the role of Piezo1 in RNA localization. Knockdown of Piezo1 with two different siRNAs (Figure 5.9A) reduced the peripheral *RAB13* RNA

localization in cells within the 50 μm wide microchannels (Figure 5.10A&B). Combination of Piezo1 knockdown with 50 μM ML-7 treatment, in the 50 μm wide microchannels, did not lead to any additive effect. The *RAB13* RNA remained perinuclear (evidenced by a significantly decreased PDI of approximately 1) compared to the control group.

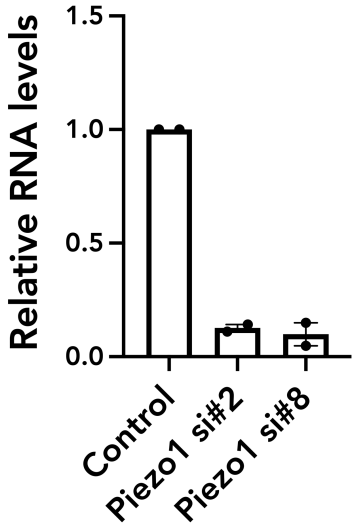

Figure 5.9: Piezo1 siRNA treatment reduces Piezo1 RNA levels.

Quantification of RNA levels measured by droplet digital PCR of Piezo1 compared to GusB housekeeping gene of A375 cells treated with indicated siRNAs. Individual dots represent one experiment. Error bars represent standard error.

Notably, in the 3 μm narrow microchannels, as seen above upon myosin inhibition, treatment with Piezo1 siRNA alone was not sufficient to alter the *RAB13* PDI (Figure 5.10C&D). Importantly, however, co-treatment with Piezo1 siRNA and 50 μM ML-7 significantly decreased the *RAB13* RNA PDI (Figure 5.10C&D). Taken together, these results confirm that in a confined environment the Piezo1 Ca^{2+} mechanosensitive ion channel and myosin activity act redundantly to maintain peripheral RNA localization.

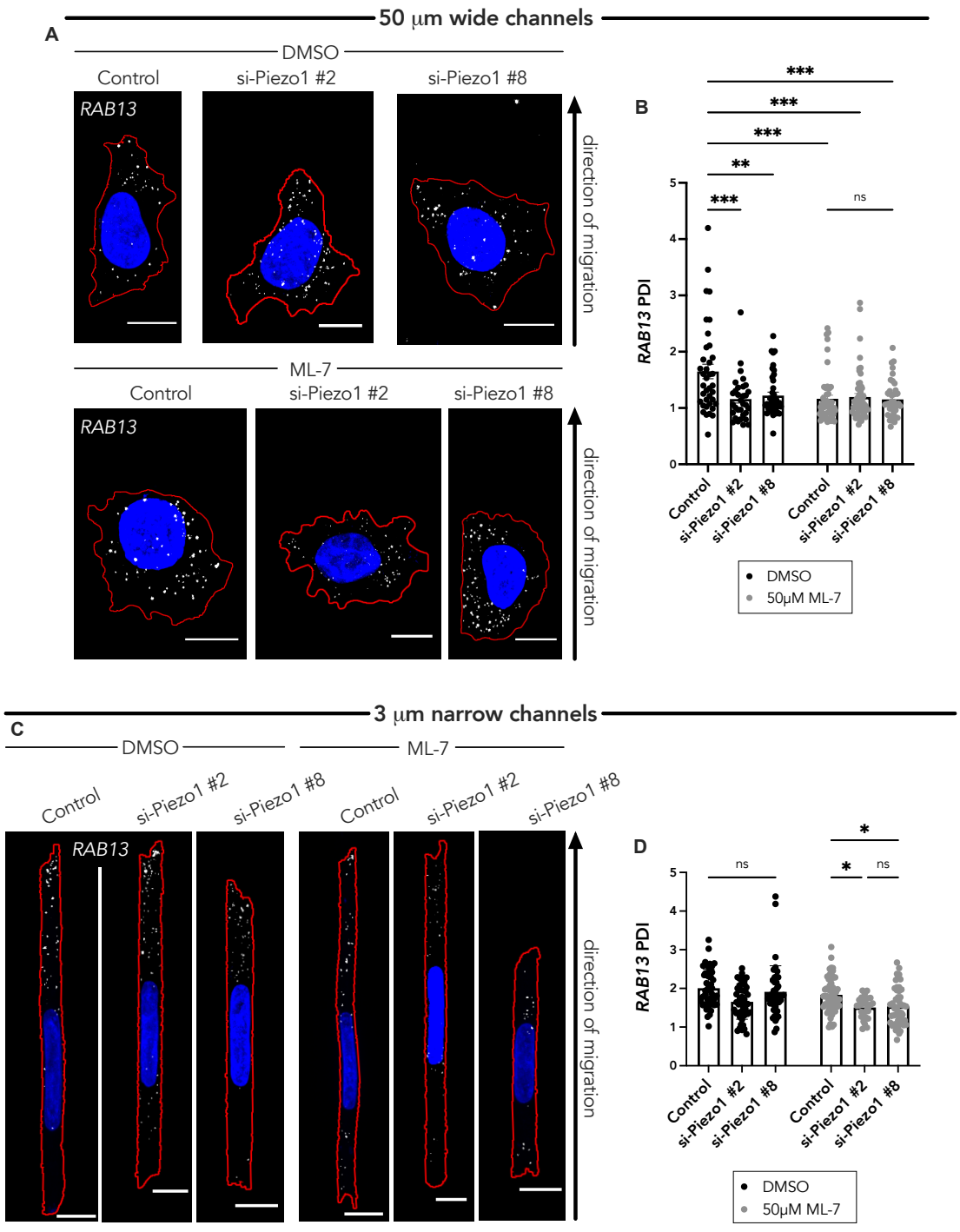

Figure 5.10: The Piezo1 channel and myosin activity function redundantly to regulate peripheral *RAB13* RNA localization in cells in confinement.

(A) Representative FISH images of *RAB13* RNA (in white dots, nucleus in blue, cell outline in red) in A375 cells in 50 μm wide microchannels treated with DMSO (vehicle control) or 50 μM ML-7 along with the indicated siRNAs.

(B) Quantification of *RAB13* PDI of A375 cells in 50 μm wide microchannels treated with DMSO or ML-7 and Piezo1 siRNAs.

(C) Representative FISH images of *RAB13* RNA (in white dots, nucleus in blue, cell outline in red) in A375 cells in 3 μm narrow microchannels. Cells were treated with DMSO (vehicle control) or 50 μM ML-7, along with the indicated siRNAs.

(D) Quantification of *RAB13* PDI of cells in 3 μm narrow microchannels. Individual dots on graphs represent individual cells pooled from three independent experiments; error bars display standard error. Scale bars: 10 μm. P values, *<0.05, **<0.01, *<0.001, ****<0.0001 by two-way ANOVA with Šídák's test.**

To determine whether this effect is mediated through the detyrosinated tubulin network (Figure 5.11A), we assessed Glu-tubulin levels under single or dual inhibition of these factors. Indeed only upon dual treatment with Piezo1 siRNA and ML-7 was there maximal decrease in Glu-tubulin levels as assessed by western blot (Figure 5.11B&C) or by immunostaining of A375 cells within the 3 μm narrow microchannels (Figure 5.11D&E). Only dual treatment with Piezo1 siRNA and ML-7 led to a significant decrease in the detyrosinated tubulin intensity (Figure 5.11E). Altogether, the above data support a model whereby in confined A375 cells both Piezo1

mechanoactivity and myosin activity can promote the formation of a detyrosinated tubulin network and consequently lead to peripheral *RAB13* RNA localization.

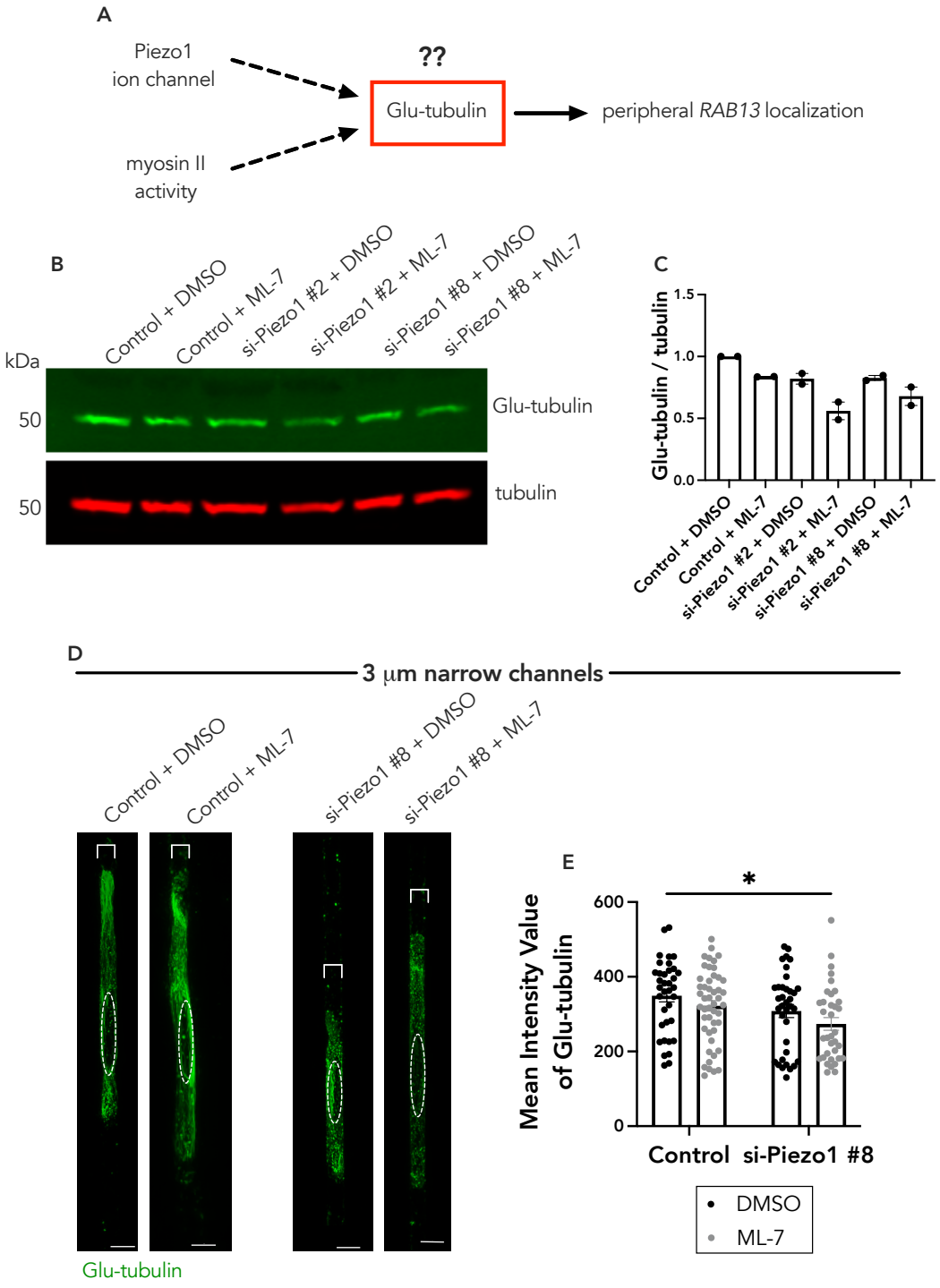

Figure 5.11: The Piezo1 channel and myosin activity function redundantly to regulate the detyrosinated tubulin network in cells in confinement.

(A) Schematic depicting the proposed redundant regulation of Glu-tubulin and RNA localization by Piezo1 and myosin.

(B) Representative western blot showing effect of Piezo1 knockdown and ML-7 co-treatment (DMSO is used as the vehicle control) on Glu-tubulin protein levels for cells on a 2D surface.

(C) Quantification of corresponding Glu-tubulin to tubulin protein levels from (B); individual dots represent one independent experiment.

(D) Representative immunofluorescence images of Glu-tubulin in A375 cells in 3 μm wide microchannels after treatment with Piezo1 siRNA and/or ML-7. Dashed white circle represents position of nucleus.

(E) Quantification of mean intensity of Glu-tubulin signal per cell. Dots represent individual cells pooled from three independent experiments. Error bars reflect standard error, scale bars: 5 μm. P values, *<0.05, by two-way ANOVA with Šídák's test.

5.2.5 Peripheral RNA localization contributes to confined migration

Peripheral localization of the *RAB13* RNA is important for cell migration in 2D and 3D settings (*242*, *249*, *266*). Targeting of the *RAB13* RNA to the periphery can be specifically inhibited using antisense morpholino oligonucleotides targeted against a functionally important GA-rich region within the 3'UTR of *RAB13*. Such oligos have been shown to specifically mislocalize the *RAB13* RNA in MDA-MB-231 cells from

peripheral regions of cells, without altering total *RAB13* RNA or protein levels (*242*). We first confirmed that these tools produce the same results in A375 cells. Indeed, morpholinos targeted against the GA-rich region in the 3'UTR of *RAB13* RNA prevented the peripheral localization of *RAB13*, as evidenced by a decrease in *RAB13* PDI, but did not alter the PDI of a perinuclear RNA, *RHOA* (Figure 5.12A-C). Significantly, and consistent with prior studies, RAB13 morpholinos also reduced cell migration speed and persistence of A375 cells on 2D unconstrained surfaces. These results support the conclusion that peripheral RAB13 is also important for migration of this cell type (Figure 5.11D&E).

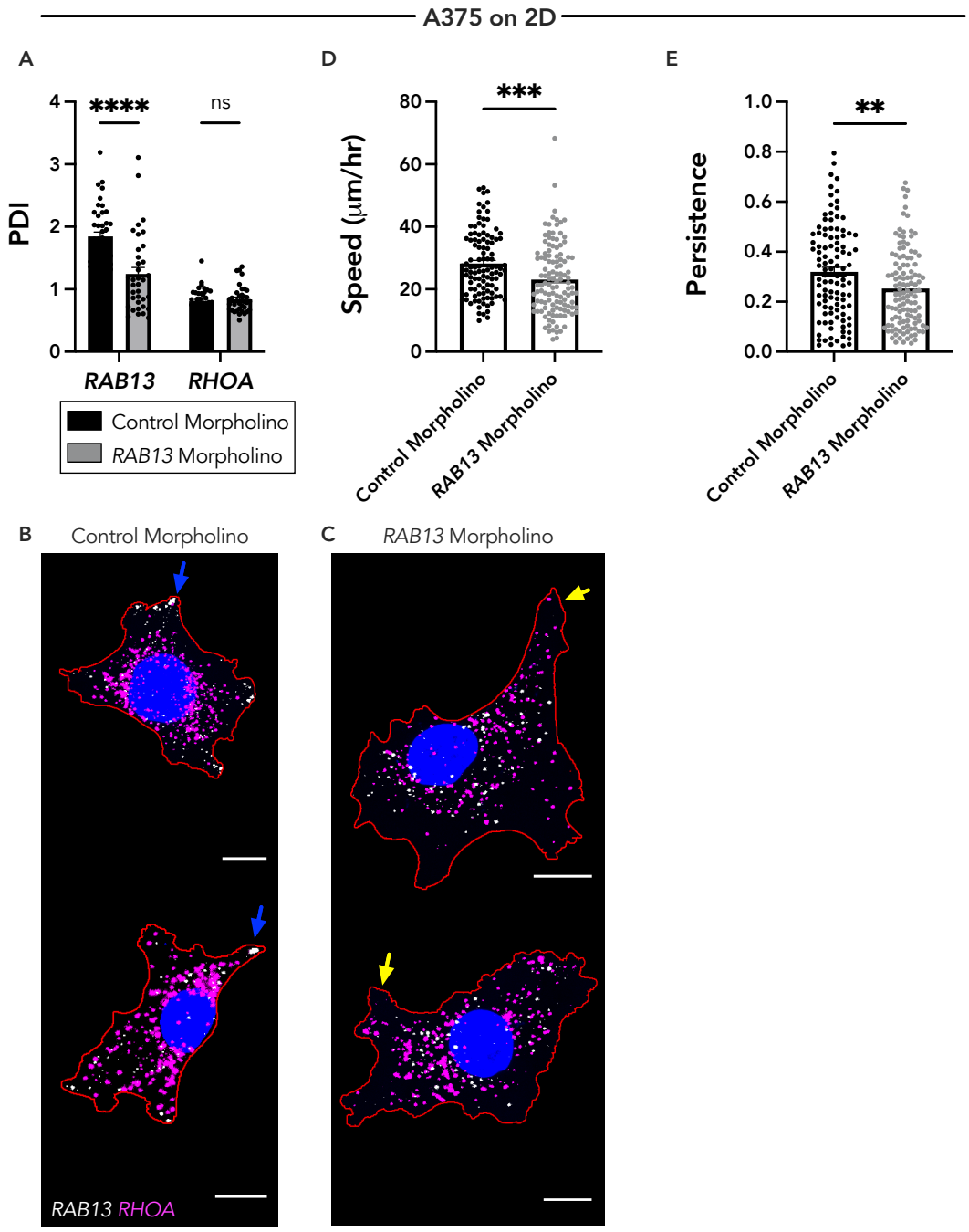

Figure 5.12: Antisense morpholino oligos targeted against localization sequences in the 3'UTR of *RAB13* can mislocalize the *RAB13* RNA and impact cell migration in A375 cells.

(A) PDI quantification of *RAB13* or *RHOA* RNAs in A375 cells treated with control morpholino oligos or *RAB13*-targeted oligos. Individual dots represent individual cells pooled from two independent experiments.

(B and C) Representative *RAB13* FISH images of A375 cells treated with (B) control morpholino oligos or (C) oligos directed against localization sequences in the 3'UTR of *RAB13*. Cell outline is in red and nucleus in blue. Blue arrows in (B) depict peripheral localization of *RAB13* RNA, while yellow arrows in (C) show lack of *RAB13* RNA at cell protrusions.

(D and E) Effect of treatment of A375 cells with control morpholino oligos or oligos directed against localization sequences in the 3'UTR of *RAB13* on (D) cell speed and (E) persistence. Individual dots represent individual cells pooled from two independent experiments.

Scale bar: 10 μm. P values, **<0.01, *<0.001, ****<0.0001, by two way ANOVA with Šídák's test (in A, D, E). Error bars represent standard error.**

To assess the role of *RAB13* RNA localization in confined migration, we seeded cells treated with antisense morpholino oligos against *RAB13* into the 50 μm wide microchannels or into the 3 μm narrow microchannels and quantified their migratory parameters. In the MDA-MB-231 cells, there was a significant decrease in cell speed in the 50 μm wide microchannels, but no significant change in the 3 μm narrow microchannels when compared to treatment with control morpholinos (Figure 5.13A). There was no change in cell persistence in either case (Figure 5.13B). By contrast, there was a significant decrease in A375 cell speed and cell persistence, in both 50 μm wide

and 3 μm narrow microchannels, upon treatment with *RAB13* morpholinos (Figure 5.13C&D). Together, these data support a model where in confinement, cells that maintain peripheral *RAB13* RNA localization (A375 cells) require this peripheral RNA accumulation for efficient migration. In contrast, cells that cannot support peripheral RNA localization in confinement (MDA-MB-231 cells), due to a lack of Glu-tubulin network, likely rely on a different migratory mechanism that does not involve peripheral *RAB13* RNA.

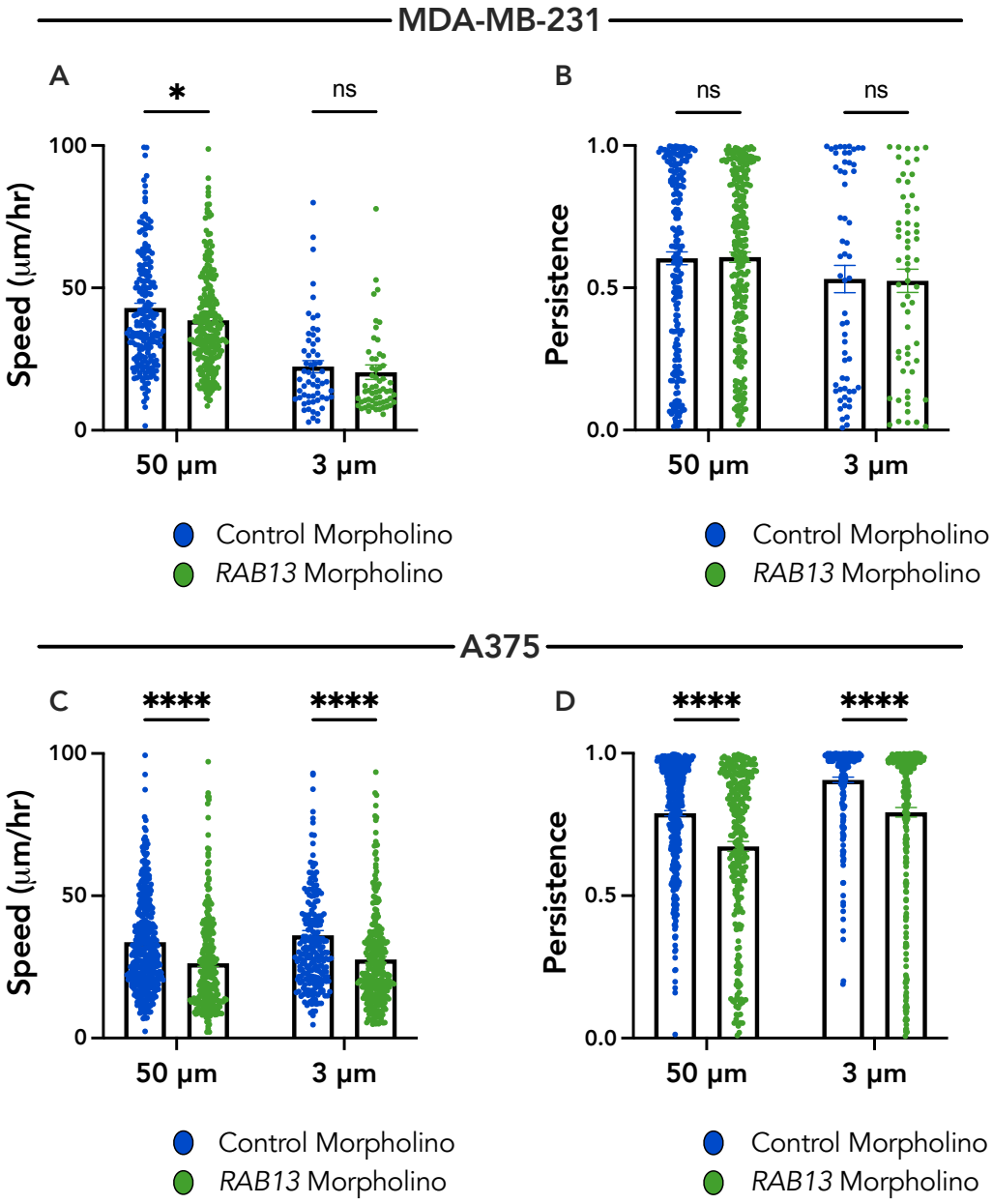

Figure 5.13: Peripheral RNA localization functionally contributes to cell migration in confinement.

(A and B) Cell speed (A) and persistence (B) of MDA-MB-231 cells in 50 μm wide and 3 μm narrow microchannels were quantified after treatment with control

morpholino oligos or oligos directed against localization sequences in the 3'UTR of *RAB13*.

(C and D) Cell speed (C) and persistence (D) of A375 cells in 50 μm wide and 3 μm narrow microchannels were quantified after treatment with control morpholino oligos or oligos directed against the 3'UTR of *RAB13* RNA. Dots represent individual cells pooled from three independent experiments. P values, *<0.05, **<0.0001 by two-way ANOVA with Šídák's test.**

5.3 Discussion

In summary, we have shown here that RNA localization in confinement is controlled by the mechanoactivity of cells. Mechanically active cells, through the Piezo1 channel or myosin activity, establish a detyrosinated tubulin network and utilize it to peripherally enrich the *RAB13* RNA. This peripheral RNA accumulation functionally contributes to cell movement through a confined space. Less mechanically active cells do not establish a pronounced detyrosinated tubulin network, do not manifest the same set of peripherally enriched RNAs, and do not require them for migration in confinement (Figure 5.14).

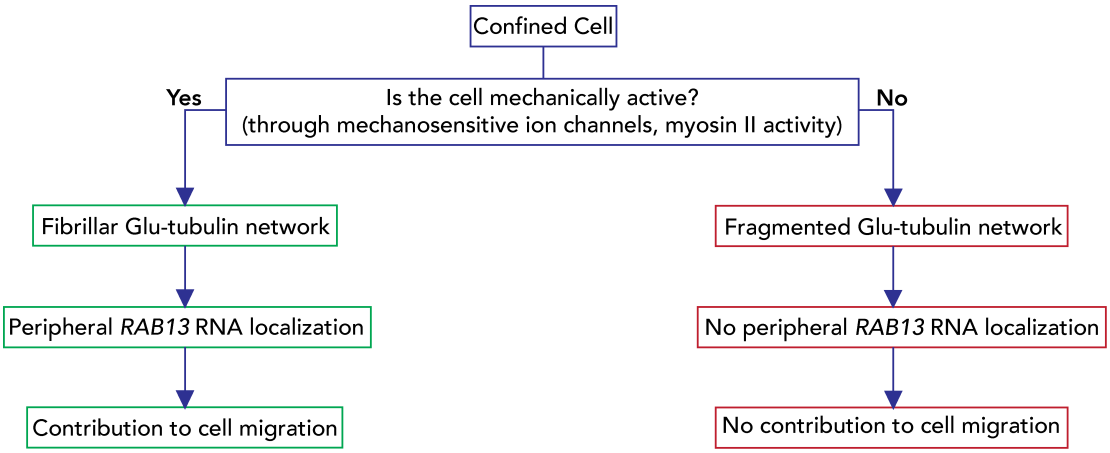

Figure 5.14: Proposed model.

Flow chart depicting how the mechanical properties of cells determine RNA localization in confined cells. Peripheral RNA targeting can promote migration through narrow spaces.

Cells in confinement have been reported to be less mechanically active than their unconfined counterparts. U2OS osteosarcoma cells soften as they move into confinement, with lower Young's moduli and denser actomyosin stress fibers at the cortical edges of the cell (*81*). Both NIH-3T3 fibroblasts and U2OS osteosarcoma cells in confinement exert lower traction forces compared to cells in unconfined environments (*57*). YAP localization can also be a marker of cell mechanoactivity, where greater nuclear YAP signal can correlate to a more mechanically active cell and greater cytoplasmic signal can correlate to a 'softer' cell (*81*, *276*). U2OS cells in confinement exclude YAP from the nucleus compared to nuclear accumulation of YAP in unconfined environments (*81*). Our results suggest that residual cell mechanoactivity can vary in confinement depending on the cell type. While both cell types tested here

appear to be less mechanically active compared to unconfined settings, A375 cells maintain a higher degree of mechanoactivity compared to MDA-MB-231 cells. This difference is also reflected in different levels of active myosin, microtubule dynamics and consequently RNA localization patterns. A375 cells are also able to move faster and more persistently in confined microchannels than MDA-MB-231 cells (Figure 5.14), suggesting a potential benefit of higher mechanoactivity in confinement. However, the underlying cause, purpose, and/or function of this difference warrants further investigation.

Entry of cells into a confined environment is accompanied by numerous changes in adhesion, cytoskeleton organization and membrane tension, all of which alter the mechanical and signaling state of the cell and ultimately influence the adopted mode of migration. Localized increases in membrane tension can drive the opening of stretch activated ion channels leading to an intracellular ion influx that can direct downstream signaling cascades (*277*). A375 cells upregulate the Piezo1 stretch-activated ion channel, which allows entry of Ca^{2+} into the cytoplasm in response to changes in membrane tension (*73*). In confined cells, Piezo1-directed Ca^{2+} influx results in activation of phosphodiesterase 1 (PDE1), which suppresses protein kinase A (PKA) through hydrolysis of cAMP (*73*). We speculate that this signaling cascade could affect APC-dependent RNA localization by leading to activation of RhoA, as RhoA and PKA are connected through a negative feedback loop (*278*). RhoA can, in turn, activate mDia1, a formin protein, which can impact both actin and microtubule dynamics (*273*). Confined A375 cells additionally maintain a residual level of active myosin, which can further promote RhoA activation (*9*, *279*).

In contrast to A375 cells, MDA-MB-231 cells do not upregulate Piezo1, but rather other mechanosensitive ion channels, such as transient receptor potential channels (TRPs) and Na^+/H^+ exchangers (NHEs) (*154*, *280*). MDA-MB-231 cells in confinement can utilize the TRPM7 channel and cortical actomyosin to mechanically probe and enter environments of varying degrees of hydrostatic pressure, but their inhibition does not affect the cells' ability to migrate once in confinement (*200*). Similarly, the MDA-MB-231 clone that has been purified from successive brain metastatic lesions (MDA-MB-231 BR) overexpresses the Piezo2 channel (*281*). In MDA-MB-231 BR cells, loss of Piezo2 does not impact confined migration, but rather the ability of the cells to enter confinement (*281*). Notably, these examples are in contrast to A375 cells, where knockdown of Piezo1 significantly reduces both confined migration and entry into confined microchannels (*73*). Together, it seems that mechanosensitive ion channels and actomyosin play cell type dependent roles in confinement sensing and migration.

We show here that changes in mechanical activity and cytoskeletal dynamics underlie different RNA localization patterns in confined cells. Peripheral *RAB13* RNA localization is maintained in unconfined and confined A375 cells and is required for their efficient migration in both environments (Fig 7, (*242*, *249*)). This functional contribution likely stems from localized RNA translation at the periphery. Indeed, translation at protrusions is important for protrusion stabilization (*243*), and the *RAB13* RNA itself is translated in peripheral protrusions. Interestingly, active *RAB13* translation is observed in extending regions while translationally silent *RAB13* RNA is found in retracting areas (*241*). The functional contribution of *RAB13* RNA silencing

at retracting areas is still unclear, however a mechanism has been described through which active *RAB13* translation, in lamellipodial regions, contributes to cell migration. Specifically, *RAB13* translation allows a co-translational interaction of the nascent RAB13 protein with its activator RABIF. This peripheral association is required to direct the RAB13 GTPase activity to support cell migration (*242*). It would be interesting to explore whether an analogous mechanism occurs during confined migration and whether a similar or different set of RAB13 effectors are involved in confined versus unconfined migration. Our results suggest that for MDA-MD-231 cells, which do not maintain peripheral *RAB13* translation in confinement, these potential RAB13 effectors are not relevant for the adopted migration mode.

An intriguing set of RNAs that become prominently peripheral in confinement, in both cell types tested here, encode ribosomal proteins (APC-independent RNAs). Their observed peripheral enrichment in both cases suggests that this might be a broader response upon entering confinement, regardless of the migration mode adopted by each cell type. This peripheral enrichment lacks directionality, occurring apparently randomly either at the front or back of cells, potentially indicating a lack of direct involvement in cell migration. Understanding the functional role of this phenomenon is hampered by our lack of knowledge of the underlying mechanisms of localization. While peripheral r-protein RNA localization can be mediated through the RNA-binding protein LARP6 and sequences in the 5'UTR (*250*), there is not currently an available way to specifically interfere with this RNA localization pathway. Changes in the location of r-protein mRNAs in polarized cells have been correlated with changes in the efficiency of their translation (*250*, *282*). Specifically, protrusion localization of r-

protein RNAs increases ribosomal protein synthesis. Such an increased r-protein production can lead to enhanced ribosome biogenesis and consequently to an increase in overall protein synthesis (*250*). Locally translated r-proteins could additionally participate in on-site ribosome remodeling, which could alter local ribosome functions (*283*). The functional relevance of either scenario in confinement is unclear. It would be interesting to assess whether overall protein synthesis changes as cells enter confinement, what is the contribution of r-protein RNA localization, and the potential functional roles of this regulation.

In summary, our work provides evidence that specific mechanical properties of cells direct the type of migration mode adopted in confinement at least partly through directing cytoplasmic RNA distributions. This work adds to the emerging picture that subcellular RNA localization is regulated by both the internal and external mechanical environment of the cell and is functionally relevant for both 2D and 3D cell migration.

While the microchannel devices are useful for studying cell migration phenotypes in confined spaces, their pliability is not reflective of all physiological settings. Furthermore, they likely do not adequately model the potential contribution of matrix remodeling by cells as they navigate confined environments *in vivo*. Further technical advances could shed light on these aspects. The presented mechanistic understanding is based on studies of the APC-dependent RNA, *RAB13*. Given that RNAs belonging to the APC-dependent group generally require detyrosinated microtubules for localization (*241*), we consider it likely that other RNAs of this group are regulated in a similar fashion, but future work would be needed to support that point. Finally, we focused on two cell lines which employ different migration

mechanisms (myosin based ameboid migration or actomyosin independent migration) in confinement and which exhibit differing levels of mechanoactivity. An expansion of this work to include additional cell types could strengthen the connections between mechanoactivity in confinement, migration mode and subcellular RNA distributions.

5.4 Methods

5.4.1 Cell culture

MDA-MB-231 cells (derived from female patient metastatic pleural effusion site of breast adenocarcinoma, ATCC) were cultured in Leibovitz's L-15 medium (ThermoFisher Scientific) supplemented with 10% FBS (ThermoFisher Scientific) and 1% Penicillin/Streptomycin (1000 U/mL; ThermoFisher Scientific) in a 37°C incubator with 50% humidity and 0% CO_2. A375 (derived from female patient with malignant melanoma, ATCC) cells were cultured in DMEM (ThermoFisher Scientific) supplemented with 10% FBS, 1% Penicillin/Streptomycin in a 37°C incubator with 50% humidity and 5% CO_2.

5.4.2 Microchannel fabrication & cell seeding

Microfluidic devices were fabricated as previously described (*66*, *128*), and summarized here in Chapter 3.4.2. All fabrication was carried out in the University of Maryland Fabrication Laboratory. 20 μg/mL collagen type I (Sigma) was added to all wells of the microfluidic device and allowed to adsorb for 1 hour at 37°C or overnight at 4°C. All wells were washed 3 times with PBS for 5 minutes each. Cells were

trypsinized for 5 minutes and centrifuged. $5x10^4$ cells were resuspended in 25 μL of serum free media (basal media supplemented with 1% Pen/Step), added to the bottom inlet, and allowed to incubate for 5 minutes at 37°C. Any remaining cell media was removed, and serum-free media was added to the bottom three inlets, while FBS-containing media was added to the top inlet to act as the chemoattractant. For 2D control experiments, coverslips were coated with 20 μg/mL collagen type I for 1 hour and then washed three times with PBS for 5 minutes each. Cells were plated at $1x10^5$ cells/mL and allowed to adhere.

5.4.3 Drug inhibitors

Cells were allowed to migrate through the microchannels for 3 hours and then media was replaced with serum-free or serum-containing media, both with drug. Cells were incubated with drug for another 3 hours, washed twice in PBS for 5 minutes each, and then fixed with 4% methanol-free paraformaldehyde for 20 minutes. Drug concentrations were as follows: Parthenolide (MDA-MB-231, 10 μM; A375, 50 μM), ML-7 (A375, 50 μM). DMSO was used as a vehicle control for all treatments.

5.4.4 Fluorescence in situ hybridization (FISH)

Cells were allowed to migrate through the microchannels for at least 3 hours but no longer than 10 hours. Cells were washed 2 times in PBS for 5 minutes each and fixed in 4% methanol-free paraformaldehyde for 20 minutes. FISH was performed with ViewRNA ISH Cell Assay kit (ThermoFisher Scientific) according to the manufacturer's instructions, with adjusted incubation times. The following probe sets were used: human RAB13 #VA1-12225; human KIF1C #VA1-3006735; human

Rpl27α #VA1-16562-01; human Rps20 #VA1-16561-01. To detect *polyA* RNAs, LNA modified oligodT probe (30 nucleotides) labeled with ATTO-655 was added during hybridization at 100nM and all amplification steps at 50nM. We use *polyA* as a marker of all RNA sequences within the cell. The entirety of the cell was stained with a cell mask stain to obtain the cell outline and nuclei were stained with DAPI.

5.4.5 Immunofluorescence (IF) & western blotting

Cells were allowed to migrate through the microchannels for at least 3 hours but no longer than 10 hours. Cells were washed 2 times in PBS for 5 minutes each and fixed in either 100% ice cold methanol (for Glu-tubulin and tubulin) or 4% methanol-free paraformaldehyde (all other proteins). Cells were again washed 3 times in PBS for 5 minutes each and blocked for one hour in PBS containing 5% goat serum and 0.3% Triton X-100. Cells were incubated with primary antibodies overnight, diluted in PBS containing 1% bovine serum albumin and 0.3% Triton X-100. The following day cells were washed 3 times in PBS for 5 minutes each and then incubated with Alexa-conjugated secondary antibodies (ThermoFisher Scientific) at 1:500 in PBS containing 1% bovine serum albumin and 0.3% Triton X-100. Cells were washed 3 times again in PBS for 5 minutes and then nuclei were stained with DAPI and imaged.

Western blots were blocked using Intercept TBS blocking buffer (Li-Cor) and incubated with primary antibodies at concentrations listed in the reference table, diluted in blocking buffer with 1% Tween-20 overnight at 4°C. Secondary antibodies conjugated with IRDye (LiCor) were used at 1:10,000 in blocking buffer with 1%

Tween-20 for one hour at room temperature. Blots were imaged using a Li-Cor Odyssey imaging system.

5.4.6 siRNA knockdown

Cells were grown to 60-70% confluency and then transfected with 20 pmoles/mL of siRNAs using Lipofectamine RNAiMAX (ThermoFisher Scientific), following the manufacturer's instructions. TTL siRNA and Piezo1 siRNA sequence #8 treated cells were analyzed 72 hours after transfection. Piezo1 siRNA sequence #2 cells were re-transfected with 20 pmol/mL siRNA at 48 hours and analyzed at 96 hours after transfection. siRNAs used were: AllStars Negative control siRNA (Qiagen, cat# 1027281); si-TTL#5 (Qiagen, cat# SI03145856; target sequence: 5'-AGGAGTTCAATCAGTACCTAA-3', si-Piezo1#2 (Qiagen, cat# SI00383656; target sequence: 5'- CAGCCTTGTATGCACCGTCAA -3'; si-Piezo1#8 (Qiagen, cat# SI04759153; target sequence: 5'- CCGGCCCTGTGCATTGATTAT -3').

5.4.7 Antisense morpholino oligonucleotides

Cells were plated and allowed to attach overnight before antisense morpholino oligonucleotides (synthesized by GeneTools, LLC) were added to the cells at final concentration of 20 μM with Endoporter (GeneTools, LLC) delivery vehicle. Cells were analyzed 72 hours post treatment.

5.4.8 Imaging

RNA FISH and IF samples were imaged using a Leica SP8 confocal microscope (with a HC PL APO 63X oil CS2 objective). Z-stacks were taken through the entire

volume of the cell at an interval of 0.3 μm per step. Migration analysis was performed on an Olympus IX83 microscope (LUCPlan FLN 20X phase objective) with an environmental chamber to maintain appropriate growth conditions. Images were taken at 5 or 10-minute intervals for 12 hours.

5.4.9 Image analysis, quantification, and statistical analysis

Non-specific background noise was subtracted from all FISH images (Figure 5.15A). RNA distribution indices were calculated using RDI Calculator (*274*). Distributions along the leading to lagging edge axis were performed using a custom MATLAB script. Glu-tubulin and tubulin IF images were processed through the Nikon Elements denoise.ai and fluorescent intensity was quantified using Imaris 9.7.0. All other IF images were quantified using ImageJ; phospho-myosin images were thresholded to remove diffuse background signal before quantification (Figure 5.15B). Cells for migration analysis were tracked using the Manual Tracking ImageJ plugin. Speed and persistence values were calculated using a custom MATLAB code by K.M.S. We measure persistence as the stepwise distance divided by the total distance the cell travelled, such that a persistence of 1 reflects a cell that moved in a straight line.

All values are represented as mean ± standard error (SEM) and data represents individual cells pooled from similarly sized, biologically independent trials. An individual cell within a single microchannel was noted as N=1. First, this allowed for the heterogeneity within a single cell line population to be factored into the analysis. Second, as each microchannel could have slight differences in shape, introduced during

fabrication, or exposure to nutrients due to its position within the device, each cell within was in a unique experimental environment and could be counted as an individual entity. Prism 9 (GraphPad) was used for all statistical analysis; the significance level was set at 0.05. For multiple comparisons, a two-way ANOVA with Šídák's test was performed. For single comparisons, an unpaired t-test assuming equal standard deviations was used.

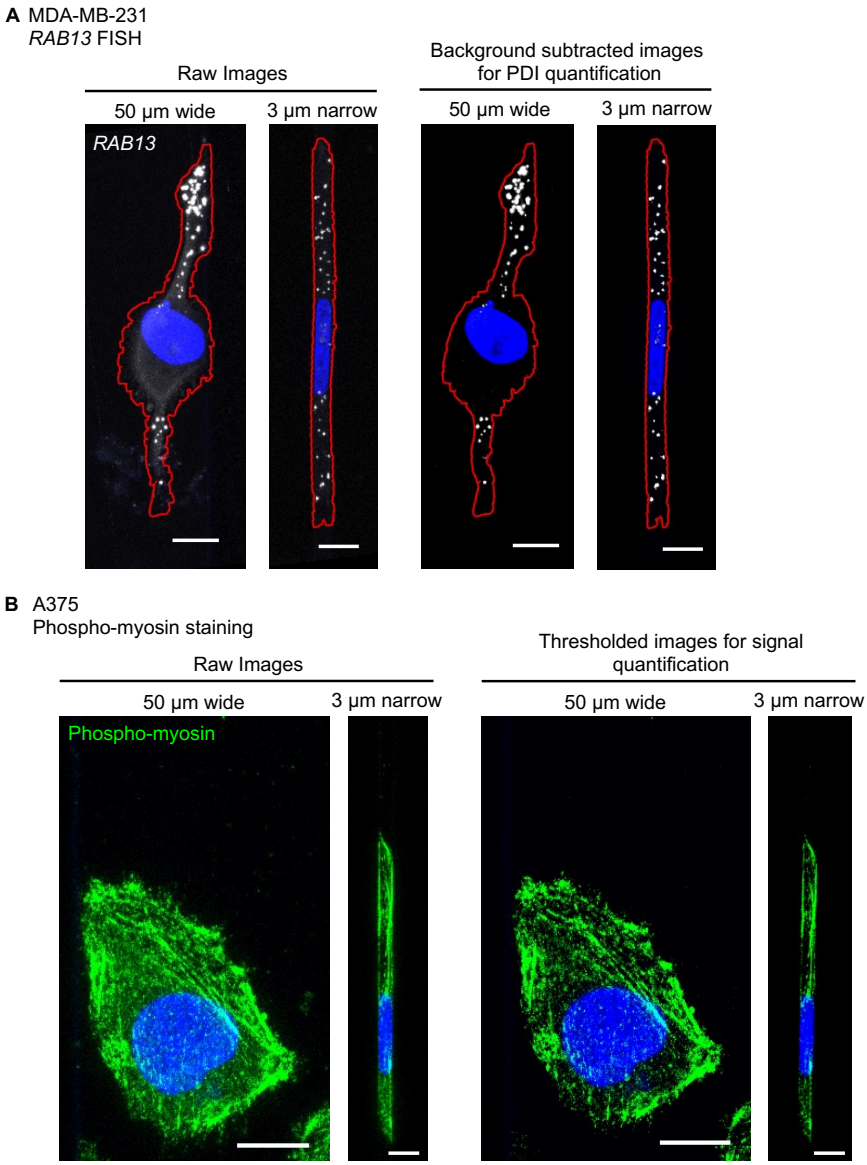

Figure 5.15: Post-processing of RNA FISH and IF images. (A) *RAB13* FISH Z-stack maximum projection images of MDA-MB-231 cells either raw signal or with background signal subtracted to remove noise. Nucleus in blue and cell outline in red. (B) Phospho-myosin IF staining of A375 cells shown with raw signal or remaining signal after threshold was applied to remove diffuse, non-fibrillar staining. Nucleus in blue.

5.5 Conclusion

Cancer cells experience mechanical confining forces during metastasis and consequently, can alter their migratory mechanisms. Localization of numerous mRNAs to cell protrusions contributes to cell polarization and migration and is controlled by proteins that can bind RNA and/or cytoskeletal elements, such as the Adenomatous Polyposis Coli (APC). Here, we demonstrate that peripheral localization of APC-dependent RNAs in cells within confined microchannels is cell type dependent. This varying phenotype is determined by the presence or absence of a fibrillar detyrosinated tubulin network. We show that this network is regulated by mechanoactivity, and that cells with mechanosensitive ion channels and increased myosin II activity direct peripheral localization of the *RAB13* APC-dependent RNA. Through specific mislocalization of the *RAB13* RNA, we show that peripheral RNA localization contributes to confined cell migration. Our results indicate that a cell's mechanical activity determines its ability to peripherally target RNAs and utilize them for movement in confinement.

Chapter 6: Conclusions and contributions to science

6.1 Physical confinement alters sarcoma cell cycle progression and division

In Chapter 3, we explored the effects of bi-axial confinement on cell cycle progression given the critical role of nuclear shape and mechanics in cell division and cell cycle progression. Our results demonstrate that bi-axial physical confinement reduces the frequency of cell division, which we found to be attributed to an arrest in the S/G2/M phase of the cell cycle and increases the frequency of abnormal division events. Cell and nuclear morphology were both altered in confinement, with the most confining channels preventing cells from undergoing the normal increase in size from G1 to S/G2/M during cell cycle progression. Finally, our results suggest that confinement induces a mechanical memory to the cells, given our observation of lasting effects on cell division and morphology, even after cells exited confinement.

Together, our results provide new insights into the possible impact of mechanical forces on primary and secondary tumor formation and growth. This work motivates research on checkpoint inhibitors or cell cycle regulators to halt tumor cell cycle progression and division. As cells in confinement can retain some control of their cell cycle, harnessing these regulatory pathways may be useful in globally disrupting cancer cell growth. In addition, we suggest an interesting mechanism by which cells acquire genetic abnormalities through abnormal cell divisions in confining environments, which can impart the cells with metastatic capabilities. This motivates

further study of these multinucleated cells or cells with chromosomal abnormalities to garner a broader understanding of metastatic cells themselves.

6.2 Global RNA translation is spatially altered in confinement and contributes to confined migration

In Chapter 4, we found that MDA-MB-231 cells display a different spatial pattern of newly synthesized proteins in confinement, enriching these tagged sequences at the peripheral edges of the cell in comparison to unconfined cells, where the spatial distribution preferentially accumulates around the nucleus. We ruled out diffusion constraints within the microchannels to explain this peripheral accumulation. We further sought to understand the role of global mRNA translation in confined cell migration and found that active translation is required to specify the direction of migration and the magnitude of movement. We proposed a novel 3-D printed microchannel transwell filter insert to collect RNA and protein from cells in confinement to pinpoint what RNA sequences are contributing to confined migration. We designed a novel 3-D printed transwell device to collect confined cell lysate to study RNA and protein alterations within this environment.

Together, this work emphasizes that confined migration requires continuous protein synthesis and motivates exploration of the proteome in cells in confinement. From a clinical standpoint, translation inhibition can be a treatment to halt cancer cell migration during metastasis. Combining translation inhibitors with local treatment strategies could effectively isolate the primary tumor or be used to ensure that

remaining cancer cells after excising the primary tumor are eradicated. In addition, using our confining microchannel transwell devices, further identification of the proteome in confinement can identify novel targets for therapeutic strategies.

6.3 RNA localization in confined cells depends on cellular mechanical activity and contributes to confined migration

In Chapter 5, we explored the role of RNA localization in cells in confinement as different migratory mechanisms can be at play. Here, we demonstrate that peripheral localization of APC-dependent RNAs in cells within confined microchannels is cell type dependent. This varying phenotype is determined by the presence or absence of a fibrillar detyrosinated tubulin network. We show that this network is regulated by mechanoactivity, and that cells with mechanosensitive ion channels and increased myosin II activity direct peripheral localization of the *RAB13* APC-dependent RNA. Through specific mislocalization of the *RAB13* RNA, we show that peripheral RNA localization contributes to confined cell migration.

Our results indicate that a cell's mechanical activity determines its ability to peripherally target RNAs and utilize them for movement in confinement. APC-dependent RNA localization is seen in invading tumor cell strands in mouse models (*266*). Therapeutically, targeting APC-dependent RNA localization can disrupt cancer cell migration and invasion. In addition, further exploration of the mechanical state of the cell and its impact on genetic, proteomic, and behavioral outcomes may be useful for therapeutic treatment development.

6.4 Concluding remarks

In summary, this dissertation expands upon the understanding of cancer cell growth and migration in physiologically relevant mechanically confined environments. Using microfluidic microchannels that model microtracks present in the tumor stroma rich in dense ECM, we investigated the effect of confinement on sarcoma cell cycle progression and division (Chapter 3). We also preliminarily explored the role of global RNA translation in confined migration for cells that employ contractility-independent migration mechanisms in confinement (Chapter 4). We focused in on a specific RNA, *RAB13*, that is enriched in the periphery of migrating cells, to explore the role of altered mechanical environments on its localization and function in confined migration (Chapter 5). Together, this work offers a unique viewpoint by combining biophysical, bioengineering, and biological methodologies to uncover important mechanisms by which cancer cell growth and migration can be modulated by cells traveling through harsh environments.

6.5 Contributions to the field

6.5.1 Contributions to science

- First study of bi-axial confinement on tumor cell cycle progression and division (Chapter 3).

- Determined that bi-axial confinement below 70 μm^2 significantly restricts cell divisions through a block in the S/G2/M stage (Chapter 3).
- Demonstrated that cells do not retain a significant mechanical imprint of bi-axial confinement on cell divisions, morphology, or cell cycle progression (Chapter 3).
- Determined that newly synthesized proteins and ribosomal protein RNAs accumulate at the peripheral edges in response to a confined environment (Chapter 4 & Chapter 5).
- Showed that mRNA translation is necessary for confined cell migration (Chapter 4).
- Showed that peripheral *RAB13* and *KIF1C* RNA localization is cell-type dependent in confined environments (Chapter 5).
- Demonstrated that peripheral *RAB13* RNA localization is dependent on the mechanical state of the cells in confined environments (Chapter 5).
- Determined that peripheral *RAB13* RNA localization contributes to confined cell migration of cells that retain some level of mechanoactivity in confinement (Chapter 5).

6.5.2 Peer-reviewed journal publications

- **RA Moriarty**, S Mili & KM Stroka. "RNA localization in confinement depends on mechanical activity and contributes to confined migration." *iScience* (2021): invited submission, submitted.

- MT Doolin*, **RA Moriarty***, KM Stroka. "Mechanosensing of physical confinement by mesenchymnal-like cells." *Frontiers in Physiology* 11 (2020): 365. *denotes equal contribution.
- **RA Moriarty**, KM Stroka. "Physical confinement alters sarcoma cell cycle progression and division." *Cell Cycle* 17.19-20 (2018): 2360-2373.
- L Yan, **RA Moriarty**, KM Stroka. "Advances in human pluripotent stem cell derived blood brain barrier models." *Theranostics* (2021): in revision.
- MA Shumakovich, CP Mencio, JS Siglin, **RA Moriarty**, H Geller, KM Stroka. "Astrocytes from the Brain Microenvironment Alter Migration and Morphology of Metastatic Breast Cancer Cells." *FASEB Journal* 31.11 (2017): 5049-5067.

6.5.3 Conference presentations

- **RA Moriarty**, KM Stroka & S Mili. "RNA localization and translation contribute to cell migration in confined environments." American Society for Cell Biology Annual Meeting, December 2019. Washington, DC. *poster presentation
- **RA Moriarty,** KM Stroka & S Mili. "Lost in translation? Investigating RNA localization and translation in confined microenvironments." NCI-UMD Partnership for Investigate Cancer Research Symposium, November 2019. College Park, MD. *oral presentation
- **RA Moriarty,** S Mili, KM Stroka. "Lost in translation? Investigating global RNA translation in confined microenvironments." Fischell Department of

Bioengineering Annual Retreat, August 2019. College Park, MD. *oral presentation

- **RA Moriarty**, KM Stroka, S Mili. "RNA translation contributes to cell migration in confinement." NCI RNA Biology Initiative Retreat, February 2019. Rockville, MD. *poster presentation
- **RA Moriarty**, KM Stroka & S Mili. "The role of RNA localization during tumor cell migration in confined spaces." UMD-NCI Partnership for Integrated Cancer Research Annual Symposium, February 2019. Bethesda, MD. *poster presentation
- **RA Moriarty**, KM Stroka. "Physical confinement alters sarcoma cell cycle progression and division." Biomedical Engineering Society Annual Meeting, October 2018. Atlanta, GA. *oral presentation
- **RA Moriarty**, KM Stroka. "Physical confinement alters sarcoma cell cycle progression and division." Fischell Department of Bioengineering Annual Retreat, August 2018. College Park, MD. *oral presentation
- **RA Moriarty,** KM Stroka. "Effect of mechanical confinement on sarcoma cell cycle progression." ResearchFest, June 2018. College Park, MD *poster presentation
- **RA Moriarty**, KM Stroka. "Effect of mechanical confinement on sarcoma cell cycle progression." UMD-NCI Partnership for Integrated Cancer Research Annual Symposium, February 2018. Bethesda, MD. *poster presentation

- **RA Moriarty**, KM Stroka. “Effect of mechanical confinement on sarcoma cell cycle progression.” Cell and Molecular Bioengineering Conference, January 2018. Key Largo, FL. *poster presentation

Chapter 7: Future work and outlook

The goal of this work was to gain a more in-depth understanding of invasive cancer cell behaviors, with a long-term goal to utilize this information to direct novel targeted treatments or therapeutics for the metastatic cancers. As such, we note several open-ended research questions, where future work can continue to explore the mechanisms driving cancer cell growth and altered migration in confined environments.

7.1: The role of the cytoskeleton in disrupting confined cell cycle progression and division

As we explored in Chapter 3, sarcoma cell division became significantly restricted in confined environments, seemingly caused by a cell cycle block in the S/G2/M stage. Previous research using uni-axial confinement had identified that the block occurs in the M stage due to inability of the cell to round up, leading to incorrect spindle capture and abnormal daughter cell geometries (*179*). This rounding is facilitated by both the actin and microtubule cytoskeleton. Interestingly, the cytoskeleton also appears altered in cells in confinement, where in S180 mouse sarcoma cells, the actin network appears diffuse and cells can migrate in confinement despite inhibition of actin polymerization (*154*). As a result, we hypothesize that in our bi-axial confined microchannels that the cell is halted in the M stage due to alterations present in the cytoskeleton in confinement. However, we anticipate that the cancer cells themselves are able to self-regulate in confinement to suppress their divisions. We

propose to use the live-cell SiR-actin and SiR-microtubule probes to image cells progressing through the cell cycle and dividing in confinement (*284*), where we would expect to see phenotypic alterations in one or both cytoskeletal elements. We hypothesize that stabilizing the actin or microtubule network through pharmacological agents may increase the number of divisions within cells in confinement. We would investigate whether the stabilization of the cytoskeleton in confinement, if it does lead to an increase in cell divisions, also results in a greater increase in abnormal divisions. In addition, we can investigate the expression of cyclins present at various stages in the cell cycle to determine the nuclear contribution to controlling cell divisions in confinement.

7.2: The role of mitochondria in confined cell migration

As we showed in Chapter 4, newly synthesized proteins are spatially rearranged in cells in confinement, and they play an integral role in confined cell migration. As translation is a key energy consumer within the cell, we think it would be of note to investigate the role of mitochondria, as the energy producers within the cell. Mitochondria can deform in response to mechanical forces, which ultimately affects their function (*285*, *286*). In invading cancer cells, mitochondria localize to the anterior side of the nucleus, and this corresponds to a higher ATP energy consumption towards the leading edge of the cell (*84*, *196*, *287*, *288*). Mitochondria are trafficked along the microtubule cytoskeleton through association with kinesins (*289*). In addition, cells alter their metabolic consumption when moving through collagen matrices of varying orientations and densities; cells in denser matrices used more energy to promote

migration which was slower than cells in aligned matrices that used less energy to move faster (*195*). During collective invasion, leader and follower cells dynamically rearrange once the leader cells' ATP/ADP ratio falls below a critical threshold (*196*). This is notable as mitochondria accumulate in areas of low ATP/ADP ratios or in areas of high Ca^{2+} accumulation (*290*). Synthesizing these studies, we think it is of interest to study the mitochondrial localization and ATP output for translation purposes of cells in confining environments. We propose that the mitochondria are integral to mRNA translation during confined migration and associate towards the peripheral edges of cells in confinement. To explore the relationship, we can partially inhibit the mitochondria's ATP production through treatment with bedaquiline (*291*) or tether the mitochondria to the ER membrane to understand the relationship between localization and translational function.

7.3: The translatome of cells in confinement

In Chapter 4, we briefly discussed a novel confining device which would facilitate the collection of a cell secretome, RNA, and protein for analysis. We detailed the future testing needed to fabricate and characterize the functionality of the device. Upon certification that it meets our criteria, we will utilize this device to understand the global mRNA and protein landscape within cells in confinement. We hypothesize that there will be an upregulation of certain genes corresponding with altered modes of migration but acknowledge that there may be no significant changes. We also note that comparison of multiple cell lines, and of multiple disease states would be of particular interest here.

In line with this, our results from Chapter 5 demonstrate that *RAB13* mRNA localization is cell type dependent in confined environments. Therefore, we would utilize this device to also test *RAB13* mRNA and protein levels in cells in confined and unconfined environments. Previous results from our lab have identified unique binding partners for RAB13 depending on the location of translation with the cell and could utilize protein pulldowns to study RAB13 binding partners in confined cell lysates. Another way we would like to focus in on the translation of *RAB13* is through the live-cell translation reporters that our lab has developed. Specifically, we would like to test cells in the seeding channel without our microfluidic microchannel devices, watch cells as they enter the microchannels, and then become fully confined. We hypothesize that during entry into the microchannels, the MDA-MB-231 cells will display a change in the RNA localization and, subsequently, local translation of *RAB13*.

7.4: Alterations in mechanoactivity of cells in confinement

As we explored in Chapter 5, the mechanoactivity of cells in confined environments appears to be cell type dependent. Interestingly, this may not correlate to the presence of mechanosensitive ion channels alone, as both cell lines we tested upregulate various mechanosensitive ion channels in confinement (*73*, *200*). In both instances, this can drive an increase in intracellular Ca^{2+} levels in confinement. However, there seems to be a difference in downstream pathways or protein interactions, as the two cell lines ultimately differ in the regulation of the detyrosinated tubulin network. We hypothesize that during entry into confinement, the MDA-MB-

231 cells may upregulate or downregulate unique pathways that ultimately lead to a less mechanically active cytoplasmic environment.

7.5 Outlook

In this dissertation, we explored the effects of physical confinement on tumor cell growth and migration. We provide three key pieces of motivating evidence mechanical cues impact cancer cell behaviors. However, there is a need to provide a more detailed understanding of changes occurring at the sub-cellular and molecular level. We acknowledge that investigating cells in 3-D systems can limit the capability of numerous molecular techniques that were developed and exclusively optimized for 2-D systems. Yet through the integration of biological, physical, and engineering sectors, new solutions can be developed to characterize and image cells in 3-D systems. Together, these 3-D mechanistic studies will explore physiologically relevant cell behaviors and advance the development of metastatic cancer therapeutics.

Appendix

Table 1

	Fraction that Divide		
Degree of Confinement	Mean	Cell Count	ANOVA
2D	0.7	22	A
50 µm	0.23	131	B
20 µm	0.147	227	BC
10 µm	0.155	99	C
6 µm	0.096	202	CD
3 µm	0.05	160	D

Table 2

		Cell Area			Cell Aspect Ratio			Nuclear Area			Nuclear Aspect Ratio		
Cell Cycle Stage	Degree of Confinement	Mean	Cell Count	ANOVA Value	Mean	Cell Count	ANOVA Value	Mean	Cell Count	ANOVA Value	Mean	Cell Count	ANOVA Value
G1	2D	958.27	249	A	3.33	249	GH	171.91	208	E	1.92	208	G
	50 µm	468.91	144	EFG	3.17	144	GH	175.58	203	E	1.97	203	FG
	20 µm	440.73	113	EFG	4.73	101	FG	196.89	138	DE	2.28	138	FG
	10 µm	412.21	78	EFG	6.74	78	F	183.38	67	E	2.85	67	F
	6 µm	328.99	99	G	15.88	99	D	169.92	135	EF	7.1	135	D
	3 µm	576.61	87	CDE	27.65	87	B	172.72	94	EF	11.11	94	B
S/G2/M	2D	1460.17	246	B	2.56	246	H	284.43	194	B	1.83	194	G
	50 µm	759.23	101	C	3.29	101	GH	305.81	93	B	1.93	93	FG
	20 µm	683.2	63	CD	4.98	63	FG	356.93	72	A	2.19	72	FG
	10 µm	541.04	67	DEF	9.09	67	E	279.84	72	BC	4.1	72	E
	6 µm	465.94	60	DEFG	19.47	60	C	239.15	59	CD	10.05	59	C
	3 µm	345.36	87	FG	32.83	87	A	135.09	80	F	15.96	80	A

Table 3

		G1			G2		
Nuclear Axis Length	Degree of Confinement	Mean	Cell Count	ANOVA Value	Mean	Cell Count	ANOVA Value
Major	2D	11.13	150	E	13.8	138	C
	50 µm	13.52	66	D	20.05	46	B
	20 µm	15.84	95	D	22.72	61	B
	10 µm	20.26	38	C	28.03	61	A
	6 µm	28.91	120	B	22.49	56	B
	3 µm	35.36	94	A	28.03	80	A
Minor	2D	5.86	150	FG	7.31	138	E
	50 µm	6.66	66	F	10.42	46	D
	20 µm	7.26	95	F	10.51	61	D
	10 µm	7.3	38	F	6.74	61	E
	6 µm	4.11	120	GH	2.36	56	F
	3 µm	3.37	94	H	1.83	80	F

Table 4

Cell Cycle Stage	Degree of Confinement	Cell Speed			Chemotactic Index		
		Mean	Count	ANOVA Value	Mean	Count	ANOVA Value
G1	2D	38.84	178	G	0.504	178	DE
	50 μm	115.22	162	B	0.51	163	DE
	20 μm	131.4	136	A	0.579	136	CDE
	10 μm	104.55	52	BCD	0.767	52	AB
	6 μm	100.61	51	BCD	0.634	51	ABCD
	3 μm	61.87	86	EF	0.729	86	AB
S/G2/M	2D	40.01	154	G	0.474	154	E
	50 μm	97.87	118	CD	0.531	118	DE
	20 μm	107.33	60	BC	0.611	60	BCDE
	10 μm	82.7	66	DE	0.718	66	ABC
	6 μm	55.2	64	FG	0.789	64	A
	3 μm	49.92	69	FG	0.739	69	AB

Table 5

	Time in Channel			
Cell Cycle Stage	Degree of Confinement	Mean	Cell Count	ANOVA
G1	2D	282	10	EF
	50 μm	316.92	13	F
	20 μm	338.57	7	F
	10 μm	290	10	F
	6 μm	298	10	F
	3 μm	317.78	9	F
S/G2/M	2D	480	7	DE
	50 μm	714.29	7	C
	20 μm	810.19	3	BC
	10 μm	650	2	CD
	6 μm	972.5	4	B
	3 μm	1206	5	A

Table 6

	Fraction that Divide			
	Degree of Confinement	Mean	Cell Count	ANOVA
During Confinement	2D	0.7	22	A
	50 μm	0.23	131	BC
	20 μm	0.15	227	CDE
	10 μm	0.15	99	BCDE
	6 μm	0.1	202	DF
	3 μm	0.05	160	EF
Post-Confinement	50 μm	0.45	7	AB
	20 μm	0.24	10	BCDEF
	10 μm	0.22	13	BCDEF
	6 μm	0.2	10	BCDEF
	3 μm	0.25	29	BCD

Table 7

			Cell Area			Cell Aspect Ratio			Nuclear Area			Nuclear Aspect Ratio		
	Cell Cycle Stage	Degree of Confinement	Mean	Cell Count	ANOVA Value	Hide	Cell Count	ANOVA Value	Mean	Cell Count	ANOVA Value	Mean	Cell Count	ANOVA Value
During Confinement	G1	2D	958.27	249	BC	3.33	249	HI	171.91	208	F	1.92	208	GH
		50 µm	468.91	144	JKL	3.17	144	HI	175.58	203	F	1.97	203	GH
		20 µm	440.73	113	JKL	4.73	101	G	196.89	138	EF	2.28	138	FG
		10 µm	412.21	78	JKL	6.74	78	F	183.38	67	EF	2.85	67	F
		6 µm	328.99	99	L	15.88	99	D	169.92	135	FG	7.1	135	D
		3 µm	576.61	87	KL	27.65	87	B	172.72	94	FG	11.11	94	B
	S/G2/M	2D	1460.17	246	A	2.56	246	HI	284.43	194	B	1.83	194	GH
		50 µm	759.23	101	DEFG	3.29	101	GHI	305.81	93	B	1.93	93	GH
		20 µm	683.2	63	EFGHI	4.98	63	FG	356.93	72	A	2.19	72	FGH
		10 µm	541.04	67	HIJK	9.09	67	E	279.84	72	BC	4.1	72	E
		6 µm	465.94	60	IJKL	19.47	60	C	239.15	59	CD	10.05	59	C
		3 µm	345.36	87	GHIJ	32.83	87	A	135.09	80	GH	15.96	80	A
Post Confinement	G1	2D	958.275	249		3.33	249		171.913	208		1.92	208	
		50 µm	659.085	152	GH	3.73	152	GH	131.195	142	EF	1.89	142	GH
		20 µm	617.658	161	GHI	2.65	161	HI	120.362	170	H	1.63	170	H
		10 µm	693.582	217	GH	2.92	217	HI	127.228	224	H	1.73	224	H
		6 µm	638.496	165	GHI	2.89	165	HI	115.362	191	H	1.88	191	GH
		3 µm	692.144	90	FGH	2.2	90	I	127.827	109	H	1.72	109	GH
	S/G2/M	2D	1460.17	246		2.56	246		284.432	194		1.83	194	
		50 µm	833.568	134	CDEF	2.77	134	HI	182.34	133	EF	1.7	133	GH
		20 µm	920.007	141	BCD	2.13	141	I	209.458	105	DE	1.73	105	GH
		10 µm	869.395	123	CDE	2.61	123	HI	186.341	125	EF	1.79	125	GH
		6 µm	850.348	121	CDEF	2.75	121	HI	181.163	126	EF	1.93	126	GH
		3 µm	1057.62	72	B	2.19	72	HI	189.287	71	EF	1.81	71	GH

Table 8

	Cell Cycle Stage	Degree of Confinement	Cell Speed			Chemotactic Index		
			Mean	Count	ANOVA Value		Count	ANOVA Value
During Confinement	G1	2D	38.84	178	GHI	0.504	178	DEF
		50 µm	115.22	162	B	0.51	163	DEF
		20 µm	131.4	136	A	0.579	136	CDE
		10 µm	104.55	52	BC	0.767	52	AB
		6 µm	100.61	51	BCD	0.634	51	ABCD
		3 µm	61.87	86	E	0.729	86	AB
	S/G2/M	2D	40.01	154	FGH	0.474	154	EF
		50 µm	97.87	118	CD	0.531	118	DEF
		20 µm	107.33	60	BC	0.611	60	BCDE
		10 µm	82.7	66	D	0.718	66	ABC
		6 µm	55.2	64	EF	0.789	64	A
		3 µm	49.92	69	EFG	0.739	69	AB
Post- Confinement	G1	2D	38.84494	178		0.504	178	
		50 µm	38.77073	150	GHI	0.559	150	DEF
		20 µm	32.04606	199	HIJ	0.519	199	D
		10 µm	29.16349	157	HIJ	0.544	157	DEF
		6 µm	26.87913	162	J	0.57	162	DE
		3 µm	28.47004	147	HIJ	0.525	147	DEF
	S/G2/M	2D	40.01398	154		0.474	154	
		50 µm	35.25458	145	GHIJ	0.497	145	DEF
		20 µm	28.38235	146	HIJ	0.519	146	DEF
		10 µm	27.91323	149	IJ	0.509	149	DEF
		6 µm	24.5743	131	J	0.506	131	DEF
		3 µm	24.20096	132	J	0.449	132	F

Table 9

		Time in Channel			
	Cell Cycle Stage	Degree of Confinement	Mean	Cell Count	ANOVA
During Confinement	G1	2D	282	10	F
		50 µm	316.923	13	F
		20 µm	338.571	7	EF
		10 µm	290	10	F
		6 µm	298	10	F
		3 µm	317.778	9	EF
	S/G2/M	2D	480	7	DE
		50 µm	714.286	7	C
		20 µm	810.187	3	BC
		10 µm	650	2	CD
		6 µm	972.5	4	B
		3 µm	1206	5	A
Post- Confinement	G1	2D	282	10	
		50 µm	259.091	11	F
		20 µm	266.667	9	F
		10 µm	370	11	EF
		6 µm	318.889	9	EF
		3 µm	327.5	8	EF
	S/G2/M	2D	480	7	
		50 µm	598.333	6	CD
		20 µm	728.333	6	B
		10 µm	755	6	BC
		6 µm	716.667	6	C
		3 µm	680	2	BCD

Movie 1

Movie 2

Movie 3

Movie 4

Please follow this link to view movies published online.

https://www.tandfonline.com/doi/suppl/10.1080/15384101.2018.1533776

Bibliography

1. R. L. Anderson, T. Balasas, J. Callaghan, R. C. Coombes, J. Evans, J. A. Hall, S. Kinrade, D. Jones, P. S. Jones, R. Jones, J. F. Marshall, M. B. Panico, J. A. Shaw, P. S. Steeg, M. Sullivan, W. Tong, A. D. Westwell, J. W. A. Ritchie, A framework for the development of effective anti-metastatic agents. *Nat. Rev. Clin. Oncol.* **16**, 185–204 (2019).
2. I. Dagogo-Jack, A. T. Shaw, Tumour heterogeneity and resistance to cancer therapies. *Nat. Rev. Clin. Oncol.* **15**, 81–94 (2017).
3. T. N. Seyfried, L. C. Huysentruyt, On the origin of cancer metastasis. *Crit. Rev. Oncog.* **18**, 43–73 (2013).
4. J. Z. Gasiorowski, C. J. Murphy, P. F. Nealey, Biophysical cues and cell behavior: The big impact of little things. *Annu. Rev. Biomed. Eng.* **15**, 155–176 (2013).
5. F. Spill, D. S. Reynolds, R. D. Kamm, M. H. Zaman, Impact of the physical microenvironment on tumor progression and metastasis. *Curr. Opin. Biotechnol.* **40** (2016), pp. 41–48.
6. C. S. Chen, J. Tan, J. Tien, Mechanotransduction at cell-matrix and cell-cell contacts. *Annu. Rev. Biomed. Eng.* **6**, 275–302 (2004).
7. J. Eyckmans, T. Boudou, X. Yu, C. S. Chen, A Hitchhiker's Guide to Mechanobiology. *Dev. Cell*. **21** (2011), pp. 35–47.
8. D. A. Fletcher, R. D. Mullins, Cell mechanics and the cytoskeleton. *Nature*. **463**, 485–492 (2010).
9. B. D. Hoffman, C. Grashoff, M. A. Schwartz, Dynamic molecular processes

mediate cellular mechanotransduction. *Nature*. **475**, 316–323 (2011).

10. T. J. Kirby, J. Lammerding, Emerging views of the nucleus as a cellular mechanosensor. *Nat. Cell Biol.* **20** (2018), pp. 373–381.
11. D. M. Graham, K. Burridge, Mechanotransduction and nuclear function. *Curr. Opin. Cell Biol.* **40**, 98–105 (2016).
12. S. Cho, J. Irianto, D. E. Discher, Mechanosensing by the nucleus: From pathways to scaling relationships. *J. Cell Biol.* **216**, 305–315 (2017).
13. M. E. Dolega, M. Delarue, F. Ingremeau, J. Prost, A. Delon, G. Cappello, Cell-like pressure sensors reveal increase of mechanical stress towards the core of multicellular spheroids under compression. *Nat. Commun.* **8**, 14056 (2017).
14. T. Stylianopoulos, J. D. Martin, V. P. Chauhan, S. R. Jain, B. Diop-Frimpong, N. Bardeesy, B. L. Smith, C. R. Ferrone, F. J. Hornicek, Y. Boucher, L. L. Munn, R. K. Jain, Causes, consequences, and remedies for growth-induced solid stress in murine and human tumors. *PNAS*. **109**, 15101–15108 (2012).
15. S. Alexander, G. E. Koehl, M. Hirschberg, E. K. Geissler, P. Friedl, Dynamic imaging of cancer growth and invasion: a modified skin-fold chamber model. *Histochem. Cell Biol.* **130**, 1147–1154 (2008).
16. P. Friedl, S. Alexander, Cancer Invasion and the Microenvironment: Plasticity and Reciprocity. *Cell*. **147**, 992–1009 (2011).
17. S. Alexander, B. Weigelin, F. Winkler, P. Friedl, Preclinical intravital microscopy of the tumour-stroma interface: Invasion, metastasis, and therapy response. *Curr. Opin. Cell Biol.* **25**, 659–671 (2013).
18. B. Weigelin, G.-J. Bakker, P. Friedl, Intravital third harmonic generation

microscopy of collective melanoma cell invasion. *IntraVital*. **1**, 32–43 (2012).

19. Y. Kienast, L. Von Baumgarten, M. Fuhrmann, W. E. F. Klinkert, R. Goldbrunner, J. Herms, F. Winkler, Real-time imaging reveals the single steps of brain metastasis formation. *Nat. Med.* **16**, 116–122 (2010).

20. K. Yamauchi, M. Yang, P. Jiang, M. Xu, N. Yamamoto, H. Tsuchiya, K. Tomita, A. R. Moossa, M. Bouvet, R. M. Hoffman, Development of real-time subcellular dynamic multicolor imaging of cancer-cell trafficking in live mice with a variable-magnification whole-mouse imaging system. *Cancer Res.* **66**, 4208–4214 (2006).

21. R. L. Siegel, K. D. Miller, A. Jemal, Cancer statistics, 2016. *CA. Cancer J. Clin.* **66**, 7–30 (2016).

22. P. S. Steeg, Tumor metastasis: mechanistic insights and clinical challenges. *Nat. Med.* **12**, 895–904 (2006).

23. B. De Craene, G. Berx, Regulatory networks defining EMT during cancer initiation and progression. *Nat. Rev. Cancer*. **13**, 97–110 (2013).

24. S. Orsulic, Y. Li, R. A. Soslow, L. A. Vitale-Cross, J. S. Gutkind, H. E. Varmus, Induction of ovarian cancer by defined multiple genetic changes in a mouse model system. *Cancer Cell*. **1**, 53–62 (2002).

25. F. Sanchez-Vega, M. Mina, J. Armenia, W. K. Chatila, A. Luna, K. C. La, S. Dimitriadoy, D. L. Liu, H. S. Kantheti, S. Saghafinia, D. Chakravarty, F. Daian, Q. Gao, M. H. Bailey, W. W. Liang, S. M. Foltz, I. Shmulevich, L. Ding, Z. Heins, A. Ochoa, B. Gross, J. Gao, H. Zhang, R. Kundra, C. Kandoth, I. Bahceci, L. Dervishi, U. Dogrusoz, W. Zhou, H. Shen, P. W. Laird, G. P.

Way, C. S. Greene, H. Liang, Y. Xiao, C. Wang, A. Iavarone, A. H. Berger, T. G. Bivona, A. J. Lazar, G. D. Hammer, T. Giordano, L. N. Kwong, G. McArthur, C. Huang, A. D. Tward, M. J. Frederick, F. McCormick, M. Meyerson, E. M. Van Allen, A. D. Cherniack, G. Ciriello, C. Sander, N. Schultz, Oncogenic Signaling Pathways in The Cancer Genome Atlas. *Cell*. **173**, 321-337.e10 (2018).

26. H. Takeshima, T. Ushijima, Accumulation of genetic and epigenetic alterations in normal cells and cancer risk. *npj Precis. Oncol.* **3**, 1–8 (2019).

27. D. Hanahan, R. A. Weinberg, The hallmarks of cancer. *Cell*. **100**, 57–70 (2000).

28. C. Compton, in *Cancer: The Enemy from Within* (Springer International Publishing, 2020; https://doi.org/10.1007/978-3-030-40651-6_2), pp. 25–48.

29. K. Polyak, R. Kalluri, The role of the microenvironment in mammary gland development and cancer. *Cold Spring Harb Perspect Biol*. **2**, a003244 (2010).

30. X. Qin, T. Li, S. Li, H. Yang, C. Wu, C. Zheng, F. You, Y. Liu, The tumor biochemical and biophysical microenvironments synergistically contribute to cancer cell malignancy. *Cell. Mol. Immunol.* **17**, 1186–1187 (2020).

31. M. J. Oudin, V. M. Weaver, Physical and chemical gradients in the tumor microenvironment regulate tumor cell invasion, migration, and metastasis. *Cold Spring Harb. Symp. Quant. Biol.* **81**, 189–205 (2016).

32. H. Y. Jung, L. Fattet, J. Yang, Molecular pathways: Linking tumor microenvironment to Epithelial-mesenchymal transition in metastasis. *Clin. Cancer Res.* **21**, 962–968 (2015).

33. J. Roche, The Epithelial-to-Mesenchymal Transition in Cancer. *Cancers (Basel).* **10**, 52 (2018).

34. T. F. Gajewski, Y. Meng, C. Blank, I. Brown, A. Kacha, J. Kline, H. Harlin, Immune resistance orchestrated by the tumor microenvironment. *Immunol. Rev.* **213** (2006), pp. 131–145.

35. P. Chiarugi, P. Cirri, Metabolic exchanges within tumor microenvironment. *Cancer Lett.* **380** (2016), pp. 272–280.

36. K. E. Allison, B. L. Coomber, B. W. Bridle, Metabolic reprogramming in the tumour microenvironment: a hallmark shared by cancer cells and T lymphocytes. *Immunology*. **152**, 175–184 (2017).

37. D. J. McGrail, Q. M. N. Kieu, J. A. Iandoli, M. R. Dawson, Actomyosin tension as a determinant of metastatic cancer mechanical tropism. *Phys. Biol.* **12** (2015), doi:10.1088/1478-3975/12/2/026001.

38. M. S. Samuel, J. I. Lopez, E. J. McGhee, D. R. Croft, D. Strachan, P. Timpson, J. Munro, E. Schröder, J. Zhou, V. G. Brunton, N. Barker, H. Clevers, O. J. Sansom, K. I. Anderson, V. M. Weaver, M. F. Olson, Actomyosin-Mediated Cellular Tension Drives Increased Tissue Stiffness and β-Catenin Activation to Induce Epidermal Hyperplasia and Tumor Growth. *Cancer Cell*. **19**, 776–791 (2011).

39. H. Qazi, Z.-D. Shi, J. M. Tarbell, Fluid Shear Stress Regulates the Invasive Potential of Glioma Cells via Modulation of Migratory Activity and Matrix Metalloproteinase Expression. *PLoS One*. **6**, e20348 (2011).

40. Y. Boucher, L. T. Baxter, R. K. Jain, “Interstitial Pressure Gradients in Tissue-

isolated and Subcutaneous Tumors: Implications for Therapy" (1990), (available at http://cancerres.aacrjournals.org/content/canres/50/15/4478.full.pdf).

41. M. C. Lampi, C. A. Reinhart-King, Targeting extracellular matrix stiffness to attenuate disease: From molecular mechanisms to clinical trials. *Sci. Transl. Med.* **10**, eaao0475 (2018).

42. J. Rodriguez, M. Muñoz, L. Vives, C. G. Frangou, M. Groudine, M. A. Peinado, Bivalent domains enforce transcriptional memory of DNA methylated genes in cancer cells. *Proc. Natl. Acad. Sci. U. S. A.* **105**, 19809–14 (2008).

43. S. Nasrollahi, C. Walter, A. J. Loza, G. V. Schimizzi, G. D. Longmore, A. Pathak, Past matrix stiffness primes epithelial cells and regulates their future collective migration through a mechanical memory. *Biomaterials*. **146**, 146–155 (2017).

44. B. B. Silver, C. M. Nelson, The Bioelectric Code: Reprogramming Cancer and Aging From the Interface of Mechanical and Chemical Microenvironments. *Front. Cell Dev. Biol.* **6**, 21 (2018).

45. C. Yang, M. W. Tibbitt, L. Basta, K. S. Anseth, Mechanical memory and dosing influence stem cell fate. *Nat. Mater.* **13**, 645–652 (2014).

46. I. Carnevale, M. Capula, E. Giovannetti, T. Schmidt, S. Coppola, A mechanical memory of pancreatic cancer cells. *bioRxiv*, 1–6 (2019).

47. A. W. Watson, A. D. Grant, S. S. Parker, M. W. Harman, M. R. Roman, B. L. Uhlorn, C. Gowan, R. Castro-Portuguez, L. K. Stolze, C. Franck, D. A. Cusanovich, M. Padi, C. E. Romanoski, G. Mouneimne, Breast Tumor

Stiffness Instructs Bone Metastasis Via Mechanical Memory. *Cell Rep.*, 1–17 (2020).

48. J. Mathur, V. Shenoy, A. Pathak, *bioRxiv*, in press, doi:10.1101/2020.03.20.000802.

49. T. Stylianopoulos, J. D. Martin, V. P. Chauhan, S. R. Jain, B. Diop-Frimpong, N. Bardeesy, B. L. Smith, C. R. Ferrone, F. J. Hornicek, Y. Boucher, L. L. Munn, R. K. Jain, Causes, consequences, and remedies for growth-induced solid stress in murine and human tumors. *PNAS*. **109**, 15101–15108 (2012).

50. Y. Boucher, L. T. Baxter, R. K. Jain, Interstitial pressure gradients in tissue-isolated and subcutaneous tumors: implications for therapy. *Cancer Res.* **50**, 4478–84 (1990).

51. S. Nasrollahi, A. Pathak, Topographic confinement of epithelial clusters induces epithelial-to-mesenchymal transition in compliant matrices. *Sci. Rep.* **6**, 18831 (2016).

52. S. Jain, V. M. L. Cachoux, G. H. N. S. Narayana, S. de Beco, J. D'Alessandro, V. Cellerin, T. Chen, M. L. Heuzé, P. Marcq, R. M. Mège, A. J. Kabla, C. T. Lim, B. Ladoux, The role of single-cell mechanical behaviour and polarity in driving collective cell migration. *Nat. Phys.* **16**, 802–809 (2020).

53. C. D. Paul, P. Mistriotis, K. Konstantopoulos, Cancer cell motility: Lessons from migration in confined spaces. *Nat. Rev. Cancer*. **17** (2017), pp. 131–140.

54. N. Walter, A. Micoulet, T. Seufferlein, J. P. Spatz, Direct assessment of living cell mechanical responses during deformation inside microchannel restrictions. *Biointerphases*. **6**, 117–125 (2011).

55. R. J. Petrie, H. Koo, *Curr. Protoc. Cell Biol.*, in press, doi:10.1002/0471143030.cb1209s63.

56. L. Milovanovic, H. Ma, Method for measurement of friction forces on single cells in microfluidic devices. *Anal. Methods*. **4**, 4303–4309 (2012).

57. P. S. Raman, C. D. Paul, K. M. Stroka, K. Konstantopoulos, Probing cell traction forces in confined microenvironments. *Lab Chip*. **13**, 4599 (2013).

58. E. Desvignes, A. Bouissou, A. Laborde, T. Mangeat, A. Proag, C. Vieu, C. Thibault, I. Maridonneau-Parini, R. Poincloux, Nanoscale Forces during Confined Cell Migration. *Nano Lett.* **18**, 6326–6333 (2018).

59. K. Wolf, M. te Lindert, M. Krause, S. Alexander, J. te Riet, A. L. Willis, R. M. Hoffman, C. G. Figdor, S. J. Weiss, P. Friedl, Physical limits of cell migration: Control by ECM space and nuclear deformation and tuning by proteolysis and traction force. *J. Cell Biol.* **201**, 1069–1084 (2013).

60. E. Zamir, B. Geiger, Molecular complexity and dynamics of cell-matrix adhesions. *J. Cell Sci.* **114**, 3583–3590 (2001).

61. M. L. Gardel, I. C. Schneider, Y. Aratyn-Schaus,, C. M. Waterman, Mechanical Integration of Actin and Adhesion Dynamics in Cell Migration. *Annu. Rev. Cell Dev. Biol.* **26**, 315–333 (2010).

62. W. R. Legant, J. S. Miller, B. L. Blakely, D. M. Cohen, G. M. Genin, C. S. Chen, Measurement of mechanical tractions exerted by cells in three-dimensional matrices. *Nat. Methods*. **7**, 969–971 (2010).

63. A. D. Doyle, M. L. Kutys, M. A. Conti, K. Matsumoto, R. S. Adelstein, K. M. Yamada, Micro-environmental control of cell migration - myosin IIA is

required for efficient migration in fibrillar environments through control of cell adhesion dynamics. *J. Cell Sci.* **125**, 2244–2256 (2012).

64. E. Cukierman, R. Pankov, D. R. Stevens, K. M. Yamada, Taking cell-matrix adhesions to the third dimension. *Science*. **294**, 1708–12 (2001).

65. S. I. Fraley, Y. Feng, R. Krishnamurthy, D. Kim, A. Celedon, G. D. Longmore, D. Wirtz, S. Louis, A distinctive role for focal adhesion proteins in three-dimensional cell motility. *Nat. Cell Biol.* **12**, 598–604 (2010).

66. E. M. Balzer, Z. Tong, C. D. Paul, W.-C. Hung, K. M. Stroka, A. E. Boggs, S. S. Martin, K. Konstantopoulos, Physical confinement alters tumor cell adhesion and migration phenotypes. *FASEB J.* **26**, 4045–56 (2012).

67. M. Bao, J. Xie, A. Piruska, W. T. S. Huck, 3D microniches reveal the importance of cell size and shape. *Nat. Commun.* **8**, 1–12 (2017).

68. W.-C. Hung, S.-H. Chen, C. D. Paul, K. M. Stroka, Y.-C. Lo, J. T. Yang, K. Konstantopoulos, Distinct signaling mechanisms regulate migration in unconfined versus confined spaces. *J. Cell Biol.* **202**, 807–24 (2013).

69. B. Pontes, P. Monzo, L. Gole, A.-L. Le Roux, A. J. Kosmalska, Z. Y. Tam, W. Luo, S. Kan, V. Viasnoff, P. Roca-Cusachs, L. Tucker-Kellogg, N. C. Gauthier, *J. Cell Biol.*, in press, doi:10.1083/jcb.201611117.

70. A. R. Houk, A. Jilkine, C. O. Mejean, R. Boltyanskiy, E. R. Dufresne, S. B. Angenent, S. J. Altschuler, L. F. Wu, O. D. Weiner, Membrane Tension Maintains Cell Polarity by Confining Signals to the Leading Edge during Neutrophil Migration. *Cell*. **148**, 175–188 (2012).

71. A. D. Doyle, K. M. Yamada, Mechanosensing via cell-matrix adhesions in 3D

microenvironments. *Exp. Cell Res.* **343**, 60–66 (2016).

72. C. T. Mierke, D. P. Zitterbart, P. Kollmannsberger, C. Raupach, U. Schlötzer-Schrehardt, T. W. Goecke, J. Behrens, B. Fabry, Breakdown of the endothelial barrier function in tumor cell transmigration. *Biophys. J.* **94**, 2832–46 (2008).

73. W.-C. Hung, J. R. Yang, C. L. Yankaskas, B. S. Wong, P.-H. Wu, C. Pardo-Pastor, S. A. Serra, M.-J. Chiang, Z. Gu, D. Wirtz, M. A. Valverde, J. T. Yang, J. Zhang, K. Konstantopoulos, Confinement Sensing and Signal Optimization via Piezo1/PKA and Myosin II Pathways. *Cell Rep.* **15**, 1430–1441 (2016).

74. Y.-W. Heng, C.-G. Koh, Actin cytoskeleton dynamics and the cell division cycle. *Int. J. Biochem. Cell Biol.* **42**, 1622–1633 (2010).

75. K. Salaita, P. M. Nair, R. S. Petit, R. M. Neve, D. Das, J. W. Gray, J. T. Groves, Restriction of receptor movement alters cellular response: physical force sensing by EphA2. *Science*. **327**, 1380–5 (2010).

76. C. F. Natale, M. Ventre, P. A. Netti, Tuning the material-cytoskeleton crosstalk via nanoconfinement of focal adhesions. *Biomaterials*. **35**, 2743–2751 (2014).

77. B. Willipinski-Stapelfeldt, S. Riethdorf, V. Assmann, U. Woelfle, T. Rau, G. Sauter, J. Heukeshoven, K. Pantel, Changes in Cytoskeletal Protein Composition Indicative of an Epithelial-Mesenchymal Transition in Human Micrometastatic and Primary Breast Carcinoma Cells. *Clin. Cancer Res.* **11**, 8006–8014 (2005).

78. D. W. Dumbauld, T. T. Lee, A. Singh, J. Scrimgeour, C. A. Gersbach, E. A. Zamir, J. Fu, C. S. Chen, J. E. Curtis, S. W. Craig, A. J. García, A. J. G. Designed, J. S. Performed, S. W. C. Contributed, How vinculin regulates force

transmission. **110** (2013), doi:10.1073/pnas.1216209110.

79. R. Windoffer, M. Beil, T. M. Magin, R. E. Leube, Cytoskeleton in motion: The dynamics of keratin intermediate filaments in epithelia. *J. Cell Biol.* **194**, 669–678 (2011).

80. J. Kim, H. Jo, H. Hong, M. H. Kim, J. M. Kim, J.-K. Lee, W. Do Heo, J. Kim, Actin remodelling factors control ciliogenesis by regulating YAP/TAZ activity and vesicle trafficking. *Nat. Commun.* **6**, 6781 (2015).

81. C. Rianna, M. Radmacher, S. Kumar, Direct Evidence that Tumor Cells Soften when Navigating Confined Spaces. *Mol. Biol. Cell*, mbcE19100588 (2020).

82. C. A. Carter, G. P. Parham, T. Chambers, Cytoskeletal Reorganization Induced by Retinoic Acid Treatment of Human Endometrial Adenocarcinoma (RL95-2) Cells Is Correlated with Alterations in Protein Kinase C-α. *Pathobiology*. **66**, 284–292 (1998).

83. D.-H. Kim, S. Cho, D. Wirtz, Tight coupling between nucleus and cell migration through the perinuclear actin cap. *J. Cell Sci.* **127**, 2528–2541 (2014).

84. S. P. Desai, S. N. Bhatia, M. Toner, D. Irimia, Mitochondrial Localization and the Persistent Migration of Epithelial Cancer cells. *Biophys. J.* **104**, 2077–2088 (2013).

85. K. Wang, A. Bruce, R. Mezan, A. Kadiyala, L. Wang, J. Dawson, Y. Rojanasakul, Y. Yang, Nanotopographical Modulation of Cell Function through Nuclear Deformation. *ACS Appl. Mater. Interfaces*. **8**, 5082–5092 (2016).

86. K. Haase, J. K. L. Macadangdang, C. H. Edrington, C. M. Cuerrier, S. Hadjiantoniou, J. L. Harden, I. S. Skerjanc, A. E. Pelling, Extracellular Forces Cause the Nucleus to Deform in a Highly Controlled Anisotropic Manner. *Sci. Rep.* **6**, 21300 (2016).

87. Doolin, Ornstein, Stroka, Nuclear Deformation in Response to Mechanical Confinement is Cell Type Dependent. *Cells*. **8**, 427 (2019).

88. P. M. Davidson, C. Denais, M. C. Bakshi, J. Lammerding, Nuclear Deformability Constitutes a Rate-Limiting Step During Cell Migration in 3-D Environments. *Cell. Mol. Bioeng.* **7**, 293–306 (2014).

89. Y. Fu, L. K. Chin, T. Bourouina, A. Q. Liu, A. M. J. Vandongen, Nuclear deformation during breast cancer cell transmigration. *Lab Chip*. **12**, 3774–3778 (2012).

90. B. Enyedi, P. Niethammer, Nuclear membrane stretch and its role in mechanotransduction. *Nucleus*. **8**, 156–161 (2017).

91. S. B. Khatau, R. J. Bloom, S. Bajpai, D. Razafsky, S. Zang, A. Giri, P.-H. Wu, J. Marchand, A. Celedon, C. M. Hale, S. X. Sun, D. Hodzic, D. Wirtz, The distinct roles of the nucleus and nucleus-cytoskeleton connections in three-dimensional cell migration. *Sci. Rep.* **2**, 488 (2012).

92. E. M. Hatch, M. W. Hetzer, Nuclear envelope rupture is induced by actin-based nucleus confinement. *J. Cell Biol.* **215** (2016), doi:10.1083/jcb.201603053.

93. C. M. Denais, R. M. Gilbert, P. Isermann, A. L. McGregor, M. te Lindert, B. Weigelin, P. M. Davidson, P. Friedl, K. Wolf, J. Lammerding, Nuclear

envelope rupture and repair during cancer cell migration. *Science*. **352** (2016), doi:10.1126/science.aad7297.

94. M. Raab, M. Gentili, H. de Belly, H. R. Thiam, P. Vargas, A. J. Jimenez, F. Lautenschlaeger, R. Voituriez, A. M. Lennon-Duménil, N. Manel, M. Piel, ESCRT III repairs nuclear envelope ruptures during cell migration to limit DNA damage and cell death. *Science*. **352**, 359–62 (2016).

95. X. Cao, E. Moeendarbary, P. Isermann, P. M. Davidson, X. Wang, M. B. Chen, A. K. Burkart, J. Lammerding, R. D. Kamm, V. B. Shenoy, A Chemomechanical Model for Nuclear Morphology and Stresses during Cell Transendothelial Migration. *Biophys. J.* **111**, 1541–1552 (2016).

96. K.-H. Chow, R. E. Factor, K. S. Ullman, The nuclear envelope environment and its cancer connections. *Nat. Rev. Cancer*. **12**, 196–209 (2012).

97. E. Infante, A. Castagnino, R. Ferrari, P. Monteiro, S. Agüera-González, P. Paul-Gilloteaux, M. J. Domingues, P. Maiuri, M. Raab, C. M. Shanahan, A. Baffet, M. Piel, E. R. Gomes, P. Chavrier, LINC complex-Lis1 interplay controls MT1-MMP matrix digest-on-demand response for confined tumor cell migration. *Nat. Commun.* **9**, 2443 (2018).

98. D. G. Thomas, A. Yenepalli, C. M. Denais, A. Rape, J. R. Beach, Y. li Wang, W. P. Schiemann, H. Baskaran, J. Lammerding, T. T. Egelhoff, Non-muscle myosin IIB is critical for nuclear translocation during 3D invasion. *J. Cell Biol.* (2015), doi:10.1083/jcb.201502039.

99. P. T. Arsenovic, I. Ramachandran, K. Bathula, R. Zhu, J. D. Narang, N. A. Noll, C. A. Lemmon, G. G. Gundersen, D. E. Conway, Nesprin-2G, a

Component of the Nuclear LINC Complex, Is Subject to Myosin-Dependent Tension. *Biophys. J.* **110**, 34–43 (2016).

100. G. Uzer, W. R. Thompson, B. Sen, Z. Xie, S. S. Yen, S. Miller, G. Bas, M. Styner, C. T. Rubin, S. Judex, K. Burridge, J. Rubin, Cell Mechanosensitivity to Extremely Low-Magnitude Signals Is Enabled by a LINCed Nucleus. *Stem Cells*. **33**, 2063–2076 (2015).

101. T. P. Driscoll, B. D. Cosgrove, S.-J. Heo, Z. E. Shurden, R. L. Mauck, Cytoskeletal to Nuclear Strain Transfer Regulates YAP Signaling in Mesenchymal Stem Cells. *Biophys. J.* **108**, 2783–2793 (2015).

102. J. Kind, L. Pagie, H. Ortabozkoyun, S. Boyle, S. S. De Vries, H. Janssen, M. Amendola, L. D. Nolen, W. A. Bickmore, B. Van Steensel, Single-cell dynamics of genome-nuclear lamina interactions. *Cell*. **153**, 178–192 (2013).

103. J. Lammerding, P. C. Schulze, T. Takahashi, S. Kozlov, T. Sullivan, R. D. Kamm, C. L. Stewart, R. T. Lee, Lamin A / C deficiency causes defective nuclear mechanics and mechanotransduction. *J. Clin. Invest.* **113**, 370–378 (2004).

104. J. Irianto, C. R. Pfeifer, R. R. Bennett, Y. Xia, I. L. Ivanovska, A. J. Liu, R. A. Greenberg, D. E. Discher, Nuclear constriction segregates mobile nuclear proteins away from chromatin. *Mol. Biol. Cell*. **27**, 4011–4020 (2016).

105. E. Makhija, D. S. Jokhun, G. V Shivashankar, Nuclear deformability and telomere dynamics are regulated by cell geometric constraints. *Proc. Natl. Acad. Sci. U. S. A.* **113**, E32-40 (2015).

106. I. Bronshtein, E. Kepten, I. Kanter, S. Berezin, M. Lindner, A. B. Redwood, S.

Mai, S. Gonzalo, R. Foisner, Y. Shav-Tal, Y. Garini, Loss of lamin A function increases chromatin dynamics in the nuclear interior. *Nat. Commun.* **6**, 8044 (2015).

107. K. Damodaran, S. Venkatachalapathy, F. Alisafaei, A. V. Radhakrishnan, D. S. Jokhun, V. B. Shenoy, G. V. Shivashankar, Compressive force induces reversible chromatin condensation and cell geometry–dependent transcriptional response. *Mol. Biol. Cell*. **29**, 3039–3051 (2018).

108. M. Le Berre, J. Aubertin, M. Piel, Fine control of nuclear confinement identifies a threshold deformation leading to lamina rupture and induction of specific genes. *Integr. Biol.* **4**, 1406 (2012).

109. B. Roy, S. Venkatachalapathy, P. Ratna, Y. Wang, D. S. Jokhun, M. Nagarajan, G. V. Shivashankar, Laterally confined growth of cells induces nuclear reprogramming in the absence of exogenous biochemical factors. *Proc. Natl. Acad. Sci. U. S. A.* **115**, E4741–E4750 (2018).

110. K. M. Stroka, Z. Gu, S. X. Sun, K. Konstantopoulos, Bioengineering paradigms for cell migration in confined microenvironments. *Curr. Opin. Cell Biol.* **30**, 41–50 (2014).

111. C. D. Paul, W.-C. Hung, D. Wirtz, K. Konstantopoulos, Engineered Models of Confined Cell Migration. *Annu. Rev. Biomed. Eng.* **18**, 159–180 (2016).

112. M. Junkin, P. K. Wong, Probing cell migration in confined environments by plasma lithography. *Biomaterials*. **32**, 1848–1855 (2011).

113. J. Yul Lim, H. J. Donahue, Cell Sensing and Response to Micro-and Nanostructured Surfaces Produced by Chemical and Topographic Patterning.

Tissue Eng. **13** (2004), doi:10.1089/ten.2006.0154.

114. A. D. Doyle, F. W. Wang, K. Matsumoto, K. M. Yamada, One-dimensional topography underlies three-dimensional fibrillar cell migration. *J. Cell Biol.* **184**, 481–490 (2009).

115. S. S. Chang, W.-H. Guo, Y. Kim, Y.-L. Wang, Guidance of Cell Migration by Substrate Dimension. *Biophys. J.* **104**, 313–321 (2013).

116. A. Ray, O. Lee, Z. Win, R. M. Edwards, P. W. Alford, D.-H. Kim, P. P. Provenzano, Anisotropic forces from spatially constrained focal adhesions mediate contact guidance directed cell migration. *Nat. Commun.* **8**, 14923 (2017).

117. A. I. Teixeira, Epithelial contact guidance on well-defined micro- and nanostructured substrates. *J. Cell Sci.* **116**, 1881–1892 (2003).

118. H. Zhang, R. Hou, P. Xiao, R. Xing, T. Chen, Y. Han, P. Ren, J. Fu, Single cell migration dynamics mediated by geometric confinement. *Colloids Surfaces B Biointerfaces*. **145**, 72–78 (2016).

119. D. Kim, K. Han, K. Gupta, K. W. Kwon, K.-Y. Suh, A. Levchenko, Mechanosensitivity of fibroblast cell shape and movement to anisotropic substratum topography gradients. *Biomaterials*. **30**, 5433–5444 (2009).

120. C. D. Paul, D. J. Shea, M. R. Mahoney, A. Chai, V. Laney, W. C. Hung, K. Konstantopoulos, Interplay of the physical microenvironment, contact guidance, and intracellular signaling in cell decision making. *FASEB J.* **30**, 2161–2170 (2016).

121. J. Ballester-Beltrán, M. Lebourg, M. Salmerón-Sánchez, Dorsal and ventral

stimuli in sandwich-like microenvironments. Effect on cell differentiation. *Biotechnol. Bioeng.* **110**, 3048–3058 (2013).

122. M. Le Berre, E. Zlotek-Zlotkiewicz, D. Bonazzi, F. Lautenschlaeger, M. Piel, Methods for two-dimensional cell confinement. *Methods Cell Biol.* **121**, 213–229 (2014).

123. P. M. Davidson, J. Sliz, P. Isermann, C. Denais, J. Lammerding, Design of a microfluidic device to quantify dynamic intra-nuclear deformation during cell migration through confining environments. *Integr. Biol.* **7**, 1534–1546 (2015).

124. C. G. Rolli, T. Seufferlein, R. Kemkemer, J. P. Spatz, Impact of Tumor Cell Cytoskeleton Organization on Invasiveness and Migration: A Microchannel-Based Approach. *PLoS One*. **5**, e8726 (2010).

125. M. A. Shumakovich, C. P. Mencio, J. S. Siglin, R. A. Moriarty, H. M. Geller, K. M. Stroka, Astrocytes from the brain microenvironment alter migration and morphology of metastatic breast cancer cells. *FASEB J.* **31**, 5049–5067 (2017).

126. D. Irimia, M. Toner, Spontaneous migration of cancer cells under conditions of mechanical confinement. *Integr. Biol.* **1**, 506–12 (2009).

127. B. Koch, A. K. Meyer, L. Helbig, S. M. Harazim, A. Storch, S. Sanchez, O. G. Schmidt, Dimensionality of Rolled-up Nanomembranes Controls Neural Stem Cell Migration Mechanism. *Nano Lett.* **15**, 5530–5538 (2015).

128. Z. Tong, E. M. Balzer, M. R. Dallas, W.-C. Hung, K. J. Stebe, K. Konstantopoulos, Chemotaxis of Cell Populations through Confined Spaces at Single-Cell Resolution. *PLoS One*. **7** (2012), doi:10.1371/journal.pone.0029211.

129. W. Xi, C. K. Schmidt, S. Sanchez, D. H. Gracias, R. E. Carazo-Salas, S. P. Jackson, O. G. Schmidt, Rolled-up functionalized nanomembranes as three-dimensional cavities for single cell studies. *Nano Lett.* **14**, 4197–4204 (2014).

130. J. K. Fisher, N. Kleckner, Magnetic force micropiston: An integrated force/microfluidic device for the application of compressive forces in a confined environment. *Rev. Sci. Instrum.* **85**, 1–6 (2014).

131. S. T. Spagnol, W.-C. Lin, E. A. Booth, B. Ladoux, H. M. Lazarus, K. N. Dahl, Early Passage Dependence of Mesenchymal Stem Cell Mechanics Influences Cellular Invasion and Migration. *Ann. Biomed. Eng.* **44**, 2123–2131 (2016).

132. Y. Alapan, M. Younesi, O. Akkus, U. A. Gurkan, Cell-Aligning Substrates: Anisotropically Stiff 3D Micropillar Niche Induces Extraordinary Cell Alignment and Elongation (Adv. Healthcare Mater. 15/2016). *Adv. Healthc. Mater.* **5**, 1833–1833 (2016).

133. E. A. Booth-Gauthier, V. Du, M. Ghibaudo, A. D. Rape, K. N. Dahl, B. Ladoux, Hutchinson-Gilford progeria syndrome alters nuclear shape and reduces cell motility in three dimensional model substrates. *Integr. Biol. (United Kingdom)*. **5**, 569–577 (2013).

134. M. T. Doolin, K. M. Stroka, Integration of Mesenchymal Stem Cells into a Novel Micropillar Confinement Assay. *Tissue Eng. Part C Methods*. **25**, 662–676 (2019).

135. A. Pathak, S. Kumar, Independent regulation of tumor cell migration by matrix stiffness and confinement. *Proc. Natl. Acad. Sci.* **109**, 10334–10339 (2012).

136. C. M. Kraning-Rush, S. P. Carey, M. C. Lampi, C. A. Reinhart-King,

Microfabricated collagen tracks facilitate single cell metastatic invasion in 3D. *Integr. Biol.* **5**, 606 (2013).

137. O. Ilina, G.-J. Bakker, A. Vasaturo, R. M. Hoffman, P. Friedl, Two-photon laser-generated microtracks in 3D collagen lattices: principles of MMP-dependent and -independent collective cancer cell invasion. *Phys. Biol.* **8**, 029501–029501 (2011).

138. A. L. Carlson, C. a. Florek, J. J. Kim, T. Neubauer, J. C. Moore, R. I. Cohen, J. Kohn, M. Grumet, P. V. Moghe, Microfibrous substrate geometry as a critical trigger for organization, self-renewal, and differentiation of human embryonic stem cells within synthetic 3-dimensional microenvironments. *FASEB J.* **26**, 3240–3251 (2012).

139. A. D. Doyle, N. Carvajal, A. Jin, K. Matsumoto, K. M. Yamada, Local 3D matrix microenvironment regulates cell migration through spatiotemporal dynamics of contractility-dependent adhesions. *Nat. Commun.* **6**, 8720 (2015).

140. N. Peela, F. S. Sam, W. Christenson, D. Truong, A. W. Watson, G. Mouneimne, R. Ros, M. Nikkhah, A three dimensional micropatterned tumor model for breast cancer cell migration studies. *Biomaterials*. **81**, 72–83 (2016).

141. N. Luciani, V. Du, F. Gazeau, A. Richert, D. Letourneur, C. Le Visage, C. Wilhelm, Successful chondrogenesis within scaffolds, using magnetic stem cell confinement and bioreactor maturation. *Acta Biomater.* **37**, 101–110 (2016).

142. D. Robert, D. Fayol, C. Le Visage, G. Frasca, S. Brulé, C. Ménager, F. Gazeau, D. Letourneur, C. Wilhelm, Magnetic micro-manipulations to probe the local physical properties of porous scaffolds and to confine stem cells. *Biomaterials*.

31, 1586–1595 (2010).

143. F. A. Pennacchio, C. Fedele, S. De Martino, S. Cavalli, R. Vecchione, P. A. Netti, Three-Dimensional Microstructured Azobenzene-Containing Gelatin as a Photoactuable Cell Confining System. *ACS Appl. Mater. Interfaces*. **10**, 91–97 (2018).

144. M. A. Kinney, T. A. Hookway, Y. Wang, T. C. McDevitt, Engineering Three-Dimensional Stem Cell Morphogenesis for the Development of Tissue Models and Scalable Regenerative Therapeutics. *Ann. Biomed. Eng.* **42**, 352–367 (2014).

145. H.-C. Chen, Boyden chamber assay. *Methods Mol. Biol.* **294**, 15–22 (2005).

146. S. M. Hamilla, K. M. Stroka, H. Aranda-Espinoza, VE-cadherin-independent cancer cell incorporation into the vascular endothelium precedes transmigration. *PLoS One*. **9**, e109748 (2014).

147. K. M. Stroka, H. N. Hayenga, H. Aranda-Espinoza, Human Neutrophil Cytoskeletal Dynamics and Contractility Actively Contribute to Trans-Endothelial Migration. *PLoS One*. **8** (2013), doi:10.1371/journal.pone.0061377.

148. M. A. Pranda, K. M. Gray, A. J. L. DeCastro, G. M. Dawson, J. W. Jung, K. M. Stroka, Tumor Cell Mechanosensing During Incorporation into the Brain Microvascular Endothelium. *Cell. Mol. Bioeng.* **12**, 455–480 (2019).

149. E. K. Paluch, I. M. Aspalter, M. Sixt, Focal Adhesion–Independent Cell Migration. *Annu. Rev. Cell Dev. Biol*. **32**, 469–90 (2016).

150. R. J. Petrie, K. M. Yamada, Fibroblasts Lead the Way: A Unified View of 3D

Cell Motility. *Trends Cell Biol.* **25**, 666–674 (2015).

151. A. Lynn McGregor, C.-R. Hsia, J. Lammerding, Squish and squeeze-the nucleus as a physical barrier during migration in confined environments. *Curr. Opin. Cell Biol.* **40**, 32–40 (2016).

152. A. J. S. Ribeiro, P. Khanna, A. Sukumar, C. Dong, K. N. Dahl, Nuclear Stiffening Inhibits Migration of Invasive Melanoma Cells. *Cell. Mol. Bioeng.* **7**, 544–551 (2014).

153. M. Tozluoğlu, A. L. Tournier, R. P. Jenkins, S. Hooper, P. A. Bates, E. Sahai, Matrix geometry determines optimal cancer cell migration strategy and modulates response to interventions. *Nat. Cell Biol.* **15** (2013), doi:10.1038/ncb2775.

154. K. M. Stroka, H. Jiang, S.-H. Chen, Z. Tong, D. Wirtz, S. X. Sun, K. Konstantopoulos, Water Permeation Drives Tumor Cell Migration in Confined Microenvironments. *Cell*. **157**, 611–623 (2014).

155. H. V. Prentice-Mott, C.-H. Chang, L. Mahadevan, T. J. Mitchison, D. Irimia, J. V. Shah, Biased migration of confined neutrophil-like cells in asymmetric hydraulic environments. *Proc. Natl. Acad. Sci.* **110**, 21006–21011 (2013).

156. R. J. Petrie, H. Koo, K. M. Yamada, Generation of compartmentalized pressure by a nuclear piston governs cell motility in a 3D matrix. *Science*. **345**, 1062–1065 (2014).

157. A. Ray, Z. M. Slama, R. K. Morford, S. A. Madden, P. P. Provenzano, Enhanced Directional Migration of Cancer Stem Cells in 3D Aligned Collagen Matrices. *Biophys. J.* **112**, 1023–1036 (2017).

158. M. Bergert, A. Erzberger, R. A. Desai, I. M. Aspalter, A. C. Oates, G. Charras, G. Salbreux, E. K. Paluch, Force transmission during adhesion-independent migration. *Nat. Cell Biol.* **17**, 524–529 (2015).

159. A. Rahman-Zaman, S. Shan, C. A. Reinhart-King, Cell Migration in Microfabricated 3D Collagen Microtracks is Mediated through the Prometastatic Protein Girdin. *Cell. Mol. Bioeng.* **11**, 1–10 (2018).

160. A. Jayo, M. Malboubi, S. Antoku, W. Chang, E. Ortiz-Zapater, C. Groen, K. Pfisterer, T. Tootle, G. Charras, G. G. Gundersen, M. Parsons, Fascin Regulates Nuclear Movement and Deformation in Migrating Cells. *Dev. Cell*. **38**, 371–383 (2016).

161. S. P. Carey, A. Rahman, C. M. Kraning-Rush, B. Romero, S. Somasegar, O. M. Torre, R. M. Williams, C. A. Reinhart-King, Comparative mechanisms of cancer cell migration through 3D matrix and physiological microtracks. *Am. J. Physiol. - Cell Physiol.* **308**, C436–C447 (2015).

162. H. P. Lee, F. Alisafaei, K. Adebawale, J. Chang, V. B. Shenoy, O. Chaudhuri, The nuclear piston activates mechanosensitive ion channels to generate cell migration paths in confining microenvironments. *Sci. Adv.* **7** (2021), doi:10.1126/sciadv.abd4058.

163. R. J. Petrie, H. M. Harlin, L. I. T. Korsak, K. M. Yamada, Activating the nuclear piston mechanism of 3D migration in tumor cells. *J. Cell Biol.* **216**, 93–100 (2017).

164. A. Pathak, Scattering of Cell Clusters in Confinement. *Biophys. J.* **111**, 1496–1506 (2016).

165. D. F. Milano, N. A. Ngai, S. K. Muthuswamy, A. R. Asthagiri, Regulators of Metastasis Modulate the Migratory Response to Cell Contact under Spatial Confinement. *Biophys. J.* **110**, 1886–1895 (2016).

166. A. Guzman, M. J. Ziperstein, L. J. Kaufman, The effect of fibrillar matrix architecture on tumor cell invasion of physically challenging environments. *Biomaterials*. **35**, 6954–6963 (2014).

167. A. Haeger, M. Krause, K. Wolf, P. Friedl, Cell jamming: Collective invasion of mesenchymal tumor cells imposed by tissue confinement. *BBA - Gen. Subj.* **1840**, 2386–2395 (2014).

168. J. M. Tse, G. Cheng, J. A. Tyrrell, S. A. Wilcox-Adelman, Y. Boucher, R. K. Jain, L. L. Munn, Mechanical compression drives cancer cells toward invasive phenotype. *PNAS.* **109**, 911–916 (2012).

169. S. Kumar, R. Kulkarni, S. Sen, Cell motility and ECM proteolysis regulate tumor growth and tumor relapse by altering the fraction of cancer stem cells and their spatial scattering. *Phys. Biol.* **13** (2016), doi:10.1088/1478-3975/13/3/036001.

170. O. Ilina, L. Campanello, P. G. Gritsenko, M. Vullings, C. Wang, P. Bult, W. Losert, P. Friedl, Intravital microscopy of collective invasion plasticity in breast cancer. *Dis. Model. Mech.* **11**, dmm034330 (2018).

171. D. L. Adams, D. K. Adams, S. Stefansson, C. Haudenschild, S. S. Martin, M. Charpentier, S. Chumsri, M. Cristofanilli, C.-M. Tang, R. K. Alpaugh, Mitosis in circulating tumor cells stratifies highly aggressive breast carcinomas. *Breast Cancer Res.* **18**, 44 (2016).

172. A. B. Al-Mehdi, K. Tozawa, A. B. Fisher, L. Shientag, A. Lee, R. J. Muschel, Intravascular origin of metastasis from the proliferation of endothelium-attached tumor cells: a new model for metastasis. *Nat. Med.* **6**, 100–102 (2000).

173. D. Gvaramia, E. Müller, K. Müller, P. Atallah, M. Tsurkan, U. Freudenberg, M. Bornhäuser, C. Werner, Combined influence of biophysical and biochemical cues on maintenance and proliferation of hematopoietic stem cells. *Biomaterials*. **138**, 108–117 (2017).

174. B. Koch, S. Sanchez, C. K. Schmidt, A. Swiersy, S. P. Jackson, O. G. Schmidt, Confinement and Deformation of Single Cells and Their Nuclei Inside Size-Adapted Microtubes. *Adv. Healthc. Mater.* **3**, 1753–1758 (2014).

175. A. Desmaison, L. Guillaume, S. Triclin, P. Weiss, B. Ducommun, V. Lobjois, Impact of physical confinement on nuclei geometry and cell division dynamics in 3D spheroids. *Sci. Rep.* **8** (2018), doi:10.1038/s41598-018-27060-6.

176. R. A. Moriarty, K. M. Stroka, Physical confinement alters sarcoma cell cycle progression and division. *Cell Cycle*. **17**, 2360–2373 (2018).

177. C. R. Pfeifer, Y. Xia, K. Zhu, D. Liu, J. Irianto, V. M. Morales García, L. M. Santiago Millán, B. Niese, S. Harding, D. Deviri, R. A. Greenberg, D. E. Discher, Constricted migration increases DNA damage and independently represses cell cycle. *Mol. Biol. Cell*. **29**, 1948–1962 (2018).

178. Y. Xia, C. R. Pfeifer, K. Zhu, J. Irianto, D. Liu, K. Pannell, E. J. Chen, L. J. Dooling, M. P. Tobin, M. Wang, I. L. Ivanovska, L. R. Smith, R. A. Greenberg, D. E. Discher, Rescue of DNA damage after constricted migration

reveals a mechano-regulated threshold for cell cycle. *J. Cell Biol.* **218**, 2542–2563 (2019).

179. O. Lancaster, M. LeBerre, A. Dimitracopoulos, D. Bonazzi, E. Zlotek-Zlotkiewicz, R. Picone, T. Duke, M. Piel, B. Baum, Mitotic Rounding Alters Cell Geometry to Ensure Efficient Bipolar Spindle Formation. *Dev. Cell*. **25**, 270–283 (2013).

180. H. T. K. Tse, W. M. Weaver, D. Carlo, Increased asymmetric and multi-daughter cell division in mechanically confined microenvironments. *PLoS One*. **7**, 1–8 (2012).

181. Z. Weihua, Q. Lin, A. J. Ramoth, D. Fan, I. J. Fidler, Formation of solid tumors by a single multinucleated cancer cell. *Cancer*. **117**, 4092–4099 (2011).

182. C. Cadart, E. Zlotek-Zlotkiewicz, M. Le Berre, M. Piel, H. K. Matthews, Exploring the function of cell shape and size during mitosis. *Dev. Cell*. **29**, 159–169 (2014).

183. A. G. Clark, E. Paluch, in *Cell Cycle in Development*, J. Z. Kubiak, Ed. (Springer Berlin Heidelberg, Berlin, Heidelberg, 2011; https://doi.org/10.1007/978-3-642-19065-0_3), pp. 31–73.

184. M. Théry, M. Bornens, Cell shape and cell division. *Curr. Opin. Cell Biol.* **18**, 648–657 (2006).

185. A. Sartorio Gehren, M. Ramos Rocha, W. Fernandes de Souza, J. Andrés Morgado-Díaz, J. Andr es Morgado-Díaz, Alterations of the apical junctional complex and actin cytoskeleton and their role in colorectal cancer progression. *Tissue Barriers* (2015), doi:10.1080/21688370.2015.1017688.

186. S. Woolner, L. L. O'Brien, C. Wiese, W. M. Bement, Myosin-10 and actin filaments are essential for mitotic spindle function. *J. Cell Biol.* **182**, 77–88 (2008).

187. A. L. Miller, The contractile ring. *Curr. Biol.* **21**, R976-8 (2011).

188. M. Chircop, Rho GTPases as regulators of mitosis and cytokinesis in mammalian cells. *Small GTPases*. **5** (2014), doi:10.4161/sgtp.29770.

189. S. P. Ramanathan, J. Helenius, M. P. Stewart, C. J. Cattin, A. A. Hyman, D. J. Muller, Cdk1-dependent mitotic enrichment of cortical myosin II promotes cell rounding against confinement. *Nat. Cell Biol.* **17**, 148–159 (2015).

190. M. Miyazaki, M. Chiba, H. Eguchi, T. Ohki, S. Ishiwata, Cell-sized spherical confinement induces the spontaneous formation of contractile actomyosin rings in vitro. *Nat. Cell Biol.* **17**, 480–489 (2015).

191. M. Barisic, R. Silva e Sousa, S. K. Tripathy, M. M. Magiera, A. V Zaytsev, A. L. Pereira, C. Janke, E. L. Grishchuk, H. Maiato, Mitosis. Microtubule detyrosination guides chromosomes during mitosis. *Science*. **348**, 799–803 (2015).

192. M. Barisic, H. Maiato, Cracking the (tubulin) code of mitosis. *Oncotarget*. **6**, 19356–7 (2015).

193. S. Nam, O. Chaudhuri, Mitotic cells generate protrusive extracellular forces to divide in three-dimensional microenvironments. *Nat. Phys.* **14**, 621–628 (2018).

194. L. Trilla-Fuertes, A. Gámez-Pozo, J. M. Arevalillo, M. Díaz-Almirón, G. Prado-Vázquez, A. Zapater-Moros, H. Navarro, R. Aras-López, I. Dapía, R.

López-Vacas, P. Nanni, S. Llorente-Armijo, P. Arias, A. M. Borobia, P. Maín, J. Feliú, E. Espinosa, J. Á. Fresno Vara, Molecular characterization of breast cancer cell response to metabolic drugs. *Oncotarget*. **9**, 9645–9660 (2018).

195. M. R. Zanotelli, Z. E. Goldblatt, J. P. Miller, F. Bordeleau, J. Li, J. A. VanderBurgh, M. C. Lampi, M. R. King, C. A. Reinhart-King, Regulation of ATP utilization during metastatic cell migration by collagen architecture. *Mol. Biol. Cell*. **29**, 1–9 (2018).

196. J. Zhang, K. F. Goliwas, W. Wang, P. V. Taufalele, F. Bordeleau, C. A. Reinhart-King, Energetic regulation of coordinated leader–follower dynamics during collective invasion of breast cancer cells. *PNAS*. **116**, 7867–7872 (2019).

197. M. Carmo-Fonseca, The Contribution of Nuclear Compartmentalization to Gene Regulation. *Cell*. **108**, 513–521 (2002).

198. J. Irianto, Y. Xia, C. R. Pfeifer, A. Athirasala, J. Ji, C. Alvey, M. Tewari, R. R. Bennett, S. M. Harding, A. J. Liu, R. A. Greenberg, D. E. Discher, DNA Damage Follows Repair Factor Depletion and Portends Genome Variation in Cancer Cells after Pore Migration. *Curr. Biol.* **27**, 210–223 (2017).

199. A. Elosegui-Artola, I. Andreu, A. E. M. Beedle, A. Lezamiz, M. Uroz, A. J. Kosmalska, R. Oria, J. Z. Kechagia, P. Rico-Lastres, A. L. Le Roux, C. M. Shanahan, X. Trepat, D. Navajas, S. Garcia-Manyes, P. Roca-Cusachs, Force Triggers YAP Nuclear Entry by Regulating Transport across Nuclear Pores. *Cell*. **171**, 1397–1410 (2017).

200. R. Zhao, A. Afthinos, T. Zhu, P. Mistriotis, Y. Li, S. A. Serra, Y. Zhang, C. L.

Yankaskas, S. He, M. A. Valverde, S. X. Sun, K. Konstantopoulos, Cell sensing and decision-making in confinement: The role of TRPM7 in a tug of war between hydraulic pressure and cross-sectional area. *Sci. Adv.* **5** (2019), doi:10.1126/sciadv.aaw7243.

201. R. W. Tilghman, C. R. Cowan, J. D. Mih, Y. Koryakina, D. Gioeli, J. K. Slack-Davis, B. R. Blackman, D. J. Tschumperlin, J. T. Parsons, Matrix Rigidity Regulates Cancer Cell Growth and Cellular Phenotype. *PLoS One*. **5**, e12905 (2010).

202. J. D. Mih, A. Marinkovic, F. Liu, A. S. Sharif, D. J. Tschumperlin, Matrix stiffness reverses the effect of actomyosin tension on cell proliferation. *J. Cell Sci.* **125**, 5974–83 (2012).

203. D. Wirtz, K. Konstantopoulos, P. C. Searson, The physics of cancer: the role of physical interactions and mechanical forces in metastasis. *Nat. Rev. Cancer*. **11**, 512–522 (2011).

204. A. Pathak, S. Kumar, Independent regulation of tumor cell migration by matrix stiffness and confinement. *Proc. Natl. Acad. Sci.* **109**, 10334–10339 (2012).

205. M. Tozluoğlu, A. L. Tournier, R. P. Jenkins, S. Hooper, P. A. Bates, E. Sahai, Matrix geometry determines optimal cancer cell migration strategy and modulates response to interventions. *Nat. Cell Biol.* **15**, 751–762 (2013).

206. H. V Prentice-Mott, C.-H. Chang, L. Mahadevan, T. J. Mitchison, D. Irimia, J. V Shah, Biased migration of confined neutrophil-like cells in asymmetric hydraulic environments. *Proc. Natl. Acad. Sci.* **110**, 21006–21011 (2013).

207. C. M. Denais, R. M. Gilbert, P. Isermann, A. L. McGregor, M. te Lindert, B.

Weigelin, P. M. Davidson, P. Friedl, K. Wolf, J. Lammerding, Nuclear envelope rupture and repair during cancer cell migration. *Science*. **352**, 353–8 (2016).

208. A. L. McGregor, C.-R. Hsia, J. Lammerding, Squish and squeeze — the nucleus as a physical barrier during migration in confined environments. *Curr. Opin. Cell Biol.* **40**, 32–40 (2016).

209. V. Baldin, J. Lukas, M. J. Marcote, M. Pagano, G. Draetta, Cyclin D1 is a nuclear protein required for cell cycle progression in G1. *Genes Dev.* **7**, 812–21 (1993).

210. M. Boehm, T. Yoshimoto, M. F. Crook, S. Nallamshetty, A. True, G. J. Nabel, E. G. Nabel, A growth factor-dependent nuclear kinase phosphorylates p27(Kip1) and regulates cell cycle progression. *EMBO J.* **21**, 3390–401 (2002).

211. H.-Y. Joo, L. Zhai, C. Yang, S. Nie, H. Erdjument-Bromage, P. Tempst, C. Chang, H. Wang, Regulation of cell cycle progression and gene expression by H2A deubiquitination. *Nature*. **449**, 1068–1072 (2007).

212. H.-W. Lo, M.-C. Hung, Nuclear EGFR signalling network in cancers: linking EGFR pathway to cell cycle progression, nitric oxide pathway and patient survival. *Br. J. Cancer*. **94**, 184–188 (2006).

213. K. Fujise, D. Zhang, J. Liu, E. T. Yeh, Regulation of apoptosis and cell cycle progression by MCL1. Differential role of proliferating cell nuclear antigen. *J. Biol. Chem.* **275**, 39458–65 (2000).

214. M. Karin, Nuclear factor-κB in cancer development and progression. *Nature*. **441**, 431–436 (2006).

215. B. Ren, H. Cam, Y. Takahashi, T. Volkert, J. Terragni, R. A. Young, B. D. Dynlacht, E2F integrates cell cycle progression with DNA repair, replication, and G(2)/M checkpoints. *Genes Dev.* **16**, 245–56 (2002).

216. A. G. Clark, E. Paluch, in *Cell Cycle in Development. Results and Problems in Cell Differentiation.*, J. Kubiak, Ed. (Springer Berlin Heidelberg, 2011; http://link.springer.com/10.1007/978-3-642-19065-0_3), pp. 31–73.

217. K. Esmaeili Pourfarhangi, E. Cardenas De La Hoz, A. R. Cohen, B. Gligorijevic, Contact guidance is cell cycle-dependent. *APL Bioeng.* **2**, 031904 (2018).

218. R. Baserga, The Relationship of the Cell Cycle to Tumor Growth and Control of Cell Division: A Review. *Cancer Res.* **25**, 581–595 (1965).

219. D. L. Adams, D. K. Adams, S. Stefansson, C. Haudenschild, S. S. Martin, M. Charpentier, S. Chumsri, M. Cristofanilli, C.-M. Tang, R. K. Alpaugh, Mitosis in circulating tumor cells stratifies highly aggressive breast carcinomas. *Breast Cancer Res.* **18**, 44 (2016).

220. A. B. Al-Mehdi, K. Tozawa, A. B. Fisher, L. Shientag, A. Lee, R. J. Muschel, Intravascular origin of metastasis from the proliferation of endothelium-attachedtumor cells: a new model for metastasis. *Nat. Med.* **6**, 100–102 (2000).

221. L. He, A. Sneider, W. Chen, M. Karl, V. Prasath, P. H. Wu, G. Mattson, D. Wirtz, Mammalian Cell Division in 3D Matrices via Quantitative Confocal Reflection Microscopy. *J. Vis. Exp*, 56364 (2017).

222. L. He, W. Chen, P.-H. Wu, A. Jimenez, B. S. Wong, A. San, K. Konstantopoulos, D. Wirtz, Local 3D matrix confinement determines division

axis through cell shape. *Oncotarget*. **7**, 6994–7011 (2015).

223. J. Fink, N. Carpi, T. Betz, A. Bétard, M. Chebah, A. Azioune, M. Bornens, C. Sykes, L. Fetler, D. Cuvelier, M. Piel, External forces control mitotic spindle positioning. *Nat. Cell Biol.* **13**, 771–778 (2011).

224. M. T. Doolin, K. M. Stroka, Physical confinement alters cytoskeletal contributions towards human mesenchymal stem cell migration. *Cytoskeleton*. **75**, 103–117 (2018).

225. Y. A. Miroshnikova, M. M. Nava, S. A. Wickström, Emerging roles of mechanical forces in chromatin regulation. *J. Cell Sci.* **130**, 2243–2250 (2017).

226. Y. Li, L. He, N. A. P. Gonzalez, J. Graham, C. Wolgemuth, D. Wirtz, S. X. Sun, Going with the Flow: Water Flux and Cell Shape during Cytokinesis. *Biophys. J.* **113**, 2487–2495 (2017).

227. B. J. Van Meer, H. De Vries, K. S. A. Firth, J. Van Weerd, L. G. J. Tertoolen, H. B. J. Karperien, P. Jonkheijm, C. Denning, A. P. Ijzerman, C. L. Mummery, Small molecule absorption by PDMS in the context of drug response bioassays. *Biochem. Biophys. Res. Commun.* **482**, 323–328 (2017).

228. G. W. Pearson, Control of Invasion by Epithelial-to-Mesenchymal Transition Programs during Metastasis. *J. Clin. Med.* **8**, 646 (2019).

229. B. Emon, J. Bauer, Y. Jain, B. Jung, T. Saif, Biophysics of Tumor Microenvironment and Cancer Metastasis - A Mini Review. *Comput. Struct. Biotechnol. J.* **16**, 279–287 (2018).

230. S. Kumar, V. M. Weaver, Mechanics, malignancy, and metastasis: The force journey of a tumor cell. *Cancer Metastasis Rev.* **28**, 113–127 (2009).

231. M. Raab, M. Raab, M. Gentili, H. De Belly, H. R. Thiam, P. Vargas, A. J. Jimenez, F. Lautenschlaeger, N. Manel, M. Piel, ESCRT III repairs nuclear envelope ruptures during cell migration to limit DNA damage and cell death. *Science*. **7611**, 359–363 (2016).

232. Y.-J. Liu, M. Le Berre, F. Lautenschlaeger, P. Maiuri, A. Callan-Jones, M. Heuzé, T. Takaki, R. Voituriez, M. Piel, Confinement and Low Adhesion Induce Fast Amoeboid Migration of Slow Mesenchymal Cells. *Cell*. **160**, 659–672 (2015).

233. K. Wolf, I. Mazo, H. Leung, K. Engelke, U. H. von Andrian, E. I. Deryugina, A. Y. Strongin, E.-B. Bröcker, P. Friedl, Compensation mechanism in tumor cell migration: mesenchymal-amoeboid transition after blocking of pericellular proteolysis. *J. Cell Biol.* **160**, 267–77 (2003).

234. R. H. Insall, L. M. Machesky, Actin Dynamics at the Leading Edge: From Simple Machinery to Complex Networks. *Dev. Cell*. **17**, 310–322 (2009).

235. A. J. Ridley, Life at the leading edge. *Cell*. **145**, 1012–1022 (2011).

236. Y. Oleynikov, R. H. Singer, Real-time visualization of ZBP1 association with β-actin mRNA during transcription and localization. *Curr. Biol.* **13**, 199–207 (2003).

237. L. A. Mingle, N. N. Okuhama, J. Shi, R. H. Singer, John Condeelis, G. Liu, Localization of all seven messenger RNAs for the actin-polymerization nucleator Arp2/3 complex in the protrusions of fibroblasts. *J. Cell Sci.* **118**, 2425–2433 (2005).

238. B. Wu, A. R. Buxbaum, Z. B. Katz, Y. J. Yoon, R. H. Singer, Quantifying

Protein-mRNA Interactions in Single Live Cells. *Cell*. **162**, 211–220 (2015).

239. M. E. Chicurel, R. H. Singer, C. J. Meyer, D. E. Ingber, Integrin binding and mechanical tension induce movement of mRNA and ribosomes to focal adhesions. *Nature*. **392**, 730–733 (1998).

240. S. Mili, K. Moissoglu, I. G. Macara, Genome-wide screen reveals APC-associated RNAs enriched in cell protrusions. *Nature*. **453**, 115–9 (2008).

241. K. Moissoglu, K. Yasuda, T. Wang, G. Chrisafis, S. Mili, Translational regulation of protrusion-localized RNAs involves silencing and clustering after transport. *Elife*. **8** (2019), doi:10.7554/eLife.44752.

242. K. Moissoglu, M. Stueland, A. N. Gasparski, T. Wang, L. M. Jenkins, M. L. Hastings, S. Mili, RNA localization and co-translational interactions control RAB13 GTPase function and cell migration. *EMBO J.* **39**, 1–19 (2020).

243. F. K. Mardakheh, A. Paul, S. Kü, A. Mccarthy, Y. Yuan, C. J. M. Correspondence, Global Analysis of mRNA, Translation, and Protein Localization: Local Translation Is a Key Regulator of Cell Protrusions. *Dev. Cell*. **35**, 344–357 (2015).

244. A. David, B. P. Dolan, H. D. Hickman, J. J. Knowlton, G. Clavarino, P. Pierre, J. R. Bennink, J. W. Yewdell, Nuclear translation visualized by ribosome-bound nascent chain puromycylation. *J. Cell Biol.* **197**, 45–57 (2012).

245. A. Gandalovičová, D. Rosel, M. Fernandes, P. Veselý, P. Heneberg, V. Čermák, L. Petruželka, S. Kumar, V. Sanz-Moreno, J. Brábek, Migrastatics—Anti-metastatic and Anti-invasion Drugs: Promises and Challenges. *Trends in Cancer*. **3**, 391–406 (2017).

246. M. Leibovitch, I. Topisirovic, Dysregulation of mRNA translation and energy metabolism in cancer. *Adv. Biol. Regul.* **67**, 30–39 (2018).

247. G.-W. Li, D. Burkhardt, C. Gross, J. S. Weissman, Quantifying absolute protein synthesis rates reveals principles underlying allocation of cellular resources. *Cell*. **157**, 624–35 (2014).

248. K. Yang, J. Yang, J. Yi, Nucleolar stress: Hallmarks, sensing mechanism and diseases. *Cell Stress*. **2**, 125–140 (2018).

249. T. Wang, S. Hamilla, M. Cam, H. Aranda-Espinoza, S. Mili, Extracellular matrix stiffness and cell contractility control RNA localization to promote cell migration. *Nat. Commun.* **8**, 896 (2017).

250. M. Dermit, M. Dodel, F. C. Y. Lee, M. S. Azman, H. Schwenzer, J. L. Jones, S. P. Blagden, J. Ule, F. K. Mardakheh, Subcellular mRNA Localization Regulates Ribosome Biogenesis in Migrating Cells. *Dev. Cell*. **55**, 298-313.e10 (2020).

251. K. Nakayama, N. Kataoka, Regulation of gene expression under hypoxic conditions. *Int. J. Mol. Sci.* **20** (2019), doi:10.3390/ijms20133278.

252. L. J. Simpson, E. Tzima, J. S. Reader, Mechanical Forces and Their Effect on the Ribosome and Protein Translation Machinery. *Cells*. **9**, 650 (2020).

253. Q. Shen, T. Hill, X. Cai, L. Bui, R. Barakat, E. Hills, T. Almugaiteeb, A. Babu, P. H. Mckernan, M. Zalles, J. D. Battiste, Y. T. Kim, Physical confinement during cancer cell migration triggers therapeutic resistance and cancer stem cell-like behavior. *Cancer Lett.* **506**, 142–151 (2021).

254. L. Bui, Q. Shen, T. Hill, S. H. Bhuiyan, R. Barakat, V. Saavedra, C. Kong, J.

D. Battiste, Y. T. Kim, Microchannel device for proteomic analysis of migrating cancer cells. *Biomed. Phys. Eng. Express*. **4**, 065026 (2018).

255. S. P. Herbert, G. Costa, Sending messages in moving cells: MRNA localization and the regulation of cell migration. *Essays Biochem.* **63** (2019), pp. 595–606.

256. C. Andreassi, A. Riccio, To localize or not to localize: mRNA fate is in 3′UTR ends. *Trends Cell Biol.* **19** (2009), pp. 465–474.

257. R. P. Jansen, mRNA localization: Message on the move. *Nat. Rev. Mol. Cell Biol.* **2**, 247–256 (2001).

258. C. Medioni, K. Mowry, F. Besse, Principles and roles of mRNA localization in animal development. *Dev.* **139** (2012), pp. 3263–3276.

259. S. L. Bullock, Cellular Cytoskeletal Motor Proteins Messengers, motors and mysteries: sorting of eukaryotic mRNAs by cytoskeletal transport. *Biochem. Soc. Trans.* **39**, 1161–1165 (2011).

260. X. Pichon, K. Moissoglu, E. Coleno, T. Wang, A. Imbert, M. Peter, R. Chouaib, T. Walter, F. Mueller, K. Zibara, E. Bertrand, S. Mili, The kinesin KIF1C transports APC-dependent mRNAs to cell protrusions. *bioRxiv* (2020), doi:10.1101/2020.11.30.403394.

261. K. Yasuda, S. F. Clatterbuck-Soper, M. E. Jackrel, J. Shorter, S. Mili, FUS inclusions disrupt RNA localization by sequestering kinesin-1 and inhibiting microtubule detyrosination. *J. Cell Biol.* **216**, 1015–1034 (2017).

262. T. Song, Y. Zheng, Y. Wang, Z. Katz, X. Liu, S. Chen, R. H. Singer, W. Gu, Specific interaction of KIF11 with ZBP1 regulates the transport of β-actin mRNA and cell motility. *J. Cell Sci.* **128**, 1001–1010 (2015).

263. V. C. Nalavadi, L. E. Griffin, P. Picard-Fraser, A. M. Swanson, T. Takumi, G. J. Bassell, Regulation of zipcode binding protein 1 transport dynamics in axons by myosin va. *J. Neurosci.* **32**, 15133–15141 (2012).

264. J. Condeelis, R. H. Singer, How and why does β-actin mRNA target? *Biol. Cell*. **97**, 97–110 (2005).

265. E. A. Shestakova, R. H. Singer, J. Condeelis, The physiological significance of β-actin mRNA localization in determining cell polarity and directional motility. *Proc. Natl. Acad. Sci.* **98**, 7045–7050 (2002).

266. G. Chrisafis, T. Wang, K. Moissoglu, A. N. Gasparski, Y. Ng, R. Weigert, S. J. Lockett, S. Mili, Collective cancer cell invasion requires RNA accumulation at the invasive front. *Proc. Natl. Acad. Sci. U. S. A.* **117**, 27423–27434 (2020).

267. G. Costa, J. J. Bradbury, N. Tarannum, S. P. Herbert, RAB13 mRNA compartmentalisation spatially orients tissue morphogenesis. *EMBO J.* **39** (2020), doi:10.15252/embj.2020106003.

268. B. Geiger, J. P. Spatz, A. D. Bershadsky, Environmental sensing through focal adhesions. *Nat. Rev. Mol. Cell Biol.* **10** (2009), pp. 21–33.

269. M. A. Schwartz, Integrins and extracellular matrix in mechanotransduction. *Cold Spring Harb Perspect Biol* (2010), doi:10.2147/CHC.S21829.

270. D. E. Discher, P. Janmey, Y. L. Wang, Tissue cells feel and respond to the stiffness of their substrate. *Science*. **310**, 1139–1143 (2005).

271. K. Zaoui, S. Honoré, D. Isnardon, D. Braguer, A. Badache, Memo - RhoA - mDia1 signaling controls microtubules, the actin network, and adhesion site formation in migrating cells. *J. Cell Biol.* **183**, 401–408 (2008).

272. F. Bartolini, L. Andres-Delgado, X. Qu, S. Nik, N. Ramalingam, L. Kremer, M. A. Alonso, G. G. Gundersen, An mDia1-INF2 formin activation cascade facilitated by IQGAP1 regulates stable microtubules in migrating cells. *Mol. Biol. Cell*. **27**, 1797–1808 (2016).

273. F. Bartolini, G. G. Gundersen, Formins and microtubules. *Biochim. Biophys. Acta - Mol. Cell Res.* **1803** (2010), pp. 164–173.

274. M. Stueland, T. Wang, H. Y. Park, S. Mili, RDI Calculator: An Analysis Tool to Assess RNA Distributions in Cells. *Sci. Rep.* **9**, 1–10 (2019).

275. H. Y. Park, T. Trcek, A. L. Wells, J. A. Chao, R. H. Singer, An Unbiased Analysis Method to Quantify mRNA Localization Reveals Its Correlation with Cell Motility. *Cell Rep.* **1**, 179–184 (2012).

276. S. Dupont, L. Morsut, M. Aragona, E. Enzo, S. Giulitti, M. Cordenonsi, F. Zanconato, J. Le Digabel, M. Forcato, S. Bicciato, N. Elvassore, S. Piccolo, Role of YAP/TAZ in mechanotransduction. *Nature*. **474**, 179–183 (2011).

277. F. Sachs, Stretch-activated ion channels: What are they? *Physiology*. **25**, 50–56 (2010).

278. E. Tkachenko, M. Sabouri-Ghomi, O. Pertz, C. Kim, E. Gutierrez, M. MacHacek, A. Groisman, G. Danuser, M. H. Ginsberg, Protein kinase A governs a RhoA-RhoGDI protrusion-retraction pacemaker in migrating cells. *Nat. Cell Biol.* **13**, 660–668 (2011).

279. E. C. Lessey, C. Guilluy, K. Burridge, From mechanical force to RhoA activation. *Biochemistry*. **51**, 7420–7432 (2012).

280. J. Canales, D. Morales, C. Blanco, J. Rivas, N. Diaz, I. Angelopoulos, O.

Cerda, A tr(i)p to cell migration: New roles of trp channels in mechanotransduction and cancer. *Front. Physiol.* **10**, 1–14 (2019).

281. C. Pardo-Pastor, F. Rubio-Moscardo, M. Vogel-González, S. A. Serra, A. Afthinos, S. Mrkonjic, O. Destaing, J. F. Abenza, J. M. Fernández-Fernández, X. Trepat, C. Albiges-Rizo, K. Konstantopoulos, M. A. Valverde, Piezo2 channel regulates RhoA and actin cytoskeleton to promote cell mechanobiological responses. *Proc. Natl. Acad. Sci.* **115**, 1925–1930 (2018).

282. A. E. Moor, M. Golan, E. E. Massasa, D. Lemze, T. Weizman, R. Shenhav, S. Baydatch, O. Mizrahi, R. Winkler, O. Golani, N. Stern-Ginossar, S. Itzkovitz, Global mRNA polarization regulates translation efficiency in the intestinal epithelium. *Science*. **357**, 1299–1303 (2017).

283. T. Shigeoka, M. Koppers, H. H. W. Wong, J. Q. Lin, R. Cagnetta, A. Dwivedy, J. de Freitas Nascimento, F. W. van Tartwijk, F. Ströhl, J. M. Cioni, J. Schaeffer, M. Carrington, C. F. Kaminski, H. Jung, W. A. Harris, C. E. Holt, On-Site Ribosome Remodeling by Locally Synthesized Ribosomal Proteins in Axons. *Cell Rep.* **29**, 3605-3619.e10 (2019).

284. G. Lukinavičius, L. Reymond, E. D'Este, A. Masharina, F. Göttfert, H. Ta, A. Güther, M. Fournier, S. Rizzo, H. Waldmann, C. Blaukopf, C. Sommer, D. W. Gerlich, H.-D. Arndt, S. W. Hell, K. Johnsson, Fluorogenic probes for live-cell imaging of the cytoskeleton. *Nat. Methods*. **11**, 731–733 (2014).

285. E. Bartolák-Suki, B. Suki, Tuning mitochondrial structure and function to criticality by fluctuation-driven mechanotransduction. *Sci. Rep.* **10**, 1–13 (2020).

286. S. C. J. Helle, Q. Feng, M. J. Aebersold, L. Hirt, R. R. Grüter, A. Vahid, A. Sirianni, S. Mostowy, J. G. Snedeker, A. Šarić, T. Idema, T. Zambelli, B. Kornmann, Mechanical force induces mitochondrial fission. *Elife*. **6** (2017), doi:10.7554/eLife.30292.

287. B. Cunniff, A. J. McKenzie, N. H. Heintz, A. K. Howe, AMPK activity regulates trafficking of Mitochondria to the leading edge during cell migration and matrix invasion. *Mol. Biol. Cell*. **27**, 2662–2674 (2016).

288. H. Alshaabi, M. Heininger, B. Cunniff, Dynamic regulation of subcellular mitochondrial position for localized metabolite levels. *J. Biochem.* **167**, 109–117 (2020).

289. P. J. Hollenbeck, W. M. Saxton, The axonal transport of mitochondria. *J. Cell Sci.* **118**, 5411–5419 (2005).

290. X. Wang, T. L. Schwarz, The Mechanism of Ca2+-Dependent Regulation of Kinesin-Mediated Mitochondrial Motility. *Cell*. **136**, 163–174 (2009).

291. M. Fiorillo, C. Scatena, A. G. Naccarato, F. Sotgia, M. P. Lisanti, Bedaquiline, an FDA-approved drug, inhibits mitochondrial ATP production and metastasis in vivo, by targeting the gamma subunit (ATP5F1C) of the ATP synthase. *Cell Death Differ.* (2021), doi:10.1038/s41418-021-00788-x.